Conference Series

Advances in Nonlinear Science

Regular and Chaotic Dynamics

Nonlinear Dynamics, Mechanics and Robotics

November 23–27, 2026

Izhevsk, Russia

Book of Abstracts

2026

Program Committee

Valery Kozlov (Steklov Mathematical Institute RAS)
Boris Bardin (Moscow Aviation Institute)
Sergey Bolotin (Steklov Mathematical Institute RAS)
Alexander Kilin (Udmurt State University)
Nikolai Lukoyanov (N. N. Krasovskii Institute of Mathematics and Mechanics UB RAS)
Ivan Mamaev (Kalashnikov Izhevsk State Technical University)
Dmitry Treschev (Steklov Mathematical Institute RAS)

Organizing Institutions

Ural Mathematical Center at UdSU
Udmurt State University
N. N. Krasovskii Institute of Mathematics and Mechanics UB RAS
Steklov Mathematical Institute RAS

Information Partners

Izhevsk Institute of Computer Science
International Journal "Regular and Chaotic Dynamics"
International Journal "Russian Journal of Nonlinear Dynamics'

Conference Webpage
http://ics.org.ru/conference/11908-rcd2026/

E-Mails
conf2026@rcd.ru, mamaev@rcd.ru

ANS Conference Series "Regular and Chaotic Dynamics: Nonlinear Dynamics, Mechanics and Robotics". Book of Abstracts. — Izhevsk : Institute of Computer Science, 2026. — 116 p.

© Izhevsk Institute of Computer Science, 2026

ISBN 978-5-4344-1134-9

Contents

W. Ali, S. A. Kolyubin
Energy-constrained variable-impedance control for state-synchronized robotic cutting . . . 7
A. A. Ardentov
The time-minimizing problem on the group $\mathrm{SE}(2)$ with control on a shifted ellipse . . . 10
A. A. Bannikov, Yu. L. Karavaev
Experimental study of force and torque characteristics of a spherical robot aerodynamic propulsion system . . . 12
B. S. Bardin, E. V. Volkov, E. A. Sukhov
On orbital stability of periodic motions near relative equilibrium positions in the planar restricted four-body problem . . . 15
I. A. Bizyaev
The two-body problem in the post-Newtonian approximation with spins . . . 17
I. A. Bizyaev, A. S. Berdnikova
Dynamics and stability of a rimless wheel on an inclined plane . . . 19
A. A. Bobrovskiy, A. O. Kazakov, N. E. Kulagin, L. M. Lerman
Numerical study of bifurcations and chaos in two different gyroscopically coupled duffing oscillators with dissipation . . . 21
S. V. Bolotin, D. V. Treschev
On the problem of stability of viscous shocks . . . 24
E. S. Briskin, D. V. Bordyugov
The motion control of mechanical systems based on the integral principle of least constraint . . . 25
M. S. Fedoseev, A. A. Ardentov
Extremal trajectories in the Markov problem with control on a triangle . . . 28
B. Gajić, V. Dragović, B. Jovanović
Dynamics of the gyroscope in R^n . . . 30
A. M. Gavrilova, E. V. Vetchanin
Influence of an attached vortex on the motion of a solid body in a fluid . . . 31
A. S. Gonchenko
On discrete Lorenz-like attractors in three-dimensional cubic maps with axial symmetry . . . 33

S. V. Gonchenko
New case of conservative $1:4$ resonance 35
T. B. Ivanova, A. A. Kilin
Integrability and bifurcation analysis of the problem of a spherical top rolling on a plane without spinning and with partial slipping 38
A. V. Ivanyukhin
Low-energy capture trajectories near the libration points 39
B. Jovanović, V. Dragović, and B. Gajić
C^0 and C^1 gluing of integrable systems 41
Yu. L. Karavaev
Specifics of using non-holonomic mechanics models in the design and control of mobile robots 43
A. O. Kazakov, N. E. Kulagin, L. M. Lerman, and K. S. Zaichikov
Invariant tori and the Smale–Williams attractor in a perturbed integrable Hamiltonian system with a saddle-focus skirt 45
O. V. Kholostova, M. V. Belichenko
Study of pendulum-type motions in an approximate problem of the dynamics of a rigid body with a vibrating suspension 47
A. A. Kilin
Rolling of a system of coupled axisymmetric bodies on a plane . . 49
A. A. Kilin, E. M. Artemova, and D. A. Solodyankin
Dynamics and control of a spherical robot with a pendulum platform on a cylindrical joint 51
A. A. Kilin, Yu. L. Karavaev, V. A. Shestakov
Accounting for surface irregularities in the control of a highly maneuverable mobile robot 52
V. A. Koryakin
Structure of the Lorenz attractor existence region in the Shimizu–Morioka system 55
K. V. Koshel, M. A. Sokolovskiy
Regular and chaotic advection induced by stationary vortex structures in a two-layer rotating fluid 58
V. V. Kozlov
Earnshaw's theorem and levitation 60
E. A. Kudryavtseva
Bifurcations through a non-semisimple hyperbolic $1:1$ resonance, with examples in rigid body dynamics 61

A. S. Kuleshov
The Hess case in the problem of motion of a heavy body with a vertically vibrating suspension point 64
D. A. Lagunov, E. M. Artemova
Motion of two thin plates in an ideal fluid 65
L. M. Lerman, N. E. Kulagin
Double Hamiltonian Hopf bifurcation 67
A. V. Maloletov
Dynamics and motion planning of a hybrid cable-driven robot with movable carriages 70
I. S. Mamaev, E. M. Artemova, and I. A. Bizyaev
Integrable systems with multivalued integrals 73
A. P. Markeev
A new algorithm for calculating the normal form coefficients of an autonomous Hamiltonian system in the neighborhood of its periodic motion 74
A. V. Nazarov, A. V. Klekovkin, Yu. L. Karavaev
Investigation of the effect of tail fin stiffness on the speed of an aquatic robot 76
A. V. Nelyubova, V. V. Zhoga
Synthesis of software control forces for a hybrid manipulator for surface processing 79
E. N. Pivovarova, A. A. Kilin
Dynamics of a spherical robot with a pendulum-rotor mechanism . 82
Yu. S. Plakhotina, A. V. Shatina
Mathematical modelling of the polar motion of a viscoelastic planet 83
E. A. Pogosyan, S. V. Gusev
A robot motion planning algorithm based on solving a system of nonconvex inequalities 85
I. Yu. Polekhin
On Lyapunov stability and integrability of the Ziegler pendulum . . 88
K. S. Ryabov
Synchronization on graphons with higher-order interactions: the spectrum of the coupling operator versus the structure of the coupling tensor 89
P. E. Ryabov
A new class of motions of the Kovalevskaya–Chaplygin–Goryachev–Yehia top: algebraic solution and reduction to elliptic quadratures . 91

K. A. Safonov
Robust chaos in replicator systems with cyclic symmetry 94
V. V. Sidorenko
Deterministic and probabilistic transitions in the dynamics of Earth co-orbitals 96
I. M. Tarabukin, O. Yu. Sumenkov
Stabilization of underactuated mechanical systems with unknown build-in controllers 98
A. M. Tuzikov
Numerical modeling of three-dimensional motion of a spherical robot with electromagnetic drive 99
A. D. Uskova
On the first caustic of elliptical billiards 102
R. A. Uvarov
Normal forms for an equilibrium with a triple-zero eigenvalue in $\mathbf{Z}_4$-symmetric systems: bifurcations and attractors 103
E. V. Vetchanin, E. M. Artemova
Control of a circular foil motion using an attached source 105
E. V. Zhuzhoma
Structurally stable systems with codimension one attractors 107
A. N. Zotov, A. R. Valeev, A. P. Tokarev, D. N. Mazidullin, and D. P. Danilov
Flexible hinges with a given characteristic for a gravity compensator 108
I. S. Zvonarev, Yu. L. Karavaev
Motion planning for a spherical robot on uneven terrain using PPO . 111
V. K. Zykov, P. N. Deryushev, R. T. Mrakov, and Yu. L. Karavaev
Visual localization of an unmanned aerial vehicle using onboard camera imagery 114

Energy-constrained variable-impedance control for state-synchronized robotic cutting

W. Ali, S. A. Kolyubin

ITMO University, Saint-Petersburg, Russia

Introduction and relevance. The combination of learned policies with variable impedance controllers for compliant execution [1] is one of the most recent contact-skill methods. A central challenge is learning a contact-rich task by encoding kinematical and dynamical priors from human demonstrations and regularizing on them rather than deterministically cloning the recorded behavior [2]. The learned reference generator supplies phase-indexed motion and interaction profiles. However, time-varying gains and moving references can inject energy, while a time-indexed reference can advance despite contact-induced delay. Recent energy-tank controllers address related passivity problems [4, 5].

The goal. Our earlier work established training of behavior-prior models for contact-rich manipulation [3] and then integrated GMR-encoded priors with variable-impedance control [2]. The present work develops an energy-constrained, state-synchronized execution architecture for a robotic arm.

The task. Human-derived scalpel cutting on different materials provides a contact-rich validation task with frictional and geometrical variability.

Methods. The learned prior supplies phase-indexed pose, velocity, wrench and impedance profiles. The contribution is their safe dynamical execution: task timing responds to physical progress while a torque-port constraint bounds power from the complete joint command.

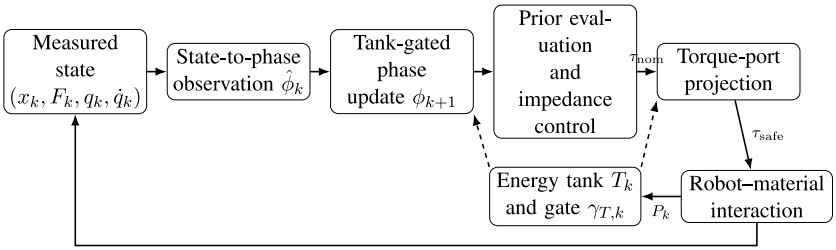


Figure 1. Sampled-data execution pipeline. Measured task state corrects phase; the tank gates progression and bounds positive joint power; delivered power settles the tank for the next sample

State-synchronized phase. At every control sample, the measured task state is projected onto the reference manifold to estimate physically consistent progress. The resulting state-corrected phase law retards or advances the reference according to the phase error, while an energy-dependent gate can suspend progression when the available storage is insufficient. In the implementation, $\hat{\phi}_k \in \arg\min_{\varphi \in \mathcal{C}_k} J_k(\varphi)$ is the locally observed phase and

$$\begin{aligned} \Delta\phi_k^{\mathrm{nom}} &= \gamma_{T,k} \frac{s_\phi h_c}{T_d}, & r_k &= h_c k_\phi (\hat{\phi}_k - \phi_k), \\ \delta\phi_k &= \mathrm{sat}_{[-\Delta\phi_k^{\mathrm{nom}},\, 2\Delta\phi_k^{\mathrm{nom}}]}(r_k), & \phi_{k+1} &= \boxed{\Pi_{[0,1]}(\phi_k + \Delta\phi_k^{\mathrm{nom}} + \delta\phi_k)}. \end{aligned} \tag{1}$$

Here h_c is the controller period, s_ϕ/T_d is the ungated nominal rate, and $\gamma_{T,k} \in [0,1]$ is the tank gate. Saturation prevents phase reversal and bounds the increment by $0 \le \phi_{k+1} - \phi_k \le 3h_c\gamma_{T,k}s_\phi/T_d$.

Discrete torque-port energy accounting. Because passivity must be assessed at the port where control action is applied, the variable-impedance command is mapped to joint torques and projected onto the discrete power constraint $\dot{q}^\top \tau_{\mathrm{safe}} \le P_{\max}$. With τ_{nom} denoting the task, posture, and model-compensation torques, the projection is

$$\boxed{\tau_{\mathrm{safe}} = \arg\min_{\tau} \|\tau - \tau_{\mathrm{nom}}\|_2^2 \quad \text{s.t. } \dot{q}_k^\top \tau \le P_{\max,k},\ P_{\max,k} = \frac{T_k - T_{\min}}{h_c}.} \tag{2}$$

The tank is updated from the power delivered after projection, closing the sampled-data accounting loop:

$$\begin{aligned} P_k &= \dot{q}_k^\top \tau_{\mathrm{safe},k}, & T_{k+1} &= \mathrm{clip}(T_k - h_c P_k, T_{\min}, T_{\max}), \\ & & \gamma_{T,k+1} &= \tanh\left(\frac{T_{k+1} - T_{\min}}{T_{\mathrm{ref}}}\right). \end{aligned} \tag{3}$$

Positive power depletes storage, negative power recharges it, and the phase gate approaches zero when usable energy is depleted. Sufficient exponential-stability conditions are also derived for the idealized regulated error dynamics with constant or sufficiently slow gain and phase variation.

Evaluation results. The method was evaluated in randomized-physics simulations of cutting with a seven-degree-of-freedom iiwa KUKA robotic manipulator. A factorial study crossed static and moving workpieces, nominal and 120 N holdback-perturbed execution, and state-driven and time-driven phase laws. All 40 executions completed with no recorded violation of the implemented torque-port power constraint. Under holdback, state feedback

visibly retarded task progress when measured motion lagged behind the reference; its accuracy benefit was scenario-dependent, and the paired cut-depth comparisons were not statistically significant. In a separate positive-power stress test, the unprojected controller exceeded its available power budget in 69.8% of samples, whereas torque projection reduced recorded violations to zero while retaining 100% task completion. To illustrate insufficient available energy, the tank was initialized at $T_0 = 1$ J ($T_{\min} = 1$ mJ, $T_{\max} = 3$ J and $T_{\mathrm{ref}} = 0.5$ J) instead of the nominal $T_0 = 50$ J. This deliberately small value is not calculated from the robot dynamics and is not used for normal runs. The tank limits the complete seven-joint command—Cartesian cutting torque, null-space posture torque and gravity/Coriolis compensation—not only the cutting interaction. At its lower energy limit, phase gating stopped the reference at $\phi = 0.024$.

Conclusion. These simulation results demonstrate torque-port energy accounting and state-aware reference synchronization.

References

[1] Jadav S., Heidersberger J., Ott C., Lee D., Shared Autonomy via Variable Impedance Control and Virtual Potential Fields for Encoding Human Demonstrations, *Proc. IEEE ICRA*, 2024, pp. 15151–15157, doi: 10.1109/ICRA57147.2024.10610761.

[2] Ali W., Kolyubin S. A., Variable Impedance Learning Control for Robotic Arms from GMR-Encoded Behavior Priors, *Journal of Instrument Engineering*, 2024, vol. 67, no. 10, pp. 893–898, doi: 10.17586/0021-3454-2024-67-10-893-898.

[3] Ali W., Kolyubin S. A., Modeling Patterns of Sensory-Motor Skills for Programming Robots in Contact Manipulation Tasks, *Journal of Instrument Engineering*, 2024, vol. 67, no. 6, pp. 500–510, doi: 10.17586/0021-3454-2024-67-6-500-510.

[4] Fu J., Maimone G., Iovene E., Zhao J., Redaelli A., Ferrigno G., De Momi E., Human-Inspired Active Compliant and Passive Shared Control Framework for Robotic Contact-Rich Tasks in Medical Applications, *IEEE Trans. Robot.*, 2025, vol. 41, pp. 2549–2568, doi: 10.1109/TRO.2025.3548493.

[5] Li Z., Deng S., Zeng C., Yang C., A Control Framework with Tactile Diffusion Policy and Variable Impedance for Unknown Surface Tracking, *IEEE Robot. Autom. Lett.*, 2026, vol. 11, no. 2, pp. 1978–1985, doi: 10.1109/LRA.2025.3645656.

The time-minimizing problem on the group $\mathrm{SE}(2)$ with control on a shifted ellipse

A. A. Ardentov

Ailamazyan Program Systems Institute of Russian Academy of Sciences, Pereslavl-Zalessky, Russia

Let us consider a wheeled robot that moves only in the forward direction. Motion along a straight line occurs at a maximum unit speed. During turns, the maximum speed decreases monotonically and smoothly as a function of the turn's radius of curvature. As the radius of curvature approaches zero, the corresponding maximum linear speed also approaches zero, which precludes the robot from rotating in place.

This model of a wheeled robot can be formulated as an optimal control problem, where the control input is defined by a vector of linear and angular velocities; the set of admissible controls is the ellipse that passes through the origin, with its center shifted to a point on the positive semi-axis of the abscissa.

Various time-minimizing problems on the group of motions of a plane $\mathrm{SE}(2)$ are known, differing in the shape of their admissible control sets. One category involves convex sets symmetric with respect to the origin, corresponding to sub-Finsler problems (specifically, sub-Riemannian problems when the set is a circle centered at the origin). Another class involves shifted control sets (not containing the origin), which restrict the robot to forward motion (e.g., the Dubins car model). The problem under consideration is of fundamental importance as a time-minimizing problem with a shifted, smooth control set that possesses a singularity at the origin; this extends the existing range of known time-optimal control models.

We apply Pontryagin maximum principle [1] to identify extremal trajectories. The vertical subsystem of the Hamiltonian system is expressed in terms of linear on the fibers of the cotangent bundle hamiltonians. We prove that only trivial abnormal trajectories (those with zero control) exist. To demonstrate the integrability of the normal Hamiltonian system, two first integrals are derived for the vertical subsystem, which can be decoupled from the overall Hamiltonian system. Next, by analyzing the phase portrait of the vertical subsystem, all types of extremals are characterized. As a result, all extremal trajectories are parameterized not by time, but by the absolute value of the robot's orientation angle. The projections of these extremal trajectories correspond to Euler's planar elasticae, excluding those with inflection points where the tangent angle undergoes only small oscillations.

The proposed time-minimizing problem can serve also as a model for describing the motion of an aircraft flying at a specified altitude or a surface watercraft. Additionally, the discovered trajectories can be applied in computer vision for reconstructing smooth image lines obscured from the observer's view.

This work is supported by the Russian Science Foundation under grant 25-21-00681 and performed in Ailamazyan Program Systems Institute of Russian Academy of Sciences.

References

[1] Pontryagin L. S., Boltyanskii V. G., Gamkrelidze R. V., Mishchenko E. F., *The mathematical theory of optimal processes*, Wiley Interscience, 1962.

Experimental study of force and torque characteristics of a spherical robot aerodynamic propulsion system

A. A. Bannikov, Yu. L. Karavaev

Kalashnikov Izhevsk State Technical University, Izhevsk, Russia

Hybrid terrestrial–aerial robots use their propeller units not only for flight, but also to reduce the ground contact load, stabilize the vehicle, and generate control torques during surface locomotion [1–3]. Designing a control system for such a vehicle requires an experimental model relating motor commands to the actual forces and torques. Nominal characteristics of individual motors and propellers do not account for the airframe configuration, mutual aerodynamic interference, or bidirectional operation. The aim of this study is to develop a force–torque test bench and an identification procedure for the four-propeller aerodynamic propulsion system of a spherical robot [4].

The propulsion system is located inside a protective spherical shell and has a quadrotor configuration with four propellers. Bidirectional electronic speed controllers allow each motor to generate forward and reverse thrust. Their combined operation produces the resultant force and control torques used for locomotion and stabilization of the spherical robot. Related control problems are considered, in particular, in [5, 6].

The aerodynamic module is mounted on a six-axis force–torque sensor that measures three force and three torque components. The displacement between the sensor and module coordinate systems is taken into account during data processing, and the measurements are reduced to the center of the module. The developed software synchronizes motor control and data acquisition, performs channel zeroing, provides a settling interval after each command change, and calculates statistical estimates. The normalized command u_i is negative for reverse thrust and positive for forward thrust.

The experimental program includes characterization of each motor in forward and reverse operation, investigation of the dead zone, assessment of repeatability, and evaluation of the supply-voltage influence. Subsequent test series address simultaneous motor operation and determine the resultant forces and torques for different command combinations. The intended outcome is the experimental mapping

$$(u_1, u_2, u_3, u_4) \longmapsto (F_x, F_y, F_z, M_x, M_y, M_z),$$

which can be used to calculate individual motor commands in the control system.

Preliminary tests were conducted to verify the test bench operation by activating the motors individually in forward and reverse directions. The measurements covered $|u_i| \leq 0.75$, with a smaller command increment near neutral and both ascending and descending sweeps. The curves presented in Fig. 1 illustrate the general relationship between axial force F_z and the motor command and are not treated as final calibration characteristics.

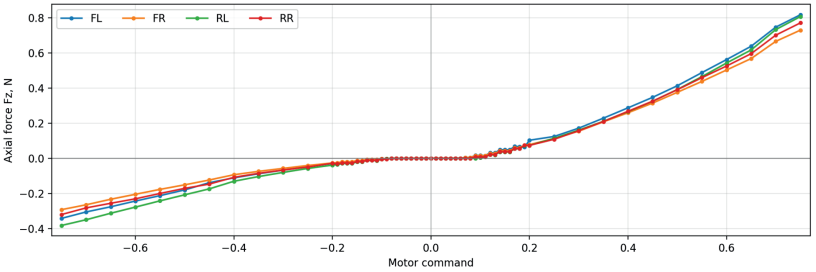


Figure 1. Axial force F_z versus command for the four motors

The preliminary results demonstrate nonlinear characteristics, a dead zone near neutral, differences between individual motors, and pronounced asymmetry between forward and reverse thrust. Consequently, a single linear coefficient is insufficient to describe the propulsion system, especially at small control inputs.

The study presents the measurement system, the automated experimental procedure, and the results of investigating the force and torque characteristics of the propulsion system. The identified relationships are used to construct a propulsion model and to develop an allocation algorithm that distributes the required forces and torques among the spherical robot motors.

The study was supported by the Russian Science Foundation, project No. 25-11-00305.

References

[1] Jia H., Bai S., Ding R. et al., A Quadrotor with a Passively Reconfigurable Airframe for Hybrid Terrestrial Locomotion, *IEEE/ASME Trans. Mechatronics*, 2022, vol. 27, no. 6, pp. 4741–4751.

[2] Zheng Z., Wang J., Wu Y. et al., Roller-Quadrotor: A Novel Hybrid Terrestrial/Aerial Quadrotor with Unicycle-Driven and Rotor-Assisted Turning, *Proc. IEEE/RSJ IROS 2023*, pp. 6927–6934.

[3] Karavaev Yu. L., Spherical Robots: An Up-to-Date Overview of Designs and Features, *Rus. J. Nonlin. Dyn.*, 2022, vol. 18, no. 4, pp. 709–750.

[4] Bannikov A. A., Artemova E. M., Solodyankin D. A., Determination of Optimal Design Parameters for a Spherical Robot with an Aerodynamic Propulsion System, *Proc. MIKMUS-2025*, 2025, pp. 147–150.

[5] Ivanova T. B., Karavaev Yu. L., Kilin A. A., Control of a Pendulum-Actuated Spherical Robot on a Horizontal Plane with Rolling Resistance, *Arch. Appl. Mech.*, 2022, vol. 92, pp. 137–150.

[6] Klekovkin A. V., Karavaev Yu. L., Nazarov A. V., Stabilization of a Spherical Robot with an Internal Pendulum During Motion on an Oscillating Base, *Rus. J. Nonlin. Dyn.*, 2024, vol. 20, no. 5, pp. 845–858.

On orbital stability of periodic motions near relative equilibrium positions in the planar restricted four-body problem

B. S. Bardin, E. V. Volkov, E. A. Sukhov

Moscow aviation institute (National research university), Moscow, Russia

The planar circular restricted four-body problem is considered in the following formulation. Three massive bodies (primaries) interact according to the Newton's law of gravitation, move in circular orbits, and are located in the triangular libration points, which are stable in the linear approximation. The masses of two of the three primaries are equal. The fourth body has infinitesimal mass and moves in the gravitational field of these primaries. All four bodies are assumed to move in the same plane. The equations of motion of the small body admit stationary solutions that describe relative equilibrium positions in the coordinate system rotating along with the equilateral triangle formed by the primaries. The stability of these relative equilibrium positions has been the subject of numerous studies; the most comprehensive investigation was performed in [1], where rigorous conclusions on Lyapunov stability has been obtained for most of the problem's parameter values.

Periodic motions, whose periods depend on the constant of the energy integral, are exist in the vicinity of stable relative equilibrium positions. The existence of such motions follows from Lyapunov's theorem on the holomorphic integral. The analytical and numerical methods are well-developed for their construction. These periodic motions are unstable in the sense of Lyapunov, but they can be orbitally stable. The most general approach for study of the orbital stability bases on introducing local coordinates in a neighborhood of periodic solutions and transforming the Hamiltonian of the problem into a normal form. Rigorous conclusions on orbital stability can then be obtained by using known stability criteria, which are written in forms of inequalities in terms of the coefficients of the Hamiltonian normal form [2].

In this paper, by using the above approach we propose an algorithm to analyze the orbital stability of periodic motions in the planar restricted four-body problem. In particular, on the basis of the method developed in [3], we show how to introduce the local variables in the vicinity of periodic motions. This algorithm allows to introduce the local variables both in the case of low energy values, when periodic solutions can be constructed in an analytical form, and for arbitrary energy values, when the periodic solutions can only be obtained numerically. We also describe a procedure for calculating

the Hamiltonian normal form in canonical polar coordinates. This procedure allows to reduce the calculation of the normal form coefficients to the sequential solution of relatively simple linear partial differential equations. Finally, we perform a nonlinear stability analysis and obtain rigorous conclusions on orbital stability of the periodic motions of the small body in a neighborhood of its relative equilibrium positions. The results of the study are presented in the form of stability diagrams.

This research was supported by the Russian Science Foundation (grant No. 25-21-00907, https://rscf.ru/project/25-21-00907/) and was carried out at the Moscow Aviation Institute (National Research University).

References

[1] Bardin B. S., Volkov E. V. The Lyapunov Stability of Central Configurations of the Planar Circular Restricted Four-Body Problem, *Cosmic Research*, 2024, vol. 62, no. 5, pp. 388–400.

[2] Markeev A. P., *Tochki libratsii v nebesnoi mekhanike i kosmodinamike (Libration Points in Celestial Mechanics and Space Dynamics)*, Moscow: Nauka, 1978.

[3] Bardin B. S., On the Method of Introduction of Local Variables in a Neighborhood of Periodic Solution of a Hamiltonian System with Two Degrees of Freedom, *Regul. Chaotic Dyn.*, 2023, vol. 28, no. 6, pp. 878–887.

The two-body problem in the post-Newtonian approximation with spins

I. A. Bizyaev

Ural Mathematical Center, Udmurt State University, Izhevsk, Russia

Consider the motion of two bodies in the center-of-mass coordinate system. Let us denote the momentum of one of the bodies by $\boldsymbol{p}$, and the distance between them by $\boldsymbol{r}$. We represent the Hamiltonian for the system under consideration in the following form:

$$H(\boldsymbol{r},\boldsymbol{p},\boldsymbol{S}^a,\boldsymbol{S}^b)=H_O(\boldsymbol{r},\boldsymbol{p})+H_{SO}(\boldsymbol{r},\boldsymbol{p},\boldsymbol{S}^a,\boldsymbol{S}^b), \tag{1}$$

where $\boldsymbol{S}^a$ and $\boldsymbol{S}^b$ are the spins of the first and second bodies.

The orbital Hamiltonian H_O includes the Newtonian term and post-Newtonian corrections:

$$H_O=H_N+H_{1PN}+H_{2PN},$$
$$H_N=\frac{\boldsymbol{p}^2}{2}-\frac{1}{r},$$

The post-Newtonian corrections in ADM (Arnowitt–Deser–Misner) coordinates are given as follows [1–3]:

$$H_{1PN}=\frac{3\eta-1}{8}\boldsymbol{p}^4-\frac{1}{2r}\left[3\boldsymbol{p}^2+\eta(\boldsymbol{p}^2+p_r^2)\right]+\frac{1}{2r^2},$$
$$H_{2PN}=\frac{1}{16}(1-5\eta+5\eta^2)\boldsymbol{p}^6+\frac{1}{8r}\left[(5-20\eta-3\eta^2)\boldsymbol{p}^4-2(\eta p_r\boldsymbol{p})^2-3\eta^2p_r^4\right]+$$
$$\frac{1}{2r^2}\left[(5+8\eta)\boldsymbol{p}^2+3\eta p_r^2\right]-\frac{1+3\eta}{4r^3},$$

where $r=\sqrt{\boldsymbol{r}^2}$ and $p_r=\dfrac{(\boldsymbol{p},\boldsymbol{r})}{r}$.

We represent the spin-orbit Hamiltonian H_{SO} in the following form [4,5]:

$$H_{SO}=\frac{\eta}{r^3}\left(2\boldsymbol{S}+\frac{3}{2}\boldsymbol{S}^*,\boldsymbol{r}\times\boldsymbol{p}\right),\quad \boldsymbol{S}=\boldsymbol{S}^a+\boldsymbol{S}^b,\quad \boldsymbol{S}^*=\zeta\boldsymbol{S}^a+\frac{1}{\zeta}\boldsymbol{S}^b.$$

The parameters entering the Hamiltonian (1) depend on the masses of the two bodies as follows:

$$\zeta=\frac{m^b}{m^a}\in(0,1],\quad \eta=\frac{m^am^b}{(m^a+m^b)^2}=\frac{\zeta}{(1+\zeta)^2}.$$

The equations of motion of the system under consideration are represented in the following form:

$$\begin{gathered} \frac{d\boldsymbol{r}}{dt} = \frac{\partial H}{\partial \boldsymbol{p}}, \quad \frac{d\boldsymbol{p}}{dt} = -\frac{\partial H}{\partial \boldsymbol{r}}, \\ \frac{d\boldsymbol{S}^a}{dt} = \frac{\partial H}{\partial \boldsymbol{S^a}} \times \boldsymbol{S}^a, \quad \frac{d\boldsymbol{S}^b}{dt} = \frac{\partial H}{\partial \boldsymbol{S^b}} \times \boldsymbol{S}^b. \end{gathered} \tag{2}$$

The Hamiltonian system (2) has five degrees of freedom. In addition to the Hamiltonian, it possesses four additional integrals that are in involution and, therefore, is integrable by the Liouville – Arnold theorem. An explicit reduction to quadratures and a subsequent qualitative analysis of the system will be carried out.

This work was carried out within the framework of the state assignment of the Ministry of Science and Higher Education of Russia (FEWS-2024-0007).

References

[1] Damour T, Jaranowski P., Schäfer G., Poincaré invariance in the ADM Hamiltonian approach to the general relativistic two-body problem, Phys. Rev. D, vol. 62, no. 2, p. 021501, 2000.

[2] Damour T, Jaranowski P., Schäfer G., Erratum: Poincaré invariance in the ADM Hamiltonian approach to the general relativistic two-body problem, Phys. Rev. D, vol. 63, no. 2, p. 029903, 2000.

[3] Buonanno A., Chen Y., Damour T. Transition from inspiral to plunge in precessing binaries of spinning black holes, Physical Review D, 2006, vol. 74, no. 10, p. 104005.

[4] Damour T., Jaranowski P., Schaefer G. Hamiltonian of two spinning compact bodies with next-to-leading order gravitational spin-orbit coupling, Physical Review D—Particles, Fields, Gravitation, and Cosmology, 2008, vol. 77, no. 6, p. 064032.

[5] Nagar A. Effective one-body Hamiltonian of two spinning black holes with next-to-next-to-leading order spin-orbit coupling, Physical Review D, 2011, vol. 84, no. 8, p. 084028.

Dynamics and stability of a rimless wheel on an inclined plane

I. A. Bizyaev, A. S. Berdnikova

Ural Mathematical Center, Udmurt State University, Izhevsk, Russia

We consider the motion of a rimless wheel [1, 2] with n equally spaced spokes of length ℓ on a fixed inclined plane. The motion consists of rotation about the supporting spoke and transitions between spokes accompanied by impacts. No slipping at the contact point is assumed. The supporting spoke changes instantaneously, and the motion is assumed to involve only one supporting spoke at a time.

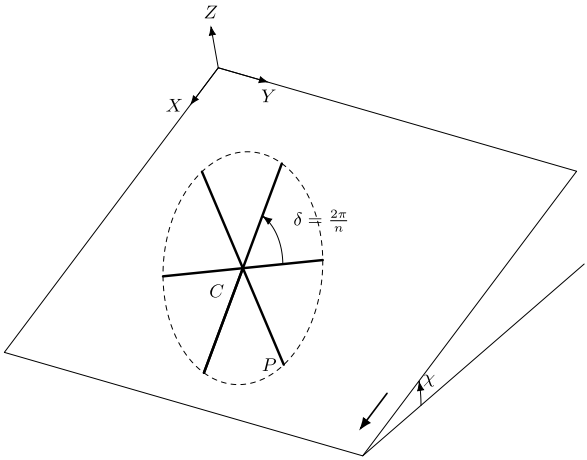


Figure 1. Schematic representation of a rimless wheel

Between impacts, the system is governed by the Euler–Poisson equations [3]

$$\dot{\boldsymbol{M}} = \boldsymbol{M} \times \boldsymbol{\omega} + mg\boldsymbol{\gamma} \times \boldsymbol{r}, \qquad \dot{\boldsymbol{\gamma}} = \boldsymbol{\gamma} \times \boldsymbol{\omega}, \qquad \boldsymbol{\omega} = \mathbf{I}^{-1}\boldsymbol{M}. \tag{1}$$

Here $\boldsymbol{M}$ is the angular momentum about the current contact point, $\boldsymbol{\gamma}$ is the upward-pointing unit vertical vector expressed in the wheel-fixed frame, and $\boldsymbol{r} = (0, 0, \ell)$ is the position vector of the center of mass relative to the contact point. The inertia tensor about the contact point P is

$$\mathbf{I} = \operatorname{diag}\bigl(J + m\ell^2,\ 2J + m\ell^2,\ J\bigr),$$

where m is the mass of the wheel, ℓ is the spoke length, and J is the central moment of inertia.

The equations (1) conserve energy and admit an area integral and a geometric integral:

$$E = \frac{1}{2}\big(\boldsymbol{M}, \mathbf{I}^{-1}\boldsymbol{M}\big) + mg(\boldsymbol{r}, \boldsymbol{\gamma}), \qquad F = (\boldsymbol{M}, \boldsymbol{\gamma}), \qquad (\boldsymbol{\gamma}, \boldsymbol{\gamma}) = 1. \quad (2)$$

At an impact (i.e., during a transition between spokes), the integrals E and F are not conserved.

To study the system, a Poincaré map is constructed numerically. A fixed point is found at which the rimless wheel remains upright and rolls at a constant speed along the line of steepest descent. For a sufficiently large number of spokes, this fixed point is asymptotically stable. In addition, the trajectory of the contact point in the rimless-wheel model is compared numerically with that of a nonholonomic rolling-disk model. It is shown that, as the number of spokes increases, the nonholonomic disk model describes the motion of the rimless wheel more accurately.

This work is supported by the Ministry of Science and Higher Education of the Russian Federation (project FEWS-2025-0004).

References

[1] McGeer T. Passive Dynamic Walking. The International Journal of Robotics Research. 1990. Vol. 9, No. 2. P. 62–82.

[2] Coleman M. J., Chatterjee A., Ruina A. Motions of a Rimless Spoked Wheel: a Simple 3D System with Impacts. Dynamics and Stability of Systems. 1997. Vol. 12, No. 3. P. 139–159.

[3] Borisov A. V., Mamaev I. S., *Rigid Body Dynamics*, De Gruyter Stud. Math. Phys., vol. 52, Berlin: De Gruyter, 2018.

Numerical study of bifurcations and chaos in two different gyroscopically coupled duffing oscillators with dissipation

A. A. Bobrovskiy[1], A. O. Kazakov[1], N. E. Kulagin[2], L. M. Lerman[1]

[1] *HSE University, Nizhniy Novgorod, Russia,*
[2] *A. N. Frumkin Institute of Physical Chemistry and Electrochemistry, Russian Academy of Science, Moscow, Russia*

A four-dimensional dynamical system obtained as a dissipative perturbation of a Hamiltonian system of two gyroscopically coupled Duffing oscillators is considered:

$$\begin{aligned} \dot{x} &= \alpha x + y - \beta u - \gamma x^5, \\ \dot{y} &= -x + \alpha y - x^3 - \beta v - \gamma y^5, \\ \dot{u} &= v + \beta x - \gamma u^5, \\ \dot{v} &= u - u^3 + \beta y - \gamma v^5. \end{aligned} \tag{1}$$

In this system, α, β, and γ are control parameters, while x, y, u, v are the phase variables. For $\gamma = 0$ and $\alpha = 0$, the system is Hamiltonian. It possesses a rich structure of invariant manifolds, periodic orbits, and homoclinic trajectories. The introduction of dissipative and excitation terms leads to a significant complication of the dynamics and to the formation of regions of periodic, quasiperiodic, and chaotic behavior. The aim of this work is to numerically investigate transformations of the phase-space structure and to construct the bifurcation picture of the system as the control parameters are varied.

Particular attention is paid to numerical methods for detecting and continuing invariant objects. Equilibria are determined by solving a system of nonlinear algebraic equations, followed by computation of the spectrum of the linearization matrix and classification of their stability. Poincaré sections and the shooting method with Newton correction are used to investigate periodic solutions. The stability of periodic orbits is determined from their Floquet multipliers. Parameter continuation of equilibria, periodic orbits, and global bifurcation structures makes it possible to trace their evolution and determine critical parameter values.

To analyze the global dynamics, long-term numerical integration is performed for a large number of initial conditions, together with computation of the largest Lyapunov exponent and construction of two-parameter diagrams (Fig. 1). In these diagrams, regions corresponding to stable periodic regimes,

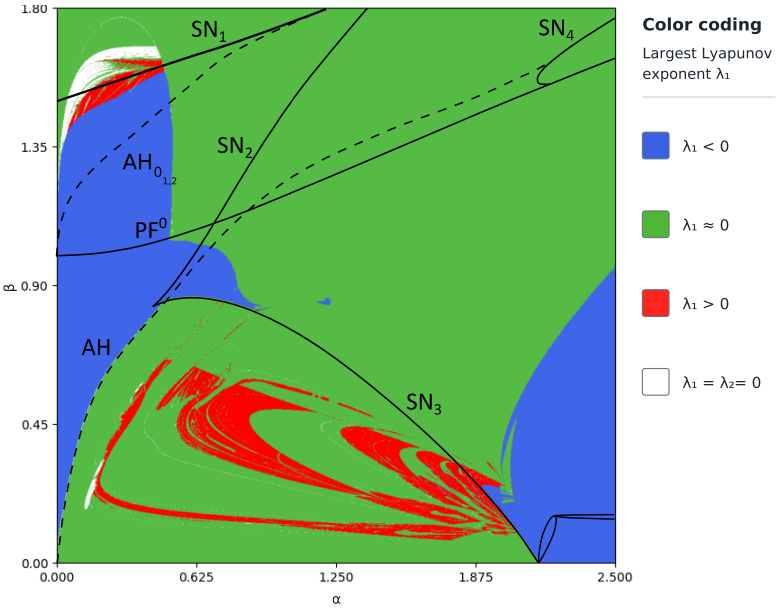


Figure 1. Bifurcation diagram of the system under consideration in the (α, β) parameter plane for $\gamma = 0.1$. The following bifurcation curves are shown: PF^0 is the pitchfork bifurcation curve of the zero equilibrium; SN_1, SN_2, SN_3, and SN_4 are saddle-node bifurcation curves; AH is the Andronov–Hopf bifurcation curve of the zero equilibrium; and $AH_{O_{1,2}}$ is the Andronov–Hopf bifurcation curve of the nonzero equilibria

quasiperiodic dynamics, and chaos are distinguished by different colors (see the color palette to the right of Fig. 1). In addition, one-parameter bifurcation diagrams for Poincaré maps are constructed. The combined use of these approaches makes it possible to relate local bifurcations of individual invariant objects to global changes in the observed dynamics.

Within the parameter regions under study, bifurcations of equilibria and periodic orbits are detected, including Andronov–Hopf bifurcations, period-doubling bifurcations, pitchfork bifurcations of periodic orbits, and Neimark–Sacker bifurcations. The latter are accompanied by the emergence of invariant tori and the formation of regions of quasiperiodic oscillations. Saddle periodic orbits and their stable and unstable manifolds, as well as homoclinic and heteroclinic structures, are also investigated numerically. Particular attention is paid to basin boundaries and global bifurcations associated with transitions from regular dynamics to chaotic attractors.

The obtained results demonstrate that the combined use of continuation methods, Lyapunov exponent analysis, Floquet multipliers, and bifurcation diagrams makes it possible to reconstruct the complex structure of the parameter space of the four-dimensional system and to trace the main scenarios of transition from simple regular dynamics to quasiperiodic and chaotic regimes.

The work is supported by Russian Science Foundation grants No.25-11-20069.

On the problem of stability of viscous shocks

S. V. Bolotin, D. V. Treschev

Steklov Mathematical Institute, Moscow, Russia

We consider the problem of spectral stability of traveling wave solutions $u = \gamma(x - Wt)$ for a system of viscous conservation laws $\partial_t u + \partial_x F(u) = \partial_x^2 u$. Such solutions correspond to heteroclinic trajectories γ of a system of ODEs. In general conditions of stability can be obtained only numerically. We propose a model class of piece-wise linear (discontinuous) vector fields F for which study of spectral stability is reduced to a linear algebra problem. We show that the stability problem makes sense in such low regularity and construct several examples of stability loss. Every such example can be smoothed to provide a smooth example of the same phenomenon. The talk is based on the paper [1].

The work is supported by the Ministry of Science and Higher Education of the Russian Federation (agreement no. 075-15-2025-303).

References

[1] Bolotin S. V., Treschev D. V. On the problem of stability of viscous shocks, *Regul. Chaot. Dyn.*, 30:6 (2025), 908–930.

The motion control of mechanical systems based on the integral principle of least constraint

E. S. Briskin, D. V. Bordyugov

Volgograd State Technical University, Volgograd, Russia

Introduction. It is well known that imposing constraints on a mechanical system subjected to active forces alters its laws of motion. Accounting for the influence of both holonomic and nonholonomic constraints on the equations of motion is commonly carried out under the assumption of constraint ideality, which yields Lagrange's equations of the second kind with undetermined multipliers [1,2]. Both analytical and numerical methods have been developed to solve mechanics problems using these equations [3,4].

However, accounting for the influence of constraints on the equations of motion can also be performed based on hypotheses distinct from the ideal constraint assumption [5]. This is particularly viable when constraints are formed not through contact interaction between the mechanical system and external bodies, but through prescribed programmed motion realized by an appropriate control system.

The necessity of introducing specific hypotheses regarding constraint properties is due to the presence in the equations of motion for mechanical systems with S degrees of freedom of S unknown constraint reactions D_j ($j = 1, S$), in addition to S unknown generalized coordinates q_i. The corresponding equations have the form:

$$\frac{d}{dt}\left(\frac{\partial T}{\partial \dot{q}^j}\right) - \frac{\partial T}{\partial q^j} = Q_j + D_j, \quad j = 1, S \tag{1}$$

where T is the kinetic energy of the system, and Q_j is the generalized active force corresponding to the j generalized coordinate q^j. Equations (1) are supplemented by the constraint equations:

$$f_n(q_1, \ldots, q_s, t) = 0, \quad (n = 1, N), \quad N < S. \tag{2}$$

Problem statement. Typically, the hypothesis of ideal constraints is adopted. Here, an alternative hypothesis regarding constraints is formulated, consisting of the requirement for a minimum of the integral of the sum of squared constraint reactions over the time interval $0 < t < \tau$, hereinafter referred to as the integral constraint. This approach is consistent with Gauss's

differential variational principle [1], which, in turn, aligns with the principle of least energy dissipation formulated by Onsager [6] in the analysis of thermodynamic processes. This formulation also agrees with L. I. Sedov's perspective [7] on the necessity of considering thermodynamic laws when formulating governing hypotheses for macroscopic mechanical systems. The minimum requirement for the integral constraint criterion corresponds to the vanishing of the isochronous variation of the functional accounting for constraint (2):

$$\delta \int_0^\tau \left[\delta^{ik} D_j D_k + \mu^n f_n\right] dt = 0 \tag{3}$$

where δ is the isochronous variation operator, δ^{ik} are the Kronecker delta symbols $j, m = 1, \ldots, S$, and μ^n are undetermined Lagrange multipliers.

Thus, the problem is posed to construct the Euler–Poisson differential equations based on functional variation (3).

Differential equations of motion of controlled mechanical systems derived from the principle of least constraint in integral form. For stationary constraints, equations (1) take the form:

$$a_{ji}\ddot{q}^i + \Gamma_{j,ik}\dot{q}^i\dot{q}^k - Q_j = D_j, \quad j = 1, \ldots, S \tag{4}$$

where a_{ji} is the inertia matrix of the mechanical system defined in the configuration space formed by generalized coordinates q^i, and $\Gamma_{j,ik}$ are Christoffel symbols of the first kind. However, these S equations alone cannot uniquely govern the motion of the mechanical system because they contain $2S$ unknown variables q^i and D_j.

To resolve this system, it suffices to introduce equations in the form:

$$\begin{gathered}\frac{d^2}{dt^2}\left(\frac{\partial \Phi}{\partial \ddot{q}^m}\right) - \frac{d}{dt}\left(\frac{\partial \Phi}{\partial \dot{q}^m}\right) + \frac{\partial \Phi}{\partial q^m} + \mu^n \frac{\partial f_n}{\partial q^m} = 0, \quad m = 1, 2 \ldots S, \\ \Phi = \delta^{jk} D_j D_k\end{gathered} \tag{5}$$

where the functional Φ is specified in accordance with (3) as:

$$\Phi = \delta^{jk}\left[a_{ji}\ddot{q}^i + \Gamma_{j,il}\dot{q}^l\dot{q}^i - Q_j\right]\left[a_{kl}\ddot{q}^i + \Gamma_{m,kp}\dot{q}^k\dot{q}^p - Q_k\right], \quad l, p = 1 \ldots S \tag{6}$$

Consequently, the system of equations (1), (2), and (5), comprising $2S + N + 1$ equations in total, contains an equal number of unknown variables: q_j, D_j, μ_n, and Φ.

Conclusion. An alternative method for incorporating constraints into the dynamic analysis of controlled mechanical systems without relying on ideal constraint assumptions has been proposed. The method is grounded

in Gauss's principle of least constraint, extended to an integral formulation. A hypothesis is formulated regarding the consistency of the proposed method with the principle of least dissipation of energy used in non-equilibrium thermodynamics. The developed method is applicable and currently utilized in investigating the dynamics of controlled motion in robotic systems.

The research was carried out with the financial support of a grant from the Russian Science Foundation No. 25-29-01736, https://rscf.ru/project/25-29-01736/

References

[1] Dobronravov V. V., *Fundamentals of Analytical Mechanics*, Moscow: Vysshaya Shkola, 1976, 264 p. (in Russian).

[2] Butenin N. V., *Introduction to Analytical Mechanics*, Moscow: Nauka, 1971, 264 p. (in Russian).

[3] Pogorelov D. Yu., Computer simulation of dynamic technical systems using the "Universal Mechanism" software package, *J. Comput. Inf. Technol.*, 2005, no. 4(10), pp. 27–34 (in Russian).

[4] Gorobtsov A. S., Software complex for calculating dynamics and kinematics of machines as systems of rigid and elastic bodies, *Engineering Journal*, 2004, no. 9(90), pp. 40–43 (in Russian).

[5] Briskin E. S., Pavlovsky V. E., Smirnaya L. D., Formation of motion properties of mechanical systems by controlling reactions of holonomic quasi-ideal constraints, *J. Comput. Syst. Sci. Int.*, 2021, no. 6, pp. 13–23.

[6] Gyarmati I., *Non-equilibrium Thermodynamics. Field Theory and Variational Principles*, Moscow: Mir, 1974, 304 p. (in Russian).

[7] Sedov L. I., *Connections of Macroscopic Mechanics with Physics*, Moscow: Moscow State Univ. Publ., 1992, Preprint No. 255, 20 p. (in Russian).

Extremal trajectories in the Markov problem with control on a triangle

M. S. Fedoseev, A. A. Ardentov

Ailamazyan Program Systems Institute of Russian Academy of Sciences, Pereslavl-Zalessky, Russia

We consider a time-optimal motion planning problem for a differential drive robot with bounded positive velocities of its driving wheels. In the classical Markov problem [1], the linear speed is constant, so travel time is proportional to path length. For the robot considered here, the maximum translational speed decreases during turning. We study a generalization of the Markov problem with a triangular control domain to account this effect.

The robot configuration is described by its planar position (x, y) and heading angle θ. The controls u_1 and u_2 are the linear and angular velocities, respectively. The equations of motion are

$$\dot{x} = u_1 \cos\theta, \qquad \dot{y} = u_1 \sin\theta, \qquad \dot{\theta} = u_2.$$

For a fixed parameter $u_1^{\max} > 1$, the admissible controls satisfy

$$1 \le u_1 \le u_1^{\max}, \qquad |u_2| \le \frac{u_1^{\max} - u_1}{u_1^{\max} - 1}.$$

The initial configuration is $(x(0), y(0), \theta(0)) = (0, 0, 0)$. The robot must reach a prescribed point $(x(T), y(T)) = (x_1, y_1)$, while the terminal heading $\theta(T)$ is free. The objective is to minimize the travel time T.

We apply the Pontryagin maximum principle [2] to classify extremal controls and derive necessary optimality conditions. Analysis of the Hamiltonian phase portrait, together with the transversality condition for the free terminal heading, yields piecewise constant candidate controls.

The resulting candidate path types are S, C, CC, CS, SCS, $CSCS$, and $SCSCS$, where S denotes a straight segment and C denotes a circular arc. The arc durations must also satisfy the switching and optimality conditions.

The candidate trajectories have been studied analytically for different values of $u_1^{\max}$. Among the extremal trajectories, optimal ones were identified, and an algorithm was developed for constructing optimal trajectories to a given terminal point (x_1, y_1) in the plane. The results are relevant to motion planning in ground robotics.

This work is supported by the Russian Science Foundation under grant 25-21-00681 and performed in Ailamazyan Program Systems Institute of Russian Academy of Sciences.

References

[1] Markov A. A., Some examples of the solution of a special kind of problem on greatest and least quantities, *Soobshch. Kharkovsk. Mat. Obshch.*, 1889, vol. 1, no. 2, pp. 250–276 (in Russian).

[2] Pontryagin L. S., Boltyanskii V. G., Gamkrelidze R. V., Mishchenko E. F., *The mathematical theory of optimal processes*, Wiley Interscience, 1962.

Dynamics of the gyroscope in R^n

B. Gajić[1], V. Dragović[1,2], B. Jovanović[2]

[1] *Mathematical Institute, Serbian Academy of Sciences and Arts, Belgrade, Serbia*
[2] *Department of Mathematical Sciences, The University of Texas at Dallas, USA*

Starting from the multidimensional integrable generalizations of the Euler top, the Lagrange top, the Lagrange bitop, and the totally symmetric case, we add to each of them a gyroscope. We provide a matrix Lax representation and we prove Liouville integrability for each of obtained systems.

References

[1] Dragović V., Gajić B., and Jovanović B., Heavy rigid body with a gyroscope in R^n, *Contemporary Mathematics,* 2026, to appear, arXiv:2601.03965 [math-ph]

Influence of an attached vortex on the motion of a solid body in a fluid

A. M. Gavrilova, E. V. Vetchanin

Ural Mathematical Center, Udmurt State University, Izhevsk, Russia

The problem of motion of a rigid body in an ideal incompressible fluid with an attached vortex, whose position relative to the profile is considered fixed, is investigated. Two approaches can be used to describe the vortex: the point vortex model [1, 2] and the massive vortex model [3], which allows one to account for the influence of pressure forces on the vortex itself. The latter is important if the vortex is generated by some mechanism immersed in the fluid.

To construct a model of the joint motion of a circular profile and a massive vortex, we consider the plane-parallel motion of two circular cylinders with radii R_1, R_2 in an ideal incompressible fluid (see Fig. 1).

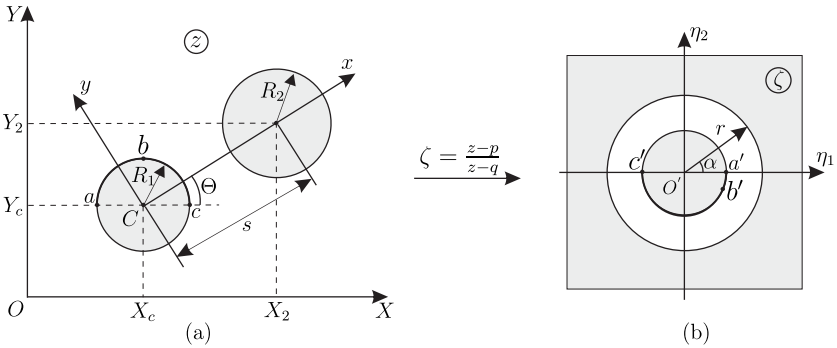


Figure 1. Schematic diagram of the system

Let us introduce the conformal mapping

$$\zeta = \frac{z-p}{z-q},$$

where $p,\ q$ — are mapping parameters related to the geometry of the cylinders. This mapping transforms the exterior of the two cylinders in the z-plane into an annular region with radii $r_1 = \dfrac{p}{R_1}$, $r_2 = \dfrac{s-p}{R_2}$ in the ζ-plane.

The fluid is assumed to undergo irrotational motion and to be at rest at infinity. Then the complex potential describing the flow has the form

$$W(\zeta) = W_{\text{motion}} + \frac{\Gamma_1}{2\pi i}\ln\zeta + \frac{\Gamma_1+\Gamma_2}{2\pi i}\sum_{k=-\infty}^{\infty}\ln\left(\frac{\zeta-\zeta_v^{2k}}{\zeta-r_2^2\zeta_v^{2k}}\right),\ \zeta_v = \frac{r_2}{r_1},$$

where $W_{\text{motion}} = W^x u_x + W^y u_y + W^\Theta\omega + W^s\dot{s}$ – is the potential describing the flow induced by the motion of the cylinders.

$$W^x = (p-q)\sum_{k=1}^{\infty}\frac{(1-r_1^{2k})\zeta^k - r_1^{2k}(r_2^{2k}-1)\zeta^{-k}}{r_2^{2k}-r_1^{2k}},$$

$$W^y = i(p-q)\sum_{k=1}^{\infty}\frac{(1+r_1^{2k})\zeta^k - r_1^{2k}(1+r_2^{2k})\zeta^{-k}}{r_2^{2k}-r_1^{2k}},$$

$$W^\Theta = i(p-q)\frac{p-qr_2^2}{1-r_2^2}\sum_{k=1}^{\infty}\frac{\zeta^k - r_1^{2k}\zeta^{-k}}{r_2^{2k}-r_1^{2k}},\ W^s = (p-q)\sum_{k=1}^{\infty}\frac{\zeta^k - r_1^{2k}\zeta^{-k}}{r_2^{2k}-r_1^{2k}}.$$

Here Γ_1, Γ_2 — are the intrinsic circulations of the cylinders; u_x, u_y — are the projections of the translational velocity onto the moving axes; ω — is the angular velocity; $\dot{s}$ — is the rate of change of the distance between the cylinders.

To transition to the problem with a massive vortex, it is necessary to let the radius of one of the cylinders tend to zero, for example, $R_2 \to 0$, while keeping the mass of the second cylinder constant.

The work was carried out within the framework of the state assignment of the Ministry of Science and Higher Education of Russia (FEWS-2024-0007).

References

[1] Kilin A. A., Gavrilova A. M., Artemova E. M., Dynamics of an Elliptic Foil with an Attached Vortex in an Ideal Fluid: The Integrable Case, *Regular and Chaotic Dynamics*, 2025, vol. 30, no. 6, pp. 931–951.

[2] Kilin A. A., Artemova E. M., Gavrilova A. M., Strange repeller in the dynamics of an elliptical foil with an attached vortex in an ideal fluid, *Computer Research and Modeling*, 2025, vol. 17, no. 6, pp. 1051–1067.

[3] Borisov A. V., Mamaev I. S., Ramodanov S. M., Dynamics of Two Interacting Circular Cylinders in Perfect Fluid, *Discrete and Continuous Dynamical Systems — Series A*, 2007, vol. 19, no. 2, pp. 235-253

On discrete Lorenz-like attractors in three-dimensional cubic maps with axial symmetry

A. S. Gonchenko

Lobachevsky State University of Nizhny Novgorod, Nizhny Novgorod, Russia

In the paper [1] we proposed a new class of three-dimensional maps of the form

$$\bar{x} = y, \;\; \bar{y} = \nu_1 x + \nu_2 y + F_1(y,z), \;\; \bar{z} = \nu_3 z + F_2(y), \qquad (1)$$

that are axial symmetric and have the constant Jacobian J. Here ν_1, ν_2, ν_3 are parameters, $J = -\nu_1\nu_3$, and sufficiently smooth functions F_1 and F_2 are such that $F_1(-y,z) \equiv -F_1(y,z)$, $F_2(-y) = F_2(y)$, which guarantees that the map is axial symmetric, i.e. invariant under the change $x \to -x, y \to -y, z \to z$. Note that these maps consist a new class of maps with constant Jacobian that is additional to the well-known class of three-dimensional Hénon maps (the linearization of (1) is not the Frobenious matrix as for the Hénon maps).

The case of such quadratic maps, i.e. the maps of the form

$$T_\pm : \; \bar{x} = y, \; \bar{y} = \nu_1 x + \nu_2 y + yz, \;\; \bar{z} = M + \nu_3 z \pm y^2,$$

was considered in our papers [1,2], in which it was shown that such maps can have discrete Lorenz attractors, including those of new types in which one-dimensional unstable separatrices of a saddle fixed point are twisted. We also demonstrated typical scenarios that start with a stable fixed point and lead to the appearance of discrete Lorenz attractors of various types, including pseudohyperbolic ones.

In this paper we continue these studies to the cubic maps of the form

$$\hat{T}_\pm : \; \bar{x} = y, \; \bar{y} = \nu_1 x + \nu_2 y + yz + Ay^3 + Byz^2, \;\; \bar{z} = M + \nu_3 z \pm y^2,$$

We study the dynamics and bifurcations in these maps. For various fixed values of ν_3, we construct bifurcation diagrams in the (ν_1, ν_2)-parameter plane, identifying regions that correspond to different types of discrete Lorenz attractors. We propose a classification of such attractors, including new types, such as semi-orientable attractors.

The work is supported by the RSciF, grant 24-11-00339.

References

[1] Gonchenko S. V., Gonchenko A, S., On discrete Lorenz-like attractors in three-dimensional maps with axial symmetry, *Chaos*, 2023, vol. 33, no. 12, 123104.

[2] Gonchenko S. V., Gonchenko A. S., Discrete Lorenz attractors of new types in three-dimensional maps with axial symmetry, *Partial Differential Equations in Applied Mathematics*, 2024, volume 11, September 2024, 100904.

New case of conservative 1 : 4 resonance

S. V. Gonchenko

Lobachevsky State University of Nizhny Novgorod, Nizhny Novgorod, Russia

It is well known that the strong resonances, that is, the bifurcation phenomena connected with the existence of fixed (periodic) points with eigenvalues $e^{\pm 2\pi p/q}$ with $q = 1, 2, 3, 4$ (respectively, the $1:1$, $1:2$, $1:3$, and $1:4$ resonances), play a very important role in the bifurcation theory of area-preserving and reversible maps. Among them, the $1:4$ resonance (with $q = 4$) is, as a rule, the most complicated and least studied.

The problem of studying bifurcations of a fixed (periodic) point with multipliers $\pm i$ can be reduced (in certain main aspects) to the analysis of local bifurcations of two-dimensional systems with Z_4-symmetry (under rotation to $\pi/2$) [1, 2]. The conservative case, when the corresponding Z_4-system is Hamiltonian, is considered as a very particular, but extremely important topic of the 1:4 resonance. Until recently, thanks to the authority of Arnold, it seemed that everything had already been done here. Indeed, he presented in [1] the following (conservative) normal form

$$\dot{z} = i\mu z + iAz|z|^2 + iB(z^*)^3 + O(|z|^5), \tag{1}$$

for such a bifurcation, where $z = x + iy$, $z^* = x - iy$, μ and $A = 1 + \beta$ are real, $B = 1$. Accordingly, generic bifurcations for $\beta \neq 0$ (always $\beta > -1$) here are such as those illustrated in Fig. 1(a) and (b). The only degenerate case is the so-called Arnold case $\beta = 0$. In this case, it is already necessary

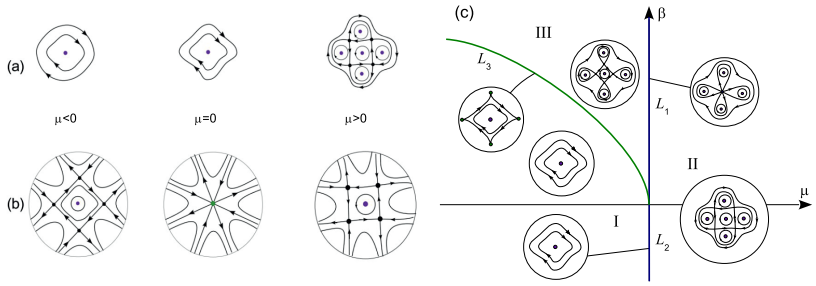


Figure 1. (a) A sketch of local bifurcations in the family (1) for (a) $\beta > 0$; (b) $\beta > 0$; (c) β varies near zero

to consider bifurcations in a two-parameter family with parameters μ and β. Main bifurcation in the corresponding conservative normal form (1) with $O(|z|^5) = iB_{32}z^3(z^*)^2 + B_{50}z^5 + B_{14}z(z^*)^4$, where B_{32} is real and $B_{14} = 5B_{50}^*$ due to conservativity ($Div \equiv 0$), were studied in [3–5]. Main elements of the corresponding bifurcation diagram are shown in Fig. 1(c).

Note that the general normal form (1) was derived under the condition $AB \neq 0$. What happens if this condition is violated? This question was "well forgotten". As we noted above, the conservative case $A \to 0$ is not specific, it fits well into the scheme of Fig. 1(b). However, the case $B = 0$ turned out to be very interesting, since it corresponds to a new degeneracy, and attention to it was stimulated from a rather unexpected side. Namely, in the papers [6, 7], generic symmetry breaking bifurcations were studied in the class of reversible two-dimensional maps. In particular, symmetric elliptic periodic points with multipliers $e^{\pm i2\pi p/q}$ (resonance $p : q$) were shown there to undergo bifurcations, at which symmetric pairs of dissipative periodic points are born, such as a sink and a source. Such local bifurcations, along with certain global bifurcations, have proven to be key for the theory of mixed dynamics [7, 8].

Undoubtedly, the case of $1 : 4$ resonance is of distinct interest. The reversible normal form in this case is as follows

$$\dot{z} = i\mu z + i\varepsilon(z^*)^3 + iz^2z^*(1 + B_{32}|z|^2) + iB_{14}z(z^*)^4 + iB_{50}z^5, \qquad (2)$$

Some examples of bifurcation diagrams are shown in Fig. 2.

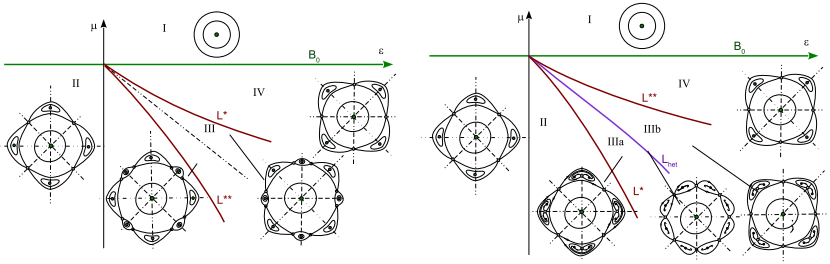


Figure 2. (a) A sketch of local bifurcations in normal form (2) for the cases (a) $B_{50}(B_{14} - B_{50}) > 0$ that includes the conservative case $B_{14} = 5B_{50}$; and (b) $B_{50}(B_{14} - B_{50}) < 0$

The work is supported by the Russian Science Foundation grant 24-11-00339.

References

[1] V. I. Arnold, Geometrical Methods in the Theory of Ordinary Differential Equations // Moscow: Nauka, 1978 (in Russian) [English transl., Springer, 1988].

[2] V. Arnold, V. Afraimovich, Y. Il'yashenko, and L. Shil'nikov, Bifurcation theory // in Encyclopedia of Mathematical Sciences (Springer, Moscow, 1986), Vol. 5.

[3] Biragov V. S., Bifurcations in a two-parameter family of conservative mappings that are close to the Hénon mapping, *Methods in Qualitative and Bifurcation Theory*, Gorky State Univ., 1987, pp. 10-24.

[4] Biragov V. S., Shilnikov L. P., On the bifurcation of a saddle-focus separatrix loop in a three-dimensional conservative dynamical system, *Methods in Qualitative and Bifurcation Theory*, Gorky State Univ., 1989, pp. 25-34.

[5] Simo C., Vieiro A., Resonant zones, inner and outer splitting in generic and low order resonances of area preserving maps, *Nonlinearity*, 2009, vol. 22, no. 5, pp. 1191-1245.

[6] Gonchenko S. V., Lamb J. S. W., Rios I., Turaev D., Attractors and repellers near generic elliptic points of reversible maps, *Dokl. Math.*, 2014, vol. 89, no. 1, pp. 65-67.

[7] Gonchenko S. V., Turaev D. V., On three types of dynamics and the notion of attractor, *Proc. Steklov Inst. Math.*, 2017, vol. 297, pp. 116-137.

[8] Gonchenko S., Reversible Mixed Dynamics: A Concept and Examples, *Discontinuity, Nonlinearity, and Complexity*, 2016, vol. 5, no. 4, pp. 365-374.

Integrability and bifurcation analysis of the problem of a spherical top rolling on a plane without spinning and with partial slipping

T. B. Ivanova, A. A. Kilin

Ural Mathematical Center, Udmurt State University, Izhevsk, Russia

The paper investigates the problem of rolling of a ball with an axisymmetric mass distribution on a horizontal plane. It is assumed that the ball does not slip during rolling in the direction of the projection of the axis of symmetry onto the supporting plane and, in addition, that there is no spinning about the vertical.

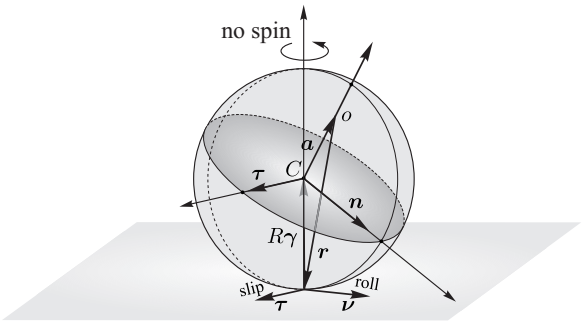


Figure 1. An unbalanced axisymmetric ball on a plane

For the system under consideration, the integrals of motion are found, a reduction to a system with one degree of freedom is performed, and the equations of motion of the reduced system are written in Hamiltonian form. In this paper, a classification of the possible types of motion is performed depending on the values of the first integrals of motion and the mass-geometric parameters, and the singularities of the system and the dynamical effects observed near them are described. The particular case of a balanced ball is considered separately, for which the bifurcation diagram in the space of the first integrals is fairly simple and illustrative, while at the same time its features associated with the degeneracy of the system of nonholonomic constraints are preserved.

The work was carried out within the framework of the state assignment of the Ministry of Science and Higher Education of Russia (FEWS-2025-0004).

Low-energy capture trajectories near the libration points

A. V. Ivanyukhin[1,2]

[1] *Research Institute of Applied Mechanics and Electrodynamics of Moscow Aviation institute, Moscow, Russia*
[2] *RUDN University, Moscow, Russia*

One approach to improving the efficiency of interplanetary transfers is the use of low-energy trajectories with a small change in energy during a transfer (transit) from one massive body to another near the libration points L_1 and L_2. Ballistic capture trajectories and free-return trajectories (periodic transit trajectories) in lunar mission design began to be studied at the dawn of the space age in [1,2]. Since low-energy transfers imply minimal changes in the energy constant along the trajectory between two massive bodies, it is reasonable to include flybys of the libration points in the transfer trajectory [3]. Estimates of orbital parameters allowing ballistic capture and long-term spacecraft residence near the smaller massive body in the restricted three-body problem have been made by many authors, in particular in [4–7].

This paper considers an approach to designing transit trajectories of temporary capture based on an analysis of the conditions for flyby of the libration points L_1 and L_2. The influence of the parameters of the libration point flyby conditions on the parameters of the transit trajectory and the duration of ballistic capture is studied. The dependence of the pericenter altitude at the first approach of the capture orbit to the smaller body and the capture duration on the magnitude and direction of the flyby velocity at the libration point is constructed. The motion along transit trajectories and the estimation of their characteristics are carried out within the framework of the circular and elliptic restricted three-body problems.

Transit trajectories of this type make it possible to obtain long-term capture orbits, low-energy departure trajectories for interplanetary missions (with a pericenter velocity lower than the parabolic one), and low-energy gravity assists (with a nearly zero hyperbolic excess velocity at the moment of entering the sphere of influence). Such trajectories can significantly reduce the total characteristic velocity costs in the design of interplanetary missions.

Examples of trajectories promising for practical use in interplanetary missions are considered in the Earth–Moon system and in the Jupiter and Saturn systems. Estimates indicate the possibility of a significant reduction in the total velocity increment for the transfer.

The study was supported by the Russian Science Foundation grant No 25-79-30009, https://rscf.ru/project/25-79-30009/.

References

[1] Egorov V. A., On the problem of capture in the restricted circular three-body problem, *Artificial Earth Satellites*, 1959, no. 3, pp. 3–12 (in Russian).

[2] Arenstorf R. F., Existence of periodic solutions passing near both masses of the restricted three-body problem, *AIAA J.*, 1963, vol. 1, no. 1, pp. 238–240.

[3] Conley C. C., Low energy transit orbits in the restricted three-body problems, *SIAM J. Appl. Math.*, 1968, vol. 16, no. 4, pp. 732–746.

[4] Belbruno E. A., Miller J. K., Sun-perturbed Earth-to-Moon transfers with ballistic capture, *J. Guidance, Control and Dyn.*, 1993, vol. 16, no. 4, pp. 770–775.

[5] Villac B. F., Scheeres D. J., On the concept of periapsis in Hill's problem, *Celest. Mech. and Dyn. Astron.*, 2004, vol. 90, pp. 165–178. DOI: https://doi.org/10.1007/s10569-004-0405-9.

[6] Topputo F., Vasile M., Bernelli-Zazzera F., Earth-to-Moon low energy transfers targeting L_1 hyperbolic transit orbits, *Ann. New York Acad. Sci.*, 2005, vol. 1065, no. 1, pp. 55–76.

[7] Ivanyukhin A. V., Low-energy transit trajectories near libration points, *Solar System Research*, 2025, vol. 59, no. 7, p. 75.

C^0 and C^1 gluing of integrable systems

B. Jovanović[1], V. Dragović[1,2], and B. Gajić[1]

[1] *Mathematical Institute, Serbian Academy of Sciences and Arts, Belgrade, Serbia*
[2] *Department of Mathematical Sciences, The University of Texas at Dallas, USA*

This work is motivated by bungee jumping. We construct classical mechanical models with almost everywhere C^∞-Hamiltonian functions that are of the class C^1 and C^0 on a given hypersurface Δ. We first model bungee jumping in $\mathbf{R}^2\{x_1, x_2\}$, as a modification of the elastic pendulum. It is a Hamiltonian system on $T^*\mathbf{R}^2$ with the Hamiltonian

$$H_1(x,p) = \frac{1}{2}(p_1^2+p_2^2)+V^*(x), \qquad V^*(x) = gx_2+\frac{1}{2}\sigma(|x|-\ell)^2\theta(|x|-\ell).$$

Here θ is the Heaviside step function, and $\sigma, g > 0$ are real parameters, the coefficient of elasticity of the spring and the gravitational constant, respectively. Thus, within the disk

$$D = \{x = (x_1, x_2) \in \mathbf{R}^2 \mid \langle x, x\rangle = x_1^2 + x_2^2 \le \ell^2\},$$

centered at the origin $O(0,0)$ and of radius ℓ, the system describes the motion of a particle of the unit mass in a homogeneous gravitational field. Outside the disk D, the motion is under the influence of an additional elastic spring.

The Hamiltonian function H_1 is C^1-smooth on $T^*\mathbf{R}^2$ and C^∞-smooth outside the hypersurface

$$\Delta = T^*_{\partial D}\mathbf{R}^2 = \{(x,p) \mid \langle x, x\rangle = x_1^2 + x_2^2 = \ell^2\}.$$

The Hamiltonian vector field is Lipschitz continuous implying the uniqueness of the solutions $(x(t), p(t))$ of the Hamiltonian system, determined by the initial data.

For the second model, we consider C^0-modification, defined by the Hamiltonian

$$H_2(x,p) = \frac{1}{2}\langle p, p\rangle + V(x), \qquad V(x) = gx_2 + \frac{1}{2}\rho(|x|^2 - \ell^2)\theta(|x| - \ell).$$

Now, the Hamiltonian vector field is not Lipschitz continuous on Δ. We can see the modified system as a C^0-gluing along Δ of two super-integrable systems: the motion in a homogeneous gravitational field in $\mathbf{R}^2$ with non-compact invariant manifolds and the motion under the influence of the Hook potential centered at $C(0, -g/\rho)$ with compact invariant manifolds.

There is a natural identification of cotangent and tangent bundles with respect to the Euclidean metric. It gives a decomposition of Δ on a part tangent to the circle ∂D, a part with outgoing velocities Δ_+, and a part with ingoing velocities Δ_-. Both flows are transversal to $\Delta_+ \cup \Delta_-$, where the dynamics can be naturally defined. However, there exists a singular set $\Xi \subset \Delta_0$, where the dynamics is not defined.

The trajectories that intersects $\Delta_+ \cup \Delta_-$ define return maps that we explicitly derive in a closed algebraic form for the value of the energy $H = h < -\rho\ell^2$.

In the limit $g = 0$, the resulting systems provide prototype examples of the Liouville–Arnol'd theorem for C^1 and C^0 Hamiltonians.

References

[1] Dragović, V., Gajić, B., Jovanović, B., From bungee to C^1 and C^0 Hamiltonian systems and their integrability and nonintegrability, arXiv:2606.00870 [math.DS].

Specifics of using non-holonomic mechanics models in the design and control of mobile robots

Yu. L. Karavaev

Kalaschnikov Izhevsk State Technical University, Izhevsk, Russia

This report examines problems in nonholonomic mechanics–specifically those involving rolling without slipping–and their application to the design and control of various robotic systems. It discusses the conditions under which nonholonomic models are applicable to real-world experiments, drawing on examples such as spherical robots [1–5], highly maneuverable robots equipped with omnidirectional (roller-based) wheels [6,7], and wheeled robots with passive trailers [8,9]. Additionally, the report explores novel designs for robots capable of moving through a fluid medium [10–13]. The presentation synthesizes recent research findings from the Laboratory for Nonlinear Analysis and Design of New Locomotion Systems at Udmurt State University and the Mobile Systems Laboratory at the M.T. Kalashnikov Izhevsk State Technical University.

The research was carried out within the framework of Russian Science Foundation grant No. 25–11–00305.

References

[1] Karavaev Y. L., Kilin A. A., Klekovkin A. V., The dynamical model of the rolling friction of spherical bodies on a plane without slipping, *Russian Journal of Nonlinear Dynamics,* 2017, vol. 13, no. 4, pp. 599–609

[2] Kilin A. A., Karavaev Y. L., Experimental research of dynamic of spherical robot of combined type, *Russian Journal of Nonlinear Dynamics,* 2015, vol. 11, no. 4, pp. 721–734

[3] Karavaev, Yu. L. Spherical Robots: An Up-to-Date Overview of Designs and Features, *Russian Journal of Nonlinear Dynamics,* 2022, vol. 18, no. 4, pp. 709-750.

[4] Ivanova T. B., Karavaev Y. L., Kilin A. A., Control of a pendulum-actuated spherical robot on a horizontal plane with rolling resistance, *Archive of Applied Mechanics,* 2022, pp. 1-14

[5] Klekovkin A. V., Karavaev Y. L., Nazarov A. V., Stabilization of a Spherical Robot with an Internal Pendulum During Motion on an Oscillating Base, *Russian Journal of Nonlinear Dynamics*, 2024, vol. 20, no. 5, pp. 845-858

[6] Kilin A. A., Karavaev Y. L., Shestakov V. A., Motion of a Four-Wheeled Omnidirectional Mobile Robot without Slipping and Detachment from the Surface, *Mekhatronika, Avtomatizatsiya, Upravlenie*, 2023, vol. 24, no. 8, pp. 403-411

[7] Mamaev I. S., Kilin A. A., Karavaev Y. L., Shestakov V. A., Criteria of Motion Without Slipping for an Omnidirectional Mobile Robot, *Russian Journal of Nonlinear Dynamics*, 2021, vol. 17, no. 4, pp. 527-546

[8] Ardentov A. A., Karavaev Y. L., Yefremov K. S., Euler Elasticas for Optimal Control of the Motion of Mobile Wheeled Robots: the Problem of Experimental Realization, *Regular and Chaotic Dynamics,* 2019, vol. 24, no. 3, pp. 312-328

[9] Kilin A. A., Ivanova T. B., Karavaev Y. L., Yefremov K. S., Theoretical and experimental investigations of the controlled motion of a roller racer, *Theoretical and Applied Mechanics*, 2025, vol. 52, no. 1, pp. 39-65

[10] Karavaev Y. L., Klekovkin A. V., Mamaev I. S., Tenenev V. A., Vetchanin E. V., A Simple Physical Model for Control of an Propellerless Aquatic Robot, *Journal of Mechanisms and Robotics,* 2022, vol. 14, no. 1, 011007, 11 pp.

[11] Karavaev Y. L., Kilin A. A., Klekovkin A. V., Experimental Investigations of the Controlled Motion of a Screwless Underwater Robot, *Regular and Chaotic Dynamics,* 2016, vol. 21, no. 7-8, pp. 918-926

[12] Vetchanin E. V., Karavaev Y. L., Kalinkin A. A., Klekovkin A. V., Pivovarova E. N., A model of a screwless underwater robot, *Bulletin of Udmurt University. Mathematics. Mechanics. Computer Science,* 2015, vol. 25, no. 4, pp. 544-553

[13] Klekovkin A. V., Chernova A. A., Karavaev Y. L., Nazarov A. V., Investigation of the motion of an aquatic robot with an internal fast-speed rotor and a non-deformable tail fin , *Bulletin of Udmurt University. Mathematics. Mechanics. Computer Science*, 2025, vol. 35, no. 4, pp. 619-642

Invariant tori and the Smale–Williams attractor in a perturbed integrable Hamiltonian system with a saddle-focus skirt

A. O. Kazakov[1], N. E. Kulagin[2], L. M. Lerman[1], and K. S. Zaichikov[1]

[1] *HSE University, Nizhny Novgorod, Russia*
[2] *A. N. Frumkin Institute of Physical Chemistry and Electrochemistry, Russian Academy of Sciences, Moscow, Russia*

We consider a smooth (analytic) Hamiltonian system on a four-dimensional symplectic manifold with Hamiltonian H, which is completely integrable in the Liouville sense. It is assumed that the system possesses an equilibrium point of saddle-focus type. The linearization at this point has a quadruple of complex eigenvalues, and the equilibrium is hyperbolic. It possesses two local invariant manifolds, stable and unstable, which belong to a critical joint level of the two first integrals. We additionally assume the existence of a homoclinic trajectory Γ asymptotic to the saddle-focus equilibrium. The homoclinic trajectory generates a family of homoclinic orbits. The union of these orbits forms a homoclinic "skirt" of the equilibrium. The main goal of the work is to investigate the dynamics of a dissipatively perturbed system in a neighborhood of this homoclinic skirt.

In local coordinates, the unperturbed system can be integrated explicitly due to the existence of two first integrals [1]. To investigate the perturbed dynamics, we construct a three-dimensional Poincaré map as a composition of local and global maps $P_\varepsilon = S \circ T$. Numerical experiments show that the resulting dynamics strongly depends on both the structure of the global return and the perturbation parameter ε.

For one of the considered maps, at small values of ε a stable invariant curve is observed. The largest Lyapunov exponent is approximately zero. With further variation of ε, the invariant curve undergoes a resonance, and the attractor becomes a period-five orbit. This periodic orbit subsequently undergoes a cascade of period-doubling bifurcations. As a result, a chaotic attractor consisting of five components is formed. With a further increase of the perturbation parameter, these components grow and merge into a single chaotic attractor.

For another variant of the global map, at small values of the perturbation parameter, the observed scenarios are similar to those described above. However, with increasing ε, stable periodic orbits disappear and a hyperbolic Smale–Williams attractor emerges. The hyperbolicity of the obtained

attractors is investigated numerically by studying the mutual orientation of the invariant subspaces. For the hyperbolic regimes, the largest Lyapunov exponent is positive, whereas the other two Lyapunov exponents are negative. This behavior is consistent with the presence of one expanding and two contracting directions in the three-dimensional Poincaré map.

For another considered global map, an attractor qualitatively similar to the previous one is obtained, but with a larger number of rotations. Thus, the structure of the global homoclinic return plays an important role in determining the bifurcation scenarios and the geometry of the resulting attractors.

This work was supported by the project HSE-BR-2025-79 implemented as part of the Basic Research Program at HSE University.

References

[1] Moser J., On the generalization of a theorem of A. Liapounoff, *Commun. Pure Appl. Math.*, 1958, vol. 11, no. 2, pp. 257–271.

Study of pendulum-type motions in an approximate problem of the dynamics of a rigid body with a vibrating suspension

O. V. Kholostova, M. V. Belichenko

Moscow Aviation Institute (National Research University), Moscow, Russia

The motion of a heavy rigid body with suspension point performing high-frequency periodic vibrations of small amplitude is considered. The study is carried out within the framework of an approximate autonomous system written in the form of the modified Euler–Poisson equations [1], to the right-hand sides of which the components of the vibration moment are added. The question of the existence of pendulum-type motions of the body is resolved. The search for pendulum-type motions is restricted to the case when the axis of these motions is one of the principal inertia axes of the body, as in the case of the Mlodzeevsky's pendulum-type motions of a heavy rigid body with a fixed point [2]. It is shown [3] that pendulum-type motions of the body exist for a wider range of laws of vibration of the suspension point. A number of properties of the vibration moment are proven. In particular, it is shown that arbitrary planar vibrations and a wide range of spatial vibrations are reduced to two basic variants of vibrations occurring along a straight line and along an ellipse. In the vibration problem (ignoring gravity), for both basic variants there are two types of pendulum-type motions around the principal axis of inertia. The first type is similar to Mlodzeevsky's pendulum-type motions for a heavy rigid body with a fixed point. For them, the body's mass center lies in the principal plane of inertia, and the axis of the pendulum-type motions is perpendicular to this plane. The second type is pendulum-type motions around the principal axis of inertia containing the center of mass of the body; it is specific to the vibration problem. Superposition of a gravitational field and a vibration field (with different locations of the straight line or the ellipse relative to the vertical) is performed. Pendulum-type motions are sought as the "sum" of two pendulum-type motions or pendulum-type motions and permanent rotations that exist in the gravitational problem (without vibration) and in that of vibration (without gravity), for the same axis in both problems. A graphical interpretation is given for the considered examples of the interaction of the gravitational and vibration fields and both basic variants of vibrations of the body's suspension point.

This research was supported by the grant of the Russian Science Foundation, No. 24-11- 00162 (https://rscf.ru/project/24-11-00162/) and was carried out at the Moscow Aviation Institute (National Research University).

References

[1] Markeyev, A.P., The Equations of the Approximate Theory of the Motion of a Rigid Body with a Vibrating Suspension Point, *J. Appl. Math. Mech.*, 2011, vol. 75, no. 2, pp. 132–139; see also: *Prikl. Mat. Mekh.*, 2011, vol. 75, no. 2, pp. 193–203.

[2] Mlodzeevsky, B., Über permanente Axen bei der Bewegung eines schweren festen Körpers um einen Punkt, *Tr. Otdel. Fiz. Nauk Ob-va Lubit. Estestvozn.*, 1894, vol. 7, no. 1, pp. 46–48 (Russian).

[3] Belichenko M.V., Kholostova O.V., On Pendulum-Type Motions and Permanent Rotations in an Approximate Problem of the Dynamics of a Rigid Body with a Vibrating Suspension, *Regul. Chaotic Dyn.*, 2025, vol. 30, no. 5, pp. 847–865.

Rolling of a system of coupled axisymmetric bodies on a plane

A. A. Kilin

Ural Mathematical Center, Udmurt State University, Izhevsk, Russia

The paper investigates the problem of rolling without slipping of a system of coupled rigid bodies on a plane. The system of coupled bodies consists of a heavy rigid body (a shell), inside which N axes are fixed. Dynamically symmetric bodies (rotors) rotate freely about these axes. The axes of symmetry of the rotors coincide with the axes about which they rotate. Thus, the mass distribution of the system does not change when the rotors rotate. A schematic representation of the system under consideration is shown in Fig. 1.

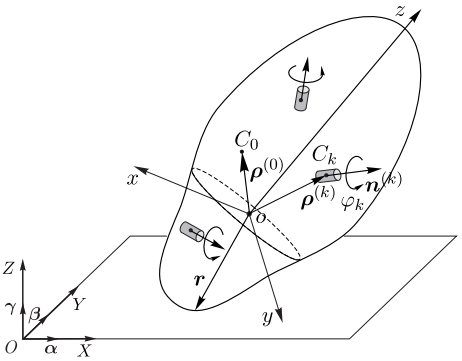


Figure 1. Schematic representation of a body with N rotors

The paper obtains the equations of motion and proves that, after reduction to the level set of one of the first integrals, the resulting system reduces to the equations of motion of a rigid body with a gyrostat rolling on a plane without slipping [1].

Рассмотрен частный случай качения по плоскости произвольного тела вращения, внутри которого A particular case is examined: the rolling of an arbitrary body of revolution on a plane, with another body of revolution rotating freely inside it. It is shown that the system is integrable. In the case of a weightless shell, this system reduces to the problem of the rolling of an axisymmetric body with partial slipping (the “omnisphere”) [2].

The work was carried out within the framework of the state assignment of the Ministry of Science and Higher Education of Russia (FEWS-2025-0004).

References

[1] Borisov, A. V. and Mamaev, I. S., The rolling motion of a rigid body on a plane and a sphere. Hierarchy of dynamics, *Regular and Chaotic Dynamics*, 2002, vol. 7, no. 2, pp. 177–200.

[2] Kilin, A. A. and Ivanova, T. B., The Integrable Problem of the Rolling Motion of a Dynamically Symmetric Spherical Top with One Nonholonomic Constraint, *Russian Journal of Nonlinear Dynamics*, 2023, vol. 19, no. 1, pp. 3–17.

Dynamics and control of a spherical robot with a pendulum platform on a cylindrical joint

A. A. Kilin, E. M. Artemova, and D. A. Solodyankin

Ural Mathematical Center Udmurt State University, Izhevsk, Russia

A model is developed for the rolling motion of a spherical shell of radius R with an internal pendulum platform, connected to the shell by a cylindrical joint whose axis passes through the center of the sphere. The platform is attached at a fixed angle χ and can generate a controlling force $\boldsymbol{F}$ (magnitude f, application angle χ) and a controlling moment $\boldsymbol{K}$ applied to the joint. A system of equations describing the dynamics of the model is derived.

The analysis shows that, in the absence of control, the system admits two families of permanent (rigid-body) rotations — with the platform tilted relative to the vertical and with the load in the bottom vertical position (rotation in place) — and one family of non-rigid rotations, in which the contact point of the shell with the plane moves along a circle.

It is shown that the system of equations admits at least two invariant manifolds corresponding to rectilinear rolling: in the first case the platform executes planar-parallel motion in a vertical plane, and in the second case the motion occurs in a plane containing the joint axis. Based on the analysis of the first invariant manifold, control strategies are proposed that correspond to simplest actuation and to feedback control. In the first case a controlling moment is chosen that ensures minimal oscillations of the system near the initial point. In the second case a moment proportional to the components of the angular velocity of the platform is proposed, which asymptotically keeps the robot on the invariant manifold. Numerical simulations are performed: phase portraits with separatrices are constructed, initial-condition maps are obtained, and the relaxation time is analyzed as a function of the feedback gain.

The work was carried out within the framework of the Russian Ministry of Education and Science State Assignment (FEWS-2025-0004).

Accounting for surface irregularities in the control of a highly maneuverable mobile robot

A. A. Kilin[1], Yu. L. Karavaev[2], V. A. Shestakov[2]

[1] *Udmurt State University, Izhevsk, Russia*
[2] *Kalashnikov Izhevsk State Technical University, Izhevsk, Russia*

Highly maneuverable mobile robots require contact between all wheel rollers and the supporting surface to ensure omnidirectional motion. The capability for omnidirectional motion require special control for such robots [1–4]. The most popular mobile robots have a design with three and four omnidirectional wheels. Three-wheeled platforms always maintain surface contact due to their geometry. In contrast, robots with four or more wheels are statically indeterminate and require a suspension mechanisms to to allow wheels to adapt to the surface profile [5, 6].

Design solutions alone are insufficient to avoid trajectory errors on uneven surfaces. Investigations into the motion three-wheeled robot demonstrate the importance of accounting for the surface profile in control [7, 8]. However, these results are limited to three-wheel configurations, and the problem remains unaddressed for robots mobile robots with a large number of wheels equipped with suspension mechanisms.

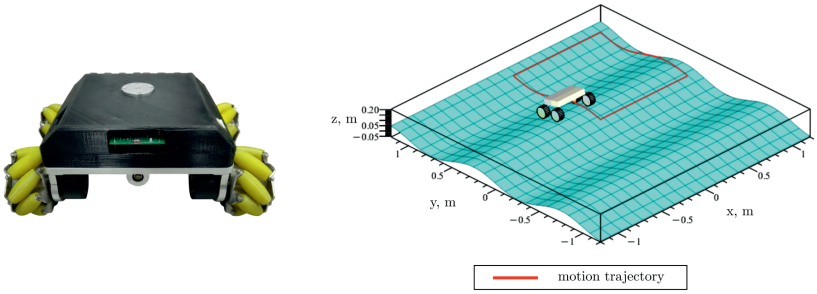
This work presents the kinematic model and control problem for a highly maneuverable mobile robot with omnidirectional wheels (mecanum or omni wheels) on an uneven surface. The robot platform consists of subplatform connected by a single degree of freedom hinge. The rotation of subplatform ensures continuous contact of all wheels with the supporting surface. Similar to the approach in [1], the omnidirectional wheel model is represented as a thin disk. The rotation of the wheel rollers will be neglected. The mobile robot prototype and the schematic representation of the robot on an uneven surface is shown in Fig. 1.

The robot's configuration on the uneven surface depends on geometric constraints, while during motion on the supporting surface the velocity constraints are imposed on the contact point of each wheel.

Taking into account this constraints, two formulations of the control problem are considered:

1. The inverse problem: determining the control that realizes the robot's motion along a specified trajectory.

2. The forward problem: determining the motion trajectory of the mobile robot for the specified control.



a) b)

Figure 1. The mobile robot prototype (a) and schematic representation of its position on an uneven surface (b)

The control algorithm for motion along a specified trajectory on the uneven surface is proposed. This algorithm can be applied to various robot designs, provided that the system of geometric constraints is solvable. Solution of the forward control problem also is considered. With in simulation, robot's motion on the specified surface along a square path is considered. The simulation results for the robot motion on the uneven surface confirm effectiveness of proposed control algorithm compared to the control obtained using the model of motion on the flat surface.

The work of Yu. L. Karavaev and V. A. Shestakov was supported by the Russian Science Foundation under grant 25-11-00305. The work of A. A. Kilin was carried out within the framework of the state assignment of the Ministry of Science and Higher Education of Russia FEWS-2026-0001.

References

[1] Borisov A. V., Kilin A. A., Mamaev I. S., Dynamics and Control of an Omniwheel Vehicle. *Regular and Chaotic Dynamics*, 2015, vol. 20, no. 2, pp. 153-172.

[2] Kilin A. A., Bobykin A. D., Control of a Vehicle with Omniwheels on a Plane, *Rus. J. Nonlin. Dyn.*, 2014, Vol. 10, no. 4, pp. 473-481.

[3] Moiseev G. N., Zobova A. A. Dynamics-Based Piecewise Constant Control of an Omnivehicle. *Rus. J. Nonlin. Dyn*, 2022, vol. 18, no. 4, pp. 661-680.

[4] Adamov B. I., Geometry and Kinematics of the Mecanum Wheel on a Plane and a Sphere, *Rus. J. Nonlin. Dyn.*, 2024, vol. 20, no. 1, pp. 43-78.

[5] Qian J., Zi B., Wang D., Ma Y. Zhang D. The design and development of an omni-directional mobile robot oriented to an intelligent manufacturing system. *Sensors*, 2017, vol. 17, pp. 1-15.

[6] Zhewen Z, Hongliu Y, Chengjia W, Pu H, Jiangui W. A comprehensive study on Mecanum wheel-based mobility and suspension solutions for intelligent nursing wheelchairs., *Sci Rep.*, 2024, vol.14, pp.1-14.

[7] Chakraborty, Nilanjan, Ghosal, Ashitava. Kinematics of wheeled mobile robots on uneven terrain., *Mechanism and Machine Theory*, 2004, vol.39, pp.1273-1287.

[8] Savaee, E., Rahmani Hanzaki, A. Anabestani, Y. Kinematic Analysis and Odometry-Based Navigation of an Omnidirectional Wheeled Mobile Robot on Uneven Surfaces., *J Intell Robot Syst*, 2023, vol.13, pp. 1-15.

Structure of the Lorenz attractor existence region in the Shimizu–Morioka system

V. A. Koryakin

Lobachevsky State University of Nizhny Novgorod, Nizhny Novgorod, Russia

The Shimizu–Morioka system

$$\begin{aligned} \dot{x} &= y, \\ \dot{y} &= x - \lambda y - xz, \qquad \alpha > 0, \quad \lambda > 0 \\ \dot{z} &= -\alpha z + x^2, \end{aligned} \tag{1}$$

is a simple model exhibiting Lorenz attractors and a rich variety of homoclinic bifurcations [1,2]. The structure of its Lorenz attractor existence region near the curve $l_{A=0}$ is illustrated in Fig. 1. This curve corresponds to tangencies between the strongly contracting invariant direction E^{ss} and the central-unstable plane E^{cu} along the unstable separatrices of the saddle equilibrium $O = (0, 0, 0)$. The separation of these subspaces is one of the conditions of pseudohyperbolicity, which ensures the robustness of Lorenz chaos.

Figure 1a shows the minimum angle between the invariant subspaces E^{ss} and E^{cu} in the parameter plane (α, λ). In the red regions, the largest Lyapunov exponent is positive and the angle remains bounded away from zero. In the blue regions, the largest Lyapunov exponent is also positive, but the angle is not bounded away from zero. The white regions correspond to stable periodic motion. Periodic windows cross the curve $l_{A=0}$, while narrow regions containing Lorenz attractors also appear below it.

The curves l_2, l_4, and l_8 in Fig. 1a correspond to symmetric homoclinic loops of the saddle O with two, four, and eight rounds, respectively. Their intersections with $l_{A=0}$ are the inclination-flip bifurcation points A_2, A_4, and A_8. The four-round homoclinic curve passes through A_2 and intersects $l_{A=0}$ again at A_4; the eight-round curve similarly connects successive levels of the cascade. Thus, the sequence of points $A_2, A_4, A_8, \ldots$ along the primary tangency curve is associated with successive doublings of the number of rounds of the homoclinic loops. Near these points, the arrangement of periodic windows and Lorenz attractor regions repeats on progressively smaller parameter scales.

In Fig. 1b, the yellow domains represent regions of existence of the Lorenz attractor. Near A_2, such regions lie on both sides of the primary curve $l_{A=0}$. Their boundaries include the heteroclinic curves l_2^{LA} and l_4^{LA}:

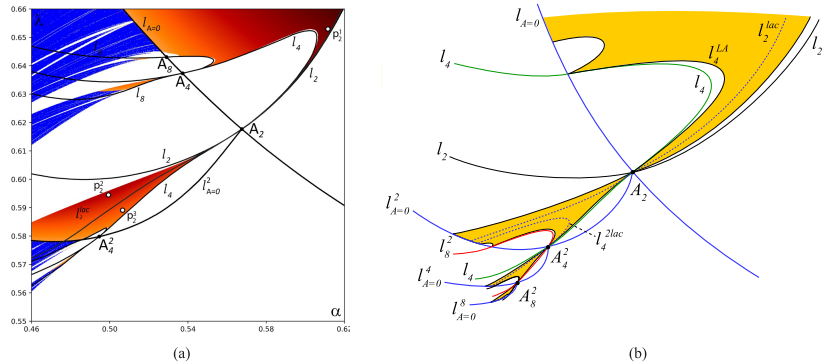


Figure 1. (a) Minimum-angle diagram for the invariant subspaces E^{ss} and E^{cu}. Red: positive largest Lyapunov exponent and angle bounded away from zero; blue: positive largest Lyapunov exponent and angle not bounded away from zero; white: stable periodic motion. (b) Schematic organization of Lorenz attractor regions (yellow) near successive tangency curves. Their intersections with homoclinic curves organize a cascade of inclination-flip bifurcations.

on these curves, the unstable separatrices of O belong to the stable manifolds of two-round and four-round saddle periodic orbits, respectively. The curve l_2^{lac} inside the yellow region marks the appearance of a lacuna, a hole surrounding a saddle periodic orbit in the attractor.

The same diagram also shows the successive tangency curves $l^2_{A=0}$, $l^4_{A=0}$, and $l^8_{A=0}$. The first of these emanates from A_2 and intersects the four-round homoclinic curve at the next inclination-flip point A_4^2. The following tangency curve emanates from A_4^2 and meets the eight-round homoclinic curve at A_8^2. This arrangement generates a second cascade, extending below the primary tangency curve. Each successive level contains further Lorenz attractor regions with a similar arrangement of bounding bifurcation curves.

Together, the two panels illustrate a hierarchical structure: one cascade follows the primary tangency curve, while the other passes through successive tangency curves. Separate Lorenz attractor regions occur below $l_{A=0}$, and their boundaries are formed by additional bifurcation curves. The repetition visible at successive levels supports the conjecture of an infinite hierarchy of such regions.

The author thanks A. Kazakov, K. Safonov, and A. L. Shilnikov for their collaboration and valuable discussions.

This work was supported by the Russian Science Foundation (grant No. 24-11-00339).

References

[1] Shilnikov A. L., On bifurcations of the Lorenz attractor in the Shimizu–Morioka model, *Physica D*, 1993, vol. 62, nos. 1–4, pp. 338–346.

[2] Shilnikov A. L., Shilnikov L. P., Turaev D. V., Normal forms and Lorenz attractors, *Int. J. Bifurcation Chaos*, 1993, vol. 3, no. 5, pp. 1123–1139.

Regular and chaotic advection induced by stationary vortex structures in a two-layer rotating fluid

K. V. Koshel[1,2], M. A. Sokolovskiy[3,4]

[1] *V. I. Il'ichev Pacific Oceanological Institute, Far Eastern Branch Russian Academy of Sciences, Vladivostok, Russia*
[2] *Institute of Applied Mathematics, Far Eastern Branch Russian Academy of Sciences, Vladivostok, Russia*
[3] *Water Problems Istitute, Russian Academy of Sciences, Moscow, Russia*
[4] *Shirshov Institute of Oceanology, Russian Academy of Sciences, Moscow, Russia*

The study of fluid particle advection in the vicinity of stationary vortex structures is a classic problem in fluid dynamics, involving the investigation of the transport of passive impurities (tracers) within a velocity field generated by vortices.

This study investigates the advection properties of fluid particles in the vicinity of stationary vortex structures in a two-layer rotating fluid. Two types of distinct stationary vortex configurations are considered:

(S1) a family of so-called M-modal structures of three vortices [1] formed from a closed trajectory (bounding a simply connected region) of a single cyclonic vortex of the upper layer and M loop-shaped trajectories ($M \geq 1$) of two vortices of different absolute values, cyclonic and anticyclonic, located in the lower layer,

(S2) a set of N-symmetric absolute choreographies [2] of a system of $2N$ vortices ($N \geq 2$) consisting of (a) a central closed quasi N-angle trajectory, common to N identical cyclonic vortices of the lower layer, and (b) N separate peripheral, also closed, trajectories of identical anticyclonic vortices of the upper layer [3, 4] under the condition of zero total intensity of the vortex system (in other words, an axisymmetric structure of N hetons [5, 6]).

References

[1] Sokolovskiy M. A., New Stationary N-Symmetric States of Three Point Vortices in a Two-Layer Rotating Fluid, *Regul. Chaot. Dyn.*, 2026, vol. 31, no. 1, pp. 116–131.

[2] Simó C., New Families of Solutions to the N-Body Problems. In *European Congress of Mathematics*. Barcelona, July 10–14, 2000, Volume I; Casacuberta C., Miró-Roig R. M., Verdera J., Xambó-Descamps S., Eds. *Progress in Mathematics*. Birkhauser Basel: Basel, Switzerland, 2001, vol. 201, pp. 101–115.

[3] Sokolovskiy M. A., Koshel K. V., Dritschel D. G., and Reinaud J. N., N-Symmetric Interaction of N Hetons. I. Analysis of the Case $N = 2$, *Phys. Fluids*, 2020, vol. 32, no. 9, 096601.

[4] Koshel K. V., Sokolovskiy M. A., Dritschel D. J., and Reinaud J. N., N-Symmetric Interaction of N Hetons. II. Analysis of the Case of Arbitrary N, *Fluids*, 2024, vol. 9, no. 6, 122.

[5] Hogg N. G. and Stommel H. M., The Heton, an Elementary Interaction Between Discrete Baroclinic Geostrophic Vortices, and its Implications Concerning Eddy Heat-Flow, *Proc. R. Soc. Lond. Math. Phys. Sci.*, 1985, vol. 397, pp. 1–20.

[6] Hogg N. G., Stommel H. M., Hetonic explosions: the breakup and spread of warm pools as explained by baroclinic point vortices, *J. Atmos. Sci*., 1982, vol. 42, no. 14, pp. 1465–1476.

Earnshaw's theorem and levitation

V. V. Kozlov

Steklov Mathematical Institute of RAS, Moscow, Russia

Various aspects of Earnshaw's theorem on the instability of equilibria of a system of interacting charges in an electrostatic field are discussed. The problem of the stability of equilibrium of a charged particle in a central electrostatic field subject to gravity is addressed. This equilibrium state is certainly unstable. However, by adding a uniform magnetic field directed along the free-fall acceleration, it can be made Lyapunov stable. This result is extended to a system consisting of several interacting charges of the same sign.

Bifurcations through a non-semisimple hyperbolic 1 : 1 resonance, with examples in rigid body dynamics

E. A. Kudryavtseva

Moscow State University, Moscow, Russia

We study an integrable Hamiltonian system with two degrees of freedom depending on a small parameter. The system is given by a Hamilton function $H^\varepsilon(q,p)$ and a first integral $F^\varepsilon(q,p)$, where $(q,p) = (q_1,q_2,p_1,p_2) \in \mathbf{R}^4$ are canonical variables and $\varepsilon \in \mathbf{R}$ is a small parameter.

Suppose that the unperturbed system has an equilibrium $x^0 = (q^0,p^0)$, at which the linearized vector field has real eigenvalues $\lambda,\lambda,-\lambda,-\lambda$ $(\lambda > 0)$ and is not diagonalizable (a Jordan block structure). Such an equilibrium is called a *non-semisimple hyperbolic* $1:1$ *resonance*.

Suppose that the system is real-analytic. We study topology of the Liouville foliation in a small saturated neighborhood of the equilibrium, and describe all possible types of bifurcations when the small parameter passes through 0, provided that the singular fiber $L^0 := \{x \in \mathbf{R}^4 \mid H^0(x) = F^0(x) = 0\}$ is compact and contains no other equilibria, where $H^0(x^0) = F^0(x^0) = 0$.

It is well known that, using linear canonical changes of variables $(q,p) \to (\widetilde{q},\widetilde{p})$ and $(H,F) \to (H,\widetilde{F} = aH+bF)$, we can transform the quadratic parts H_2^0, F_2^0 to the normal form

$$H_2^0 = \lambda\widetilde{S} + \widetilde{X}, \quad F_2^0 = \widetilde{S},$$

where

$$S = p_1q_1 + p_2q_2, \quad X = p_1q_2, \quad Y = p_2q_1, \quad Z = p_1q_1 - p_2q_2.$$

Using non-linear local canonical changes $(q,p) \to (\hat{q},\hat{p}) = (\hat{q}^\varepsilon(q,p),\hat{p}^\varepsilon(q,p))$ and $(H,F) \to (H,\hat{F} = \hat{F}^\varepsilon(H,F))$, we can transform H^ε, F^ε to a local normal form

$$H^\varepsilon = \hat{X} + \varphi^\varepsilon(\hat{Y},\hat{S}), \quad \hat{F}^\varepsilon = \hat{S},$$

in a small neighborhood of the equilibrium $x^0 = (\hat{q}^0,\hat{p}^0) = (0,0)$.

In particular, we have a 1-parameter family of equilibria $x^\varepsilon = (\hat{q}^\varepsilon,\hat{p}^\varepsilon) = (0,0)$. The eigenvalues $\pm\lambda_1^\varepsilon, \pm\lambda_2^\varepsilon$ of the linearized vector field at the equilibrium x^ε collide at $\varepsilon = 0$ (i.e., $\lambda_1^0 = \lambda_2^0$).

The following natural questions arise. What is a possible behavior of eigenvalues along this family (how do they collide at a $1:1$ resonance)? How does a local bifurcation diagram look like?

We prove the following *local properties* of *any* such singularity:

- Locally, there exist two families of commuting anti-canonical involutions $\tau^\varepsilon_\pm$ that preserve H^ε and F^ε, rendering the system reversible w.r.t. them, where $\tau^\varepsilon_\pm(\hat q_1,\hat q_2,\hat p_1,\hat p_2)=\pm(\hat p_2,\hat p_1,\hat q_2,\hat q_1)$.
- The singular fiber $L^0\ni x^0$ contains exactly four 1-dimensional local orbits $\mathcal{O}_j$ of the local Hamiltonian $\mathbf{R}^2$-action generated by H^0 and F^0 (comprizing two incoming and two outgoing separatrices of x^0). Together with the equilibrium x^0, these local orbits $\mathcal{O}_j$ $(1\le j\le 4)$ form two intersecting lines defined by $\hat p_2\hat q_1=\hat p_1=\hat q_2=0$.

We prove the following properties of such singularities, assuming that $a:=\partial^2_{\hat Y^2}\varphi^0(0,0)\ne 0$ or $\partial^3_{\varepsilon\hat Y^2}\varphi^0(0,0)\ne 0$, and that the singular fiber L^0 is compact and contains no other equilibria:

- Near the equilibrium x^0, the bifurcation is fiberwise topologically equivalent to one of 5 *local topological types* determined by 5 local normal forms (with different local bifurcation diagrams): 4 types with $a\ne 0$ (denoted by $\mathcal{KL}_{1:1}$) and one type with $a=0$ (denoted by $\mathcal{KL}^\triangle_{1:1}$).
- For each local type, we characterize the behavior of the eigenvalues $\lambda^\varepsilon_1,\lambda^\varepsilon_2$ of the linearized Hamiltonian vector field at the equilibrium x^ε, classifying them as *splitting real*, *passing real*, *crossing complex*, or *merging real* when ε passes through 0.
- Each of the 4 local $\mathcal{KL}_{1:1}$ bifurcation types correspond to *two semiglobal* bifurcation types distinguished by the topological conditions (a) $\mathcal{O}_1=\mathcal{O}_2$ or (b) $\mathcal{O}_1=\mathcal{O}_3$, whereas the local $\mathcal{KL}^\triangle_{1:1}$ type corresponds to a unique semiglobal type.
- One of 4 local $\mathcal{KL}_{1:1}$ types (and thus 2 of the 8 associated semiglobal types) yields a *locally structurally stable* bifurcation with respect to real-analytic integrable perturbations; the $\mathcal{KL}^\triangle_{1:1}$ bifurcation is *semiglobally structurally stable*.

Thus, we have exactly 9 topologically distinct *semiglobal bifurcation types*: eight of type $\mathcal{KL}_{1:1}$ and one of type $\mathcal{KL}^\triangle_{1:1}$. Three of these yield *structurally stable* bifurcations: two $\mathcal{KL}_{1:1}$ types and one $\mathcal{KL}^\triangle_{1:1}$ type. Their properties are as follows:

- If $a\ne 0$ (meaning that two semiglobal $\mathcal{KL}_{1:1}$ bifurcation types correspond to the same local type), a pair of real eigenvalues $\lambda^\varepsilon_1,\lambda^\varepsilon_2$ collides and moves into the complex plane. Consequently, the equilibrium changes from a saddle-saddle to a focus-focus type (i.e., the eigenvalues *split*, similarly to a Hamiltonian Hopf bifurcation). The local

bifurcation diagram in the (H, F, ε) space is the union of a swallowtail surface and the analytic continuation of its self-intersection line. Such a bifurcation appears, for instance, in the Clebsch case of rigid body dynamics.

- If $a = 0$ (corresponding to the $\mathcal{KL}^{\triangle}_{1:1}$ bifurcation type), the equilibrium x^{ε} remains of hyperbolic-hyperbolic type for any sufficiently small $\varepsilon \neq 0$ (i.e., the eigenvalues $\lambda^{\varepsilon}_1, \lambda^{\varepsilon}_2$ *pass* through each other along the real axis). The local bifurcation diagram in the (H, F, ε) space has the shape of a "flipping triangle". This type of bifurcation appears, for example, in the Kovalevskaya top when the parameter (area constant) passes through $g = \pm\sqrt{2}$.

To the best of our knowledge, the latter bifurcation type, $\mathcal{KL}^{\triangle}_{1:1}$ (the triangle-flipping bifurcation), has not been previously described in the literature. On one hand, it is structurally stable and is therefore preserved under any integrable perturbation of the system. On the other hand, this bifurcation does not appear in the classification of all *generic local* bifurcations [1] (where $a \neq 0$).

This apparent paradox arises because a given bifurcation can be generic in the semiglobal setting while being highly non-generic locally. By the local properties of non-semisimple hyperbolic $1:1$ bifurcations, the equilibrium x^0 has one-dimensional incoming and outgoing orbits constituting its stable and unstable separatrices, which are always permuted by locally existing momentum-preserving anti-canonical involutions. In a semiglobal setting, however, these separatrices must close into a loop in L^0 (i.e., a homoclinic orbit). Consequently, the reduced 1-degree-of-freedom system corresponding to this homoclinic orbit must possess an anti-canonical symmetry. This symmetry (reversibility) imposes a severe restriction on the local bifurcation with $a = 0$, rendering it *non-generic* among *local* bifurcations through a non-semisimple $1:1$ resonance.

The talk is based on a joint work with Lev Lerman.

The work is supported by the Russian Science Foundation (project No 24-71-10100).

References

[1] Kudryavtseva E. A., Lerman L. M., Bifurcations in Integrable Systems with Three Degrees of Freedom. I, *Proc. Steklov Inst. Math.*, 2024, vol. 327, pp. 130–207.

The Hess case in the problem of motion of a heavy body with a vertically vibrating suspension point

A. S. Kuleshov

Department of Mechanics and Mathematics, Lomonosov Moscow State University, Moscow, Russia

The problem of the motion of a rigid body in a uniform gravity field is considered. It is assumed, that one point of the rigid body (the suspension point) undergoes prescribed vertical high-frequency periodic oscillations (vibrations) of the small amplitude. The mass distribution in the body is arbitrary. This problem was first investigated by A.P. Markeev [1, 2], who derived an approximate system of differential equations, that does not depend on time explicitly and describes the motion of the rigid body relative to the coordinate system moving translationally with the suspension point. In the paper by O.V. Kholostova [3] conditions were established under which this approximate system possesses a particular first integral, similar to the Hess integral in the classical problem of the motion of a heavy rigid body with a fixed point.

In this talk we present a further study of an approximate system of equations of motion of a rigid body under the conditions formulated by O.V. Kholostova [3]. It is shown that the problem of integrating this approximate system reduced to finding the general solution of a certain second-order linear homogeneous differential equation with variable coefficients. A method is demonstrated for transforming the coefficients of the corresponding linear differential equation to the rational form. Using the Kovacic algorithm we found conditions to the parameters of the problem under which the second order linear differential equation can be solved in terms of liouvillian functions. Under these conditions the approximate system of equation of motion of a rigid body can be integrated by quadratures.

References

[1] Markeev A. P., On the Theory of Motion of a Rigid Body with a Vibrating Suspension, *Dokl. Phys.*, 2009, vol. 54, no. 8, pp. 392–396; see also: *Dokl. Akad. Nauk*, 2009, vol. 427, no. 6, pp. 771–775.

[2] Markeyev, A. P., The Equations of the Approximate Theory of the Motion of a Rigid Body with a Vibrating Suspension Point, *J. Appl. Math. Mech.*, 2011, vol. 75, no. 2, pp. 132–139; see also: *Prikl. Mat. Mekh.*, 2011, vol. 75, no. 2, pp. 193–203.

[3] Kholostova O. V., On the Dynamics of a Rigid Body in the Hess Case at High–Frequency Vibrations of a Suspension Point, *Russian J. Nonlinear Dyn.*, 2020, vol. 16, no. 1, pp. 59–84.

Motion of two thin plates in an ideal fluid

D. A. Lagunov, E. M. Artemova

Ural Mathematical Center, Udmurt State University, Izhevsk, Russia

We consider the planar motion of a thin wing consisting of two rigid plates aligned along a straight line (see Fig. 1) in an ideal incompressible fluid, under the following assumptions:

- The circulation around any closed contour is zero.
- The motion takes place in a gravitation field.
- The fluid flow is potential.

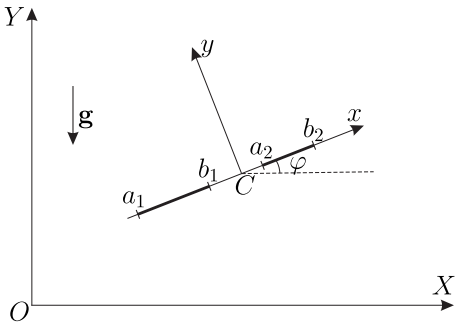


Figure 1. Schematic representation of the system under consideration and the introduced coordinate systems

To describe the fluid motion, we use the potential derived by Sedov [1]

$$\frac{dw}{dz} = -iv\left(1 - \sqrt{\frac{(z-a_1)(z-a_2)}{(z-b_1)(z-b_2)}}\right) + \\ + \frac{\Gamma_0 z + \gamma_0}{2\pi i\sqrt{(z-a_1)(z-a_2)(z-b_1)(z-b_2)}} - \\ - i\omega\left(z - \left(z - \frac{1}{2}(b_1+b_2-a_1-a_2)\right)\sqrt{\frac{(z-a_1)(z-a_2)}{(z-b_1)(z-b_2)}}\right). \tag{1}$$

For the system under consideration, the equations of motion have been formulated in Hamiltonian form, the Hamiltonian and additional first integrals

have been obtained, particular solutions have been found, and an asymptotic analysis of the motion as $t \to \infty$ has been carried out.

This work was carried out within the framework of the state assignment of the Ministry of Science and Higher Education of the Russian Federation (FEWS-2024-0007).

References

[1] Sedov L. I., *Two-Dimensional Problems in Hydrodynamics and Aerodynamics*, Moscow: Nauka, 1966 (In Russian).

Double Hamiltonian Hopf bifurcation

L. M. Lerman[1], N. E. Kulagin[2]

[1] *HSE University, Nizhny Novgorod, Russia*
[2] *A. N. Frumkin Institute of Physical Chemistry and Electrochemistry, Russian Academy of Science, Moscow, Russia*

The bifurcation, which name is in the title, has been met for the first time (as we aware of) when studying periodically modulated localized patterns of the Swift-Hohenberg equation [1], but it was not investigated there. Here we want to discuss principal features of this bifurcations in more details. Suppose in the linear symplectic space $(\mathbf{R^8}, \mathbf{\Omega})$ with the linear symplectic form Ω a smooth Hamilton function H is defined in a neighborhood U of the origin O being an equilibrium of the Hamiltonian vector field X_H, i.e. $dH(O) = 0$. We assume the linearization matrix JR, $R = D^2H(O)$, of the linear system has two pairs of double imaginary eigenvalues $\pm i\omega_1, \pm i\omega_2$, $\omega_1 \neq \omega_2$, being each non semi-simple. By a linear symplectic change of variables we can reduce the quadratic part H_2 to the form

$$H_2 = \omega_1(p_2q_1 - p_1q_2) \pm \frac{1}{2}(q_1^2 + q_2^2) + \omega_2(p_4q_3 - p_3q_4) \pm \frac{1}{2}(q_3^2 + q_4^2) + \\ + \frac{\varepsilon_1}{2}(p_1^2 + p_2^2) + \frac{\varepsilon_2}{2}(p_3^2 + p_4^2),$$

where coefficients $\omega_k, k = 1, 2$, are smooth functions of parameters $\varepsilon_1, \varepsilon_2$. In the class of smooth Hamiltonians such equilibrium is degenerated of co-dimension two, so it has to be examined in a generic two-parameter unfolding. The infinitesimally symplectic operator JR is decomposable: the symplectic space $\mathbf{R}^8$ decomposes into direct sum of two invariant symplectic four-dimensional subspaces in which the restriction of the operator generates indecomposable non semi-simple infinitesimal symplectic operator with two double non semi-simple pure imaginary eigenvalues.

Assuming the Hamiltonian to be analytic and proceeding along the lines of the normal form methods, we transform formally the Hamiltonian to the normal form of the type

$$\bar{\mathbf{H}} = \omega_1 S_1 + \omega_2 S_2 + N_1 + N_2 + \nu M_1 + \mu M_2 + \\ + \sum_{i,j,k,l \geq 0, i+j+k+l=2} A_{ijkl} S_1^i S_2^j M_1^k M_2^l,$$

where S_1, S_2, $S_1 = p_2q_1 - p_1q_2$, $S_2 = p_4q_3 - p_3q_4$, and the nilpotent part consisting of two functions N_1, N_2, $N_1 = (q_1^2 + q_2^2)/2$, $N_2 = (q_3^2 + q_4^2)/2$, where $\{S_i, N_j\} = 0$, $i, j = 1, 2$. We observe that quadratic functions S_1, S_2 are first integrals of the Hamiltonian system and each of them generate the Hamiltonian action of the group S^1, so both of them generate the action of the torus T^2 in $\mathbf{R^8}$.

Let us restrict the study, as the first step, on the normal form of the fourth order

$$\bar{\mathbf{H}}^{\nu,\mu} = \omega_1 S_1 + \omega_2 S_2 + N_1 + N_2 + \nu M_1 + \mu M_2 + A M_1^2 + B M_1 M_2 + C M_2^2,$$

The reduction w.r.t. T^2-action leads to a 2-DOF Hamiltonian system (Marsden-Weinstein). The first question here: is this system integrable, what is its structure?

We introduce new symplectic variables following to Sokolsky

$$\begin{aligned}
p_1 &= r_1 \cos\varphi_1, q_1 = P_1 \cos\varphi_1 + \tfrac{k_1}{r_1} \sin\varphi_1,\\
p_2 &= r_1 \sin\varphi_1, q_2 = P_1 \sin\varphi_1 - \tfrac{k_1}{r_1} \cos\varphi_1,\\
p_3 &= r_2 \cos\varphi_2, q_3 = P_2 \cos\varphi_2 + \tfrac{k_2}{r_2} \sin\varphi_2,\\
p_4 &= r_2 \cos\varphi_2, q_4 = P_2 \sin\varphi_2 - \tfrac{k_2}{r_2} \cos\varphi_2,
\end{aligned}$$

Despite the functions defining the change have singularities at points of two planes $p_1 = p_2 = 0$ and $p_3 = p_4 = 0$, these variables are very convenient. The Hamiltonian H in these variables becomes

$$\begin{aligned}
H = \omega_1 k_1 + \omega_2 k_2 + \frac{1}{2}(P_1^2 + k_1^2/r_1^2) + \frac{1}{2}(P_2^2 + k_2^2/r_2^2) +\\
+ \frac{\varepsilon_1}{2} r_1^2 + \frac{\varepsilon_2}{2} r_2^2 + \frac{1}{4}[A r_1^4 + 2B r_1^2 r_2^2 + C r_2^4].
\end{aligned}$$

So, k_1, k_2 become new parameters (they are integrals), φ_1, φ_2 are cyclic variables, hence the system casts as the 2-DOF system in variables (P_1, P_2, r_1, r_2) which depends on four parameters $k_1, k_2, \varepsilon_1, \varepsilon_2$. One needs to study this system and understand how its structure changes with parameters.

The most simple form the system takes at zeroth values of parameters k_1, k_2, in which case its phase space has no singularities and is $\mathbf{R^4}$. At nonzeroth k_1, k_2 the phase space is the manifold with conic singularities and its study becomes more complicated. It is was remarking that this system in $\mathbf{R^4}$ at some isolated values of coefficients A, B, C is integrable, see for instance, [2], but for almost all values of coefficients the system is nonintegrable. The system has two invariant planes on which the restriction of the system give one of possible Duffing systems. In particular, when one of the

subsystems has a saddle with two homoclinic loops and the second system has a nonlinear center, then this system is nonintegrable due to theorems of [3] and [4].

Theorem. *For all values of the ratio B/A, except for integer values $l(l-1)/2, l \in \mathbf{N}$, the system is nonintegrable.*

In case when the equilibrium at the origin is the saddle, on both invariant planes we have two Duffing systems with homoclinic orbits. In this cae, to prove nonintegrability we apply the Ziglin method and its elaboration in works Simo, Morales-Ruiz, Ramis and others. It is based on the examination of the linearized differential equations on some particular solution, for instance, a periodic solution on the invariant plane $P_1 = r_1 = 0$.

Now about the stationary Swift-Hohenberg equation $\alpha u + \beta u^2 - u^3 - (1+\Delta)^2 u = 0$ and its solutions $u(x,y)$, $(x,y) \in \mathbf{R^2}$, Δ is the Laplacian. We were sought for solutions of the wall type that is localized in variable x and periodic in variable y. Using the Bubnov-Galerkin method, we expanded the solution we sought in a Fourier series in y, whose coefficients are functions of x decaying to zero at infinity. Truncating the series up to finite number of modes, we come to the system of the second order equations of the Euler-Lagrange type. In the simplest case, after going to the Hamiltonian system, we come to the Hamiltonian system of 8 equations depending on two parameters α, β and at $\alpha = 0$ the system has an equilibrium at the origin of the type indicated above. For negative α the equilibrium becomes the double saddle-focus and its homoclinic orbit, when they exist, correspond to needed solution.

I intend to discuss the features of the orbit structure, its bifurcations, integrability and nonintegrability, homoclinic and super-homoclinic orbits, periodic orbits, etc. The preliminary version of the paper is [5].

The work is supported by the National Science Foundation, grant 22-11-00027.

References

[1] Kulagin N. E., Lerman L. M., On periodically modulated rolls in the generalized Swift-Hohenberg equation: Galerkin' approximations, *Physica D: Nonlinear Phenomena*, 2023, vol. 454, 133845.

[2] Lakshmanan M., Sahadevan R. *Phys. Reports*, 1993, vol. 224. Nos. 1& 2.

[3] Grotta Ragazzo C., *Comm. Math. Phys.* 1994, vol. 166, 255.

[4] Lerman L. M., *Selecta Math. Sov.*, 1991, vol. 10, No.3, 297.

[5] Lerman L. M., Mazrooei-Sebdani R., Kulagin N. E., Double Hamiltonian Hopf Bifurcation: normalization and normal form non-integrability, *https://arxiv.org/abs/2505.23991v1*, 37 pp.

Dynamics and motion planning of a hybrid cable-driven robot with movable carriages

A. V. Maloletov

Innopolis University, Innopolis, Russia

Cable-driven parallel robots (CDPRs) are a class of parallel manipulators in which the mobile platform is suspended and actuated by flexible cables connected to winches. Coordinated control of cable lengths enables the positioning and orientation of the platform within the robot workspace. Owing to their relatively simple mechanical structure, potentially large workspace, and suitability for handling equipment such as 3D-printing extruders and robotic manipulators, cable-driven systems are of interest in various engineering applications. However, their design and control present significant challenges associated with cable flexibility, structural deformation, nonlinear dynamics, and the coordination of multiple actuators.

This study considers an eight-cable parallel robot equipped with movable carriages carrying cable guide pulleys. The winches are mounted on four vertical supports, while the carriages allow the cable departure points to be repositioned. The system is characterized by a redundant number of actuated degrees of freedom, elastic components, and a large number of design and control parameters. Consequently, its optimization requires the simultaneous consideration of structural configuration and motion-control laws.

The movable carriages can operate in different modes. In continuous operation, carriage actuators move synchronously with the corresponding winches, increasing the number of degrees of freedom controlled simultaneously. Although this approach provides additional flexibility, it complicates control and can substantially increase actuator loads when coordination errors occur. An alternative is to reposition the carriages while the mobile platform is stationary. In this mode, only the actuator associated with the cable being adjusted operates at a given time, reducing actuator loads and relaxing carriage-positioning accuracy requirements. The latter approach effectively preserves the operating principle of a cable-driven robot with fixed guide pulleys whose positions can be changed between motion segments.

A central objective of this work is to develop a mathematical model that accounts for the coupled dynamics of the mobile platform, cables, and supporting structures. When cable spans are short and sufficiently stiff synthetic fibers are used, cable elasticity may sometimes be neglected. Similarly, support deformation can be ignored when the supporting structure behaves

approximately as a rigid frame. These simplifications, however, may be inadequate when accurate motion prediction and actuator-load estimation are required. The proposed modeling framework therefore incorporates the elastic behavior of the cables and supports.

The mobile platform and its equipment are represented as a system of rigid bodies subject to kinematic constraints and described by ordinary differential and algebraic equations. Cable dynamics are modeled using partial differential equations describing flexible, heavy strings. Cable tension and material damping are taken into account using a Voigt-type constitutive model. The vertical supports are represented by cantilever beams based on the Bernoulli–Euler beam theory. In this approximation, an algebraic relationship connects the force exerted by a cable to the deformation of the support at the cable departure point. The applicability of this simplified representation to other support configurations, including mast-type structures, requires further investigation.

The resulting mathematical model combines ordinary differential equations, partial differential equations, and algebraic relations. Its numerical solution is obtained by decomposing the original system into subsystems of ordinary differential equations and partial differential equations. These subsystems are solved separately, and their solutions are subsequently coordinated through successive iterations. This procedure provides a computationally efficient way to obtain a consistent solution without directly integrating the entire coupled system as a single monolithic model.

The inverse kinematics problem is formulated as the determination of winch and carriage coordinates corresponding to a prescribed trajectory of the mobile platform. In the presence of elastic cables and deformable supports, this problem cannot generally be solved using purely geometric relationships. Cable deformations depend on the forces acting on the cables; these forces depend on the motion laws; and the resulting motion depends, in turn, on the deformations. Therefore, the required actuator coordinates are determined through the dynamic model by minimizing the residual between the calculated and prescribed generalized coordinates of the platform.

The optimization framework accounts for several criteria associated with motion accuracy, dynamic behavior, stability, and actuator loading. Trajectory-tracking errors in the translational and angular coordinates are considered together with sensitivities of the platform coordinates to actuator-coordinate variations. The latter criteria characterize the influence of actuator-control errors on platform positioning. Dynamic performance is evaluated through the amplitudes of translational and angular oscillations caused by rapid velocity changes, control-system delays, and external disturbances, including

wind loads. Platform stability is characterized by a measure of the resistance to overturning. Actuator performance is assessed through cable-drive forces and their sensitivities to actuator-coordinate errors, with normalization based on the maximum allowable force of each actuator.

Since these criteria vary throughout the motion, optimization is performed using functionals derived from their time-dependent values rather than isolated instantaneous measurements. The optimization variables are divided into two groups: structural parameters, which are selected during robot design and remain fixed during operation, and control parameters, which define the motion laws and vary over time. The resulting problem is a multi-parameter, multi-objective optimization problem in which the aim is to identify Pareto-optimal solutions that balance competing performance requirements. Multidimensional search methods are considered for structural design optimization, whereas control-law synthesis relies on combinations of orthogonal functions or methods of variational calculus to reduce computational demands.

The developed dynamic model and inverse-kinematics solution method have been tested in the control system of a laboratory cable-driven robot. The multi-objective optimization methods have also been applied in the development of a cable-driven system prototype for a construction 3D printer. These results demonstrate the practical applicability of the proposed modeling and optimization framework to the design and control of cable-driven parallel robots with elastic components and movable cable guide carriages.

References

[1] Zi B., Qian S., *Design, Analysis and Control of Cable-Suspended Parallel Robots and Its Applications*, Springer Singapore, 2017.

[2] Pott A., *Cable-Driven Parallel Robots: Theory and Application*, Springer International Publishing, 2018.

[3] Galimov M. M., Klimchik A. S., Maloletov A. V., et al., Building 3D printer, *Russian Federation Patent 2753324 C1*, Aug. 13, 2021.

[4] Maloletov A. V., Fadeev M. Y., Klimchik A. S., Error Analysis in Solving the Inverse Problem of the Cable-driven Parallel Underactuated Robot Kinematics and Methods for their Elimination, *IFAC-PapersOnLine*, 2019, vol. 52, no. 13, pp. 1156–1161. DOI:10.1016/j.ifacol.2019.11.352.

[5] Tachia M. J., Maloletov A. V., Applications of Dynamic Models for Cable-Driven Parallel Robots: A Comprehensive Review, *Russian Journal of Nonlinear Dynamics*, 2026, vol. 22, no. 1, pp. 139–200. DOI:10.20537/nd251101.

Integrable systems with multivalued integrals

I. S. Mamaev[1], E. M. Artemova[2], and I. A. Bizyaev[2]

[1] *Kalashnikov Izhevsk State Technical University, Izhevsk, Russia*
[2] *Udmurt State University, Izhevsk, Russia*

In this talk, we intend to discuss a number of systems in mechanics and vortex dynamics, namely, those whose integrals are not single-valued functions of phase variables. We will consider some qualitative features of the behavior of the trajectories of such systems.

A new algorithm for calculating the normal form coefficients of an autonomous Hamiltonian system in the neighborhood of its periodic motion

A. P. Markeev

Moscow Aviation Institute (National Research University), Moscow, Russia

A material system with two degrees of freedom is considered, the motion of which is described by a time-independent system of Hamilton's equations. It is assumed that the system possesses a periodic solution and that the Hamiltonian function is analytic in the neighborhood of the corresponding trajectory. The parameters of the material system under study are assumed to lie within the region of orbital stability in the first (linear) approximation of the periodic solution. A new numerical-analytical algorithm is proposed for determining the normal form of the nonlinear equations of perturbed motion. This algorithm relies on approaches to the normalization of Hamiltonian systems developed previously [1, 2]. It does not require the construction of a coordinate transformation to normalize the time-dependent Hamiltonian function of perturbed motion; instead, the study of the qualitative behavior of perturbed trajectories reduces to analyzing the algebraic properties of a specially constructed generating function for the point mapping for the period. As an application, the problem of the orbital stability of the periodic motion of a dynamically symmetric rigid body about a fixed point is solved for a specific case of Grioli precession [3, 4]. The body's moments of inertia are chosen such that a third-order resonance occurs. It is shown that, despite the presence of this resonance, the precession is orbitally stable.

This research was supported by the grant of the Russian Science Foundation, No. 24-11- 00162 (https://rscf.ru/project/24-11-00162/) and was carried out at the Moscow Aviation Institute (National Research University).

References

[1] Markeev A. P., *Libration Points in Celestial Mechanics and Cosmodynamics*. M.: Nauka, 1978.

[2] Markeyev A. P., An algorithm for normalizing Hamiltonian systems in the problem of the orbital stability of periodic motions, *JAMM*, 2002, vol.66, no. 6, pp. 889–896.

[3] Grioli G., Esistenza e determinazione delle precessioni regolari dinamicamente possibili per un solido pesante asimmetrico, *Ann. Mat. Pura ed Appl.*, 1947. Ser. 4, t. 26, fasc. 3–4, pp.271–281.

[4] Markeyev A. P., The stability of the Grioli precession, *JAMM*, 2003, vol. 67, no. 4, pp. 497–510.

Investigation of the effect of tail fin stiffness on the speed of an aquatic robot

A. V. Nazarov, A. V. Klekovkin, Yu. L. Karavaev

Kalashnikov Izhevsk State Technical University, Izhevsk, Russia

The motion of aquatic robots without external propellers can be achieved through periodic rotation of internal rotors [3,4]. Previous studies investigated nondeformable tail fins for the considered robot prototype [1], while the influence of tail fin flexibility was studied for robots driven by internal moving masses [2]. The potential of elastic tail elements for improving swimming efficiency was also demonstrated in [5].

The experiments were conducted using a prototype with an airfoil-shaped hull measuring $200 \times 80 \times 80$ mm, manufactured from PLA plastic. Propulsion is achieved through periodic changes in the rotational speed of an internal rotor mounted on the shaft of a brushless motor. The maximum rotor speed is 20090 rpm. Six interchangeable rectangular tail fins with a thickness of 1 mm were manufactured. The effective transverse stiffness of the fins was determined using a cantilever bending test with an applied load according to $k = mg/\delta$, where m is the mass of the load and δ is the deflection at the point of force application. The fin parameters are presented in Table 1.

The control signal provided periodic changes in rotor speed within the range of 0–20090 rpm. To improve the agreement between the actual and desired rotor speed profiles, the PWM signal was adjusted in steps of 10% at a frequency of 25 Hz.

The experiments were performed in a 2×1.2 m pool with control periods ranging from $T = 1.0$ to 5.0 s in increments of 0.5 s. Three repeated experiments were conducted for each combination of tail fin and control period. Robot trajectories were obtained from video recordings at 30 frames/s by tracking a marker attached to the robot hull. For comparison of different operating conditions, the mean steady-state speed was calculated over an interval corresponding to two control periods.

As shown in Fig. 1, the fins made of TPU 95A provided higher swimming speeds than PETG fins of the same length. The maximum speed of approximately 0.18 m/s was achieved with fin H3 (105 mm, $k = 2.4$ N/m) at a control period of $T = 1$ s. Under the same conditions, the speed with fin H4 (105 mm, $k = 42.7$ N/m) was approximately 0.08 m/s.

Thus, the experiments demonstrate that the robot speed depends on the combined effects of tail fin length, stiffness, and control period. Reducing the

Table 1. Tail fin parameters

Fin	L, mm	Material	k, N/m
H1	70	TPU 95A	5.9
H2	70	PETG	106.7
H3	105	TPU 95A	2.4
H4	105	PETG	42.7
H5	140	TPU 95A	1.8
H6	140	PETG	18.6

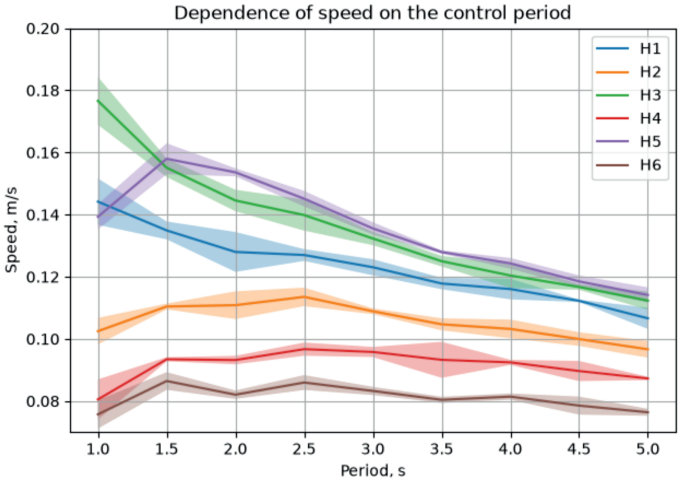


Figure 1. Robot speed as a function of the control period

fin stiffness generally leads to an increase in swimming speed. However, the fin length should be selected in combination with the control parameters.

This research was supported by the Russian Science Foundation (project No. 25-11-00305).

References

[1] Klekovkin A. V., Chernova A. A., Karavaev Y. L., Nazarov A. V., Investigation of the motion of an aquatic robot with an internal fast-speed rotor and a non-deformable tail fin, *Bulletin of Udmurt University. Mathematics. Mechanics. Computer Science*, 2025, vol. 35, no. 4, pp. 619–642.

[2] Klekovkin A. V., Karavaev Y. L., Kilin A. A., Nazarov A. V., The influence of tail fins on the speed of an aquatic robot driven by internal moving masses, *Computer Research and Modeling*, 2024, vol. 16, no. 4, pp. 869–882.

[3] Klekovkin A. V., Karavaev Y. L., Mamaev I. S., The Control of an Aquatic Robot by a Periodic Rotation of the Internal Flywheel, *Russian Journal of Nonlinear Dynamics*, 2023, vol. 19, no. 2, pp. 265–279.

[4] Pollard B., Tallapragada P., An aquatic robot propelled by an internal rotor, *IEEE/ASME Transactions on Mechatronics*, 2016, vol. 22, no. 2, pp. 931–939.

[5] Chivkula P., Tallapragada P., Spin Swimmer: A Fast, Efficient and Agile Fish-Like Robot, *IEEE Robotics and Automation Letters*, 2025, vol. 10, no. 10, pp. 10942–10949.

Synthesis of software control forces for a hybrid manipulator for surface processing

A. V. Nelyubova, V. V. Zhoga

Volgograd State Technical University, Volgograd, Russia

Manipulator systems are used to perform many technological operations for surface contact processing. They are used to grind and polish the surfaces of parts in order to improve the quality and speed of processing. The main task of the manipulator control system is to ensure that the tool moves along a given trajectory with the required kinematic parameters, providing the required force at the point of contact between the tool and the surface. Based on the original kinematic scheme, a design of a technological module based on a hybrid structure manipulator has been developed [1]. The task is to calculate the program forces in the actuators of the manipulator when moving the tool along the workpiece surface along the selected trajectory, taking into account the technological force required at the contact point. The trajectory of the tool's contact point movement along the curve is found as the intersection of two surfaces [2]. The reaction is considered to be the geometric sum of the reactions of the two surfaces. Supposed the forces acting on the tool from the surfaces are directed normal to each surface.

Defined law of motion $x_M(t)$, $y_M(t)$, $z_M(t)$ of the contact point M of the tool with the surface. By solving the positioning problem [1], we determined the configuration of the manipulator at the current moment in time through its generalized coordinates.

$$\psi(t) = \operatorname{arctg}\left(-\frac{\sqrt{x_M^2 + (y_M + OD)^2}}{z_M + DK}\right),\ \delta(t) = \operatorname{arctg}\left(-\frac{x_M}{y_M + OD}\right),$$
$$L(t) = \sqrt{x_M^2 + (y_M + OD)^2 + (z_M + DK)^2}. \tag{1}$$

On the side of the curve formed by the intersection of two surfaces, a reaction force acts on point M of the manipulator's tool $\mathbf{N}(t) = \mathbf{N}_1(t) + \mathbf{N}_2(t)$, equal in magnitude to the required technological force and determined as the geometric sum of the normal reactions of each surface. The configuration of mechanism [1] of the manipulator is described by a vector of generalized coordinates $\overline{q}\,[q_1 = L(t),\ q_2 = \psi(t),\ q_3 = \delta(t),\ q_4 = \varphi(t)]$ specified in the coordinate system of the additional link.

To form the differential equations of motion of the manipulator Lagrange's equations of the second kind are used. In matrix form, the dynamic equations take the form [3]

$$A(q)\ddot{q} + B(q,\dot{q})\dot{q} + C(q) = D(q)F(t) + Q_N, \tag{2}$$

with $A(q)$ – inertial diagonal matrix; $B(q,\dot{q})$, $D(q)$ – matrices of the mechanism's parameters, its generalized coordinates, and generalized velocities; $C(q)$ – matrix of potential forces; $F(t)$ – vector of control forces: $[F_1\ F_2\ F_3\ F_4]$, acting on the part of the executive units; Q_N – vector of generalized forces, calculated using the specified technological forces

$$\begin{aligned} Q_L &= \frac{N_x\delta x + N_y\delta y + N_z\delta z}{\delta L}, \quad Q_\psi = \frac{N_x\delta x + N_y\delta y + N_z\delta z}{\delta\psi}, \\ Q_\delta &= \frac{N_x\delta x + N_y\delta y + N_z\delta z}{\delta\delta}. \end{aligned} \tag{3}$$

The expressions for possible displacements in expressions (3) are found using the results of solving the direct kinematics of the manipulator [1]

$$x_M = L\sin\psi\sin\delta, \quad y_M = -OD - L\sin\psi\cos\delta, \quad z_M = -DK + L\cos\psi.$$

By substituting the values of the generalized coordinates, generalized velocities, and accelerations found from (1) into equations (2) at each point in time, as well as the values of the generalized technological forces (3), we obtain a system of four algebraic equations with respect to the sought-after programmable control forces $F_1(t)$, $F_2(t)$, $F_3(t)$, $F_4(t)$, which ensure the movement of the contact point of the manipulator's working tool along a given curve according to a given law, taking into account the specified reaction. The obtained expressions are used to form the control system [4].

As an example of implementing the given algorithm, we consider the movement of the tool along a curve formed by the intersection of a cylinder and a plane. The curve is represented in the form of a semicircle perpendicular to the Oy axis.

The resulting algorithm enables the tool to move along a trajectory with calculated forces in the manipulator's drives. This algorithm for determining control forces can also be extended to the case where the reaction force has a technological component directed tangentially to the trajectory.

The research was funded by the Russian Science Foundation No. 25-21-00902, https://rscf.ru/en/project/25-21-00902/

References

[1] Nelyubova A. V., Zhoga V. V., Analysis of Kinematic and Dynamic Parameters of a Manipulator-Tripod with Passive Link, in *Advances in Mechanical Engineering: Selected Contributions from the Conference "Modern Mechanical Engineering: Science and Education"*, Cham: Springer, 2026, pp. 149–156.

[2] Butenin N. V., Luntz Ya. L., Merkin D. R., *Course in Theoretical Mechanics. Dynamics*, Moscow: Nauka, 1979, 543 p.

[3] Lurye A. I., *Analytical Mechanics*, Moscow: Fizmatlit, 1961, 824 p.

[4] Krutko P. D., *Control of Robot Executive Systems*, Moscow: Nauka, 1991, 332 p.

Dynamics of a spherical robot with a pendulum-rotor mechanism

E. N. Pivovarova, A. A. Kilin

Ural Mathematical Center, Udmurt State University, Izhevsk, Russia

The dynamics of a system modeling the rolling of a combined-type spherical robot over a surface (in the particular case, over a plane) is studied. The robot is a spherical shell with a one-dimensional pendulum mounted at its center and carrying a rotor (see, for example, [1,2]). The translational motion of the spherical robot is provided by oscillations of the pendulum, while a change in the direction of motion is provided by rotation of the rotor. It is assumed that there is no slipping at the point of contact between the shell and the supporting surface.

Particular attention is paid to the analysis of particular solutions corresponding to the rolling of the spherical robot along a circle. Their stability is studied, and issues of stabilizing these solutions are also considered.

This work was carried out within the framework of the state assignment of the Ministry of Science and Higher Education of the Russian Federation (FEWS-2025-0004).

References

[1] Kilin A. A., Pivovarova E. N., Ivanova T. B., *Spherical robot of combined type: Dynamics and control*, Regular and Chaotic Dynamics, 2015, 20(6), 716–728.

[2] Borisov A. V., Kilin A. A., Karavaev Yu. L., Klekovkin A. V., *Stabilization of the motion of a spherical robot using feedbacks*, Applied Mathematical Modelling, 2019, 69, 583–592.

Mathematical modelling of the polar motion of a viscoelastic planet

Yu. S. Plakhotina, A. V. Shatina

MIREA — Russian Technological University, Moscow, Russia

The rotational motion of a deformable viscoelastic planet is investigated under the influence of gravitational fields generated by a natural satellite and a massive attracting center. The planet is modelled as a homogeneous isotropic viscoelastic body that assumes a spherical shape in its undeformed state. The attracting center and the satellite are modelled as material points.

The equations for the rotational motion of the planet are derived using an asymptotic method of motion separation for systems containing elastic elements of high stiffness [1, 2]. The generating motion is taken to be the motion of the planet-satellite system in the gravitational field of a fixed attracting center, with the barycenter of the system moving along a fixed Keplerian elliptical orbit. In this context, the planet is modelled as an absolutely rigid homogeneous sphere, while the satellite and the attracting center are treated as material points. The equations of the satellite's orbital motion relative to the center of mass of the planet are obtained using the Lagrange planetary equations [3].

Based on the generating motion, a system of ordinary differential equations is derived for the coordinates of the angular velocity vector of the viscoelastic planet and the orbital elements. The theoretical results are applied to study variations in the Earth's angular velocity under the influence of the gravitational fields of the Moon and the Sun. Graphs are plotted to describe the time dependent variation of the coordinates of the dimensionless angular velocity vector over a period of 30 days for various initial values of the orbital parameters. Trajectories are plotted to illustrate the mutual variation of the angular velocity vector coordinates, which characterise the motion of the Earth's pole. A graph illustrating the variation of the planet's relative angular velocity is also presented. An equation describing the dissipative evolution of the rotational angular velocity of a viscoelastic planet is derived; this equation enables an estimate of the coefficient of internal viscous friction for the Earth within the stated model problem.

The results obtained enable prediction of variations in the angular velocity of a viscoelastic planet under the influence of solid-body tides.

References

[1] Vil'ke V. G., *Analytical and Qualitative Methods of Mechanics of Systems with an Infinite Number of Degrees of Freedom*, Moscow: LENAND, 2023, 200 p.

[2] Vil'ke V. G., Shatina A. V., On the Translational-Rotational Motion of a Viscoelastic Sphere in the Gravitational Field of an Attracting Center and a Satellite, *Cosmic Research*, 2004, vol. 42, no. 1, pp. 95–106.

[3] Sazonov V. V., Barbashova T. F., *Lectures on Space Flight Mechanics. Special Course*, Moscow: Moscow University Press, 2018, 152 p.

A robot motion planning algorithm based on solving a system of nonconvex inequalities

E. A. Pogosyan, S. V. Gusev

Sirius University of Science and Technology, Sirius Federal Territory, Russia

Motion planning for a robot in an environment with known obstacles is one of the key problems in robotics. It arises, in particular, in the navigation of mobile robots, the control of robotic manipulators, and the transportation of bulky objects in the presence of obstacles. Its solution can be reduced to constructing a trajectory that satisfies a given system of inequality constraints describing the admissible region of motion with account of the obstacle locations.

The idea of reducing robot control problems to solving systems of inequalities was first formulated by V. A. Yakubovich in [1]. To solve such systems, he developed the method of recurrent objective inequalities [2]. Further development of this approach led, in particular, to the dividing ellipsoids method, designed for solving systems of nonconvex recurrent inequalities [3]. The aim of this work is to adapt the dividing ellipsoids method to the problem of planning robot trajectories in an environment with obstacles.

The dividing ellipsoids method generalizes the classical ellipsoid method to systems of nonconvex inequalities. It is based on an iterative procedure for finding a feasible solution of the system under the assumption that there are no hidden equalities. Within this approach, the original system of nonconvex inequalities defined in the space $\mathbb{R}^n$ is transformed into a system of convex inequalities defined on a nonconvex surface in the space $\mathbb{R}^{n+1}$. A detailed description of the corresponding transformations and of the theoretical foundations of the method is given in [3].

Let us briefly outline the main steps of the algorithm. 0) An initial ellipsoid is chosen and placed in a list. 1) The last ellipsoid (a_k, E_k) of the list, which contains the set of feasible solutions, is taken. 2) A candidate solution z_k of the system of inequalities is chosen in it. 3) All constraints are checked at the point z_k. 4) If they are all satisfied, a solution is found. 5) If there is an inequality violated both at the point a_k and at z_k, the ellipsoid method with gradient descent is applied (Fig. 1a); otherwise the ellipsoid is divided along its major axis (Fig. 1b). 6) The resulting one or two ellipsoids are placed in the list. 7) Go to step 1. Convergence of the algorithm is proved in the case where a solution of the system of inequalities exists.

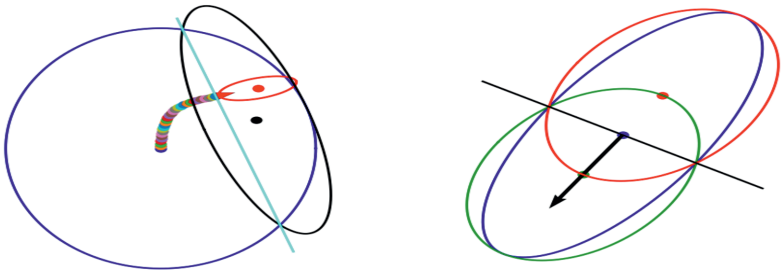


Figure 1. (a) The ellipsoid method; (b) the method of division along the major axis

As an example of applying the algorithm to robot motion construction, we consider the problem of finding a route for transporting a load through a narrow passage, also known as the "piano movers problem". The trajectory is constructed by a smooth parameterization from the initial state $X_A = [x_A, y_A, \alpha_A]$ to the final state $X_B = [x_B, y_B, \alpha_B]$ using polynomials of fixed degree.

The parameterization of the trajectory and orientation is

$$X(s) = (1-s)X_A + sX_B + s(1-s)P(s), \tag{1}$$

where $s \in [0,1]$ is the natural parameter and $P(s)$ is a vector of polynomials with unknown coefficients to be determined.

The obstacles are given analytically, which allows explicit computation of the gradients of the functions defining them. Two types of obstacles are considered, ellipses and half-planes:

$$\begin{cases} F_i^{\text{ell}}(u) = 1 - (u-c_i)^T E_i (u-c_i) \le 0, \\ F_k^{\text{hp}}(u) = (u-u_k)^T n_k \le 0, \end{cases} \tag{2}$$

where $u \in \mathbb{R}^2$; c_i and E_i are the center and the matrix of the ellipse; u_k and n_k are a point on the boundary line and its normal vector.

Substituting parameterization (1) into the analytic expressions of the constraints (2) and discretizing in the parameter s, we obtain a system of inequalities for the dividing ellipsoids algorithm, in which the unknowns are the coefficients of the polynomials $P(s)$.

We briefly present the result of one of the experiments, which addresses the construction of a trajectory for transporting a "T"-shaped load on the plane, with length 5 and width 4. The main challenge is to pass through a narrow passage of width 3.6. Figure 2 shows the key stages of the robot's trajectory constructed by the proposed algorithm.

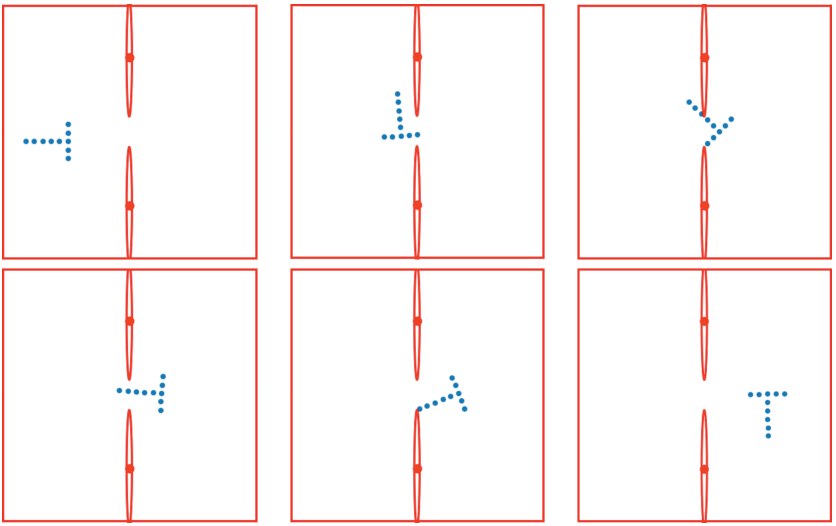


Figure 2. Construction of a trajectory for transporting a “T”-shaped load

References

[1] Yakubovich V. A., On the Theory of Adaptive Systems, *Dokl. Akad. Nauk SSSR*, 1968, vol. 182, no. 3, pp. 518–521 (Russian).

[2] Fomin V. N., Fradkov A. L., Yakubovich V. A., *Adaptive Control of Dynamic Plants*, Moscow, 1981 (Russian).

[3] Gusev S. V., Shishkin S. L., The Dividing Ellipsoids Algorithm: A Method for Solving Systems of Nonconvex Inequalities, *Avtomat. i Telemekh.*, 1999, no. 7, pp. 25–33 (Russian).

On Lyapunov stability and integrability of the Ziegler pendulum

I. Yu. Polekhin[1,2,3]

[1] *Steklov Mathematical Institute of the Russian Academy of Sciences, Moscow, Russia*
[2] *Moscow Institute of Physics and Technology, Dolgoprudny, Russia*
[2] *Lomonosov Moscow State University, Moscow, Russia*

The Ziegler pendulum is a well-known non-conservative system consisting of a planar double pendulum with a follower force directed along one of its links. Gravity is assumed to be absent. This system is primarily known for the so-called "Ziegler paradox": adding friction to the system causes an equilibrium position that was stable in the linear approximation to become unstable. In this context, one usually speaks of a loss of stability without proving Lyapunov stability in the frictionless system. The talk will address the Ziegler paradox in a nonlinear formulation for the Ziegler pendulum with symmetry. Questions concerning the integrability of this system will also be discussed.

This work was supported by the Russian Science Foundation (Project No. 26-61-00003).

Synchronization on graphons with higher-order interactions: the spectrum of the coupling operator versus the structure of the coupling tensor

K. S. Ryabov

HSE University, Nizhny Novgorod, Russia

The Kuramoto model on a dense weighted network (graphon) is a standard framework for synchronization on structured populations. For the pairwise model the critical coupling K_c is determined by the spectrum of the coupling operator W, and the limit $N \to \infty$ is well defined and analytically tractable [1]. We study its generalization to *higher-order* (three-body) interactions, in which the coupling weight is a third-rank tensor T, and ask how the pairwise and the higher-order couplings compete. The model reads

$$\dot{\varphi}_i = \omega_i + \frac{K_1}{N}\sum_j W_{ij}\sin(\varphi_j - \varphi_i) + \frac{K_2}{N^2}\sum_{j,k} T_{ijk}\,\sin(2\varphi_j - \varphi_k - \varphi_i),$$

$$\omega_i \sim g(\omega),$$

where i, j, k are free node indices (no summation convention; all sums are explicit). We consider the flag-complex tensor $T_{ijk} = W_{ij}W_{ik}$ (triangles spanned on the edges of the graph) and the separable tensor $T_{ijk} = t_i t_j t_k$, which lets us tune the alignment of T with the eigenmodes of W.

Our first result is that the *linear threshold is set by the spectrum of W alone and does not depend on K_2*. Linearizing about the incoherent state, the higher-order term contains the product $z_2\overline{z_1} = O(\varepsilon^2)$ of the first and second harmonics and therefore drops out, so that $K_c = 2/(\pi g(0)\,\lambda_{\max}(W))$ is unchanged, with the same unstable eigenmode v_1. The triples instead change the *nature* of the transition: they make it explosive (subcritical, with hysteresis), the loop area growing monotonically with K_2 (Fig. 1).

Our second result concerns the *competition of the two spectra*. Near threshold $z_1 \approx A\,v_1$ and the second harmonic is slaved, $z_2 \sim A^2$, so the higher-order term contributes to the cubic coefficient of the amplitude equation, $\dot{A} = \sigma(K_1)A + (c_{\text{pair}} + K_2 c_T)|A|^2 A + \ldots$, where c_T is proportional to the projection of the tensor onto the leading mode, $c_T \propto \langle T, v_1 \otimes v_1 \otimes v_1 \rangle$. The transition turns subcritical beyond $K_2^* = -c_{\text{pair}}/c_T$; hence a tensor aligned with v_1 triggers explosive synchronization much earlier (small K_2^*) than a misaligned one. Thus the explosiveness is governed not by the magnitude of K_2 but by how the "spectrum" of T overlaps the leading mode of W.

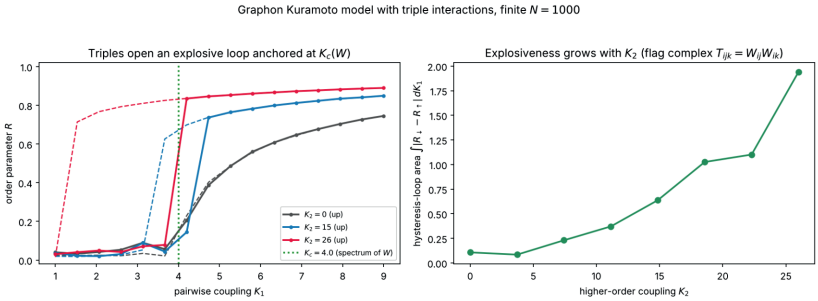


Figure 1. Graphon Kuramoto model with triple interactions (assortative SBM, flag-complex tensor, finite $N = 10^3$). Left: forward (solid) and backward (dashed) sweeps of the order parameter $R(K_1)$ for several K_2; the onset stays anchored at K_c (set by the spectrum of W) for any K_2, while the triples open an explosive hysteresis loop. Right: the hysteresis-loop area grows with the higher-order coupling K_2.

Direct finite-N simulations confirm all three statements, and the results agree with the Ott–Antonsen mean-field reduction [2]; the mean-field special case $W \equiv 1$, $T \equiv 1$ reproduces the abrupt-switching scenario of [3]. A natural next step is the analytic $N \to \infty$ theory for a dense coupling tensor (hypergraphon) and the full (K_1, K_2) phase diagram with its codimension-two tricritical point.

This work was supported by the project HSE-BR-2025-79 implemented as part of the Basic Research Program at HSE University.

References

[1] Chiba H., Medvedev G. S., The Mean Field Analysis of the Kuramoto Model on Graphs: I. The Mean Field Equation and Transition Point Formulas, *Discrete Contin. Dyn. Syst.*, 2019, vol. 39, no. 1, pp. 131–155.

[2] Ott E., Antonsen T. M., Low Dimensional Behavior of Large Systems of Globally Coupled Oscillators, *Chaos*, 2008, vol. 18, no. 3, 037113.

[3] Skardal P. S., Arenas A., Higher Order Interactions in Complex Networks of Phase Oscillators Promote Abrupt Synchronization Switching, *Commun. Phys.*, 2020, vol. 3, 218.

A new class of motions of the Kovalevskaya–Chaplygin–Goryachev–Yehia top: algebraic solution and reduction to elliptic quadratures

P. E. Ryabov[1,2,3]

[1] *Financial University under the Government of the Russian Federation, Moscow, Russia*
[2] *Moscow Institute of Physics and Technology (National Research University), Dolgoprudny, Russia*
[3] *MIREA — Russian Technological University (RTU MIREA), Moscow, Russia*

For the integrable case of the Kovalevskaya–Chaplygin–Goryachev–Yehia top, a new invariant submanifold is found and its invariance is proved. On this submanifold an algebraic solution is obtained: all phase variables are expressed in terms of one auxiliary variable, and the integration reduces to elliptic quadratures.

The motion of a rigid body about a fixed point is described by the Euler–Poisson equations

$$\dot{\boldsymbol{M}} = \boldsymbol{M} \times \frac{\partial H}{\partial \boldsymbol{M}} + \boldsymbol{\alpha} \times \frac{\partial H}{\partial \boldsymbol{\alpha}}, \qquad \dot{\boldsymbol{\alpha}} = \boldsymbol{\alpha} \times \frac{\partial H}{\partial \boldsymbol{M}},$$

where $\boldsymbol{M} = (M_1, M_2, M_3)$ is the angular momentum, $\boldsymbol{\alpha} = (\alpha_1, \alpha_2, \alpha_3)$ is the unit vertical, and $\boldsymbol{\omega} = (\omega_1, \omega_2, \omega_3)$ is the angular velocity. The inertia tensor satisfies the Kovalevskaya condition $A = B = 2C$, and $M_1 = 2\omega_1, M_2 = 2\omega_2, M_3 = \omega_3 + \lambda$, with λ being a constant gyrostatic moment along the symmetry axis.

The system possesses the first integrals

$$H = \omega_1^2 + \omega_2^2 + \tfrac{1}{2}\omega_3^2 + \gamma\alpha_1 + c(\alpha_1^2 - \alpha_2^2) + \delta\tfrac{\boldsymbol{\alpha}^2}{\alpha_3^2} = h,$$
$$\Gamma = \alpha_1^2 + \alpha_2^2 + \alpha_3^2 = 1, \quad L = 2\omega_1\alpha_1 + 2\omega_2\alpha_2 + (\omega_3 + \lambda)\alpha_3 = \ell.$$

The generalization of the Kovalevskaya–Chaplygin case [1] to a singular potential was obtained by Goryachev [2], while the gyrostatic moment and the additional integral F were introduced by Yehia [3]. On the zero level of the area integral, $\ell = 0$, the system is integrable in quadratures. The integral F has the form [3]:

$$F = \Big[\omega_1^2 - \omega_2^2 - \gamma\alpha_1 + c\alpha_3^2 + \frac{\delta(\alpha_2^2 - \alpha_1^2)}{\alpha_3^2}\Big]^2 + \Big(2\omega_1\omega_2 - \gamma\alpha_2 - \frac{2\delta\alpha_1\alpha_2}{\alpha_3^2}\Big)^2$$
$$+ 2\lambda(\omega_3 - \lambda)\Big[\omega_1^2 + \omega_2^2 + \delta\Big(1 + \frac{\boldsymbol{\alpha}^2}{\alpha_3^2}\Big)\Big] - 4\lambda\alpha_3[\omega_1(c\alpha_1 + \gamma) - c\alpha_2\omega_2].$$

Consider the function

$$F_R = \Big[4c\Big(\omega_1^2+\omega_2^2+\lambda\omega_3+\delta\frac{\boldsymbol{\alpha}^2}{\alpha_3^2}\Big)+(2c\alpha_1+\gamma)^2+4c^2(\alpha_2^2-1)\Big]^2 + 4c\Big[4c\omega_1\alpha_3+\gamma(\omega_3+\lambda)-2\lambda(\gamma+2c\alpha_1)\Big]^2.$$

This function is not an independent integral: on the level $\ell = 0$ it is functionally expressed through the known integrals H, F, and L. It is precisely this form of F_R that allows one to single out a new class of motions of the Kovalevskaya–Chaplygin–Goryachev–Yehia top in the form of an invariant submanifold $\mathcal{M}$.

On $L = \ell = 0$ and $\Gamma = 1$, the set $\mathcal{M}$ defined by $Z_1 = 0, Z_2 = 0$, where

$$Z_1 = 4c\Big(\omega_1^2+\omega_2^2+\lambda\omega_3+\delta\frac{\boldsymbol{\alpha}^2}{\alpha_3^2}\Big)+(2\alpha_1 c+\gamma)^2+4c^2(\alpha_2^2-1),$$
$$Z_2 = 4c\omega_1\alpha_3+\gamma(\omega_3+\lambda)-2\lambda(\gamma+2c\alpha_1),$$

is an invariant submanifold for the system with Hamiltonian H.

Set $h_1 = h+\lambda^2/2$, $c = -p^2$, $p > 0$. Introduce the auxiliary variable u instead of ω_3: $\omega_3 = \lambda - \frac{2Bu}{D(u)}$, $B = \sqrt{4p^2(h_1+p^2)-\gamma^2}$, $D(u) = 1+2p^2u^2$. Using $H = h$, $\Gamma = 1$, $Z_1 = Z_2 = 0$, and $L = 0$, all phase variables are expressed explicitly as algebraic functions of u. Namely, from $Z_1 = Z_2 = 0$ and $L = 0$ we find $\alpha_3^2 = \frac{\Sigma(u)}{8p^4} - \alpha_1^2$, $\alpha_2^2 = \frac{\Delta(u)^2B^2}{8p^4D(u)^2}$, where $\Delta(u) = 1-2p^2u^2$, $\Sigma(u) = \frac{4p^4\left(1+12p^2u^2+4p^4u^4\right)-\Delta(u)^2\left(4h_1p^2-\gamma^2\right)}{D(u)^2}$. Substituting these expressions into the energy integral $H = h$ yields the equation for α_1:

$$\Big(-4Bp^2\big[12p^4u^2+4p^6u^4+p^2\big(1-2\alpha_1^2D(u)^2\big)+\alpha_1D(u)^2\gamma\big]+ +B\Delta(u)^2\big(4h_1p^2-\gamma^2\big)+64p^6uD(u)\lambda\Big)^2 - A^2E(u)^2 = 0,$$

where

$$A = \sqrt{2}\sqrt{B^2(\gamma^2M_0-32p^6\delta)-32p^6M_0\lambda^2},$$
$$E(u) = 1-4p^4u^4, M_0 = -4h_1p^2+4p^4+\gamma^2.$$

This equation is quartic in α_1 and splits into two quadratic equations in α_1, so its four roots are explicit:

$$(\alpha_1)_{1,2} = \frac{\gamma}{4p^2} \pm \frac{\sqrt{T_0-2AE(u)}}{4\sqrt{B}\,p^2D(u)}, \quad (\alpha_1)_{3,4} = \frac{\gamma}{4p^2} \pm \frac{\sqrt{T_0+2AE(u)}}{4\sqrt{B}\,p^2D(u)},$$

where $T_0 = 8Bp^2\big[p^2 + 12p^4u^2 + 4p^6u^4 - h_1\Delta(u)^2\big] + B\big(3 - 4p^2u^2 + 12p^4u^4\big)\gamma^2 - 128\lambda p^6 uD(u)$. Finally, the angular velocity components are given by

$$\omega_1 = \frac{2\alpha_1\lambda p^2 D(u) - Bu\gamma}{2\alpha_3 p^2 D(u)}, \quad \omega_2 = -\frac{\Phi(u)}{8\alpha_2\alpha_3 p^4 D(u)^3}, \quad \omega_3 = \lambda - \frac{2Bu}{D(u)},$$

where $\Phi(u) = -8B^3p^2u^3 + BuD(u)^2N + 8B^2p^2u^2D(u)\lambda + D(u)^3M_0\lambda$, $N = 4h_1p^2 + 4(2\alpha_1^2 - 1)p^4 - 4\alpha_1p^2\gamma - \gamma^2$. The differential equation for $u(t)$ is $\left(\frac{du}{dt}\right)^2 = R(u), R(u) = \frac{T_0 \mp 2AE(u)}{32p^4B}$, where the sign $\mp$ corresponds to the branches $(\alpha_1)_{1,2}$ and $(\alpha_1)_{3,4}$. Since $R(u)$ is a polynomial of the fourth degree, the integration reduces to an elliptic quadrature, and all phase variables are determined by u and Jacobi elliptic functions.

On $\mathcal{M}$ defined above, for $\delta > 0$ the manifold is compact and the energy is bounded, while for $\delta < 0$ the energy is unbounded from below near the singularity $\alpha_3 = 0$. In the compact case, the motion on $\mathcal{M}$ is periodic, and the trajectory is a closed orbit.

The work was supported by the Russian Science Foundation (project no. 25-21-00086) at the Moscow Institute of Physics and Technology (National Research University).

References

[1] S. A. Chaplygin, New particular solution of the problem of motion of a rigid body in a fluid, *Proc. Dept. Phys. Sci. Soc. Lovers Nat. Sci.*, 1903, vol. 11, no. 2, pp. 7–10.

[2] D. N. Goryachev, New cases of integrability of dynamical Euler equations, *Izv. Varshav. Univ.*, 1916, no. 3, pp. 1–13.

[3] H. M. Yehia, New integrable problems in the dynamics of rigid bodies with the Kovalevskaya configuration: I. The case of axisymmetric forces, *Mech. Res. Commun.*, 1996, vol. 23, no. 5, pp. 423–427.

Robust chaos in replicator systems with cyclic symmetry

K. A. Safonov

Higher School of Economics, Nizhny Novgorod, Russia

Replicator equations are widely used to describe evolutionary dynamics in populations, where the relative abundance of each type changes according to its fitness relative to the population average. In this talk, we consider the evolutionary dynamics of four interacting types governed by the replicator equations

$$\dot{x}_i = x_i\big(f_i(x) - \phi(x)\big), \quad i = 1, \dots, 4, \qquad \phi(x) = \sum_{j=1}^{4} x_j f_j(x),$$

where $x_i \geq 0$, $\sum_{i=1}^{4} x_i = 1$, and $f_i(x)$ denotes the fitness of type i.

We focus on replicator systems that are equivariant under the cyclic permutation

$$(x_1, x_2, x_3, x_4) \mapsto (x_2, x_3, x_4, x_1),$$

which generates the symmetry group $\mathbb{Z}_4$. Our goal is to investigate the emergence of robust chaotic dynamics in this class of systems.

Recent studies [1, 2] have shown that the bifurcation of an equilibrium with three zero eigenvalues in systems with $\mathbb{Z}_4$-symmetry can lead to the emergence of robust Lorenz-like attractors. We apply this bifurcation mechanism to replicator dynamics. We derive general sufficient conditions on the fitness functions f_i for the existence of an equilibrium with three zero eigenvalues. We then establish conditions ensuring the emergence of robust chaotic attractors through its bifurcation. We also construct explicit examples of replicator systems satisfying these conditions, thereby demonstrating that this mechanism can be realized in concrete models.

Thus, replicator systems constitute another class of dynamical systems in which robust chaos emerges through a local bifurcation of a highly degenerate equilibrium. This complements the results of [3], where the same bifurcation mechanism was demonstrated in a system of four coupled phase oscillators.

The work was supported by the RSF grant No. 25-11-20069.

References

[1] E. Karatetskaia, A. Kazakov, K. Safonov, and D. Turaev (2024). Multi-winged Lorenz attractors due to bifurcations of a periodic orbit with multipliers $(-1, i, -i)$. Nonlinearity, 37(12), 125009.

[2] E. Karatetskaia, A. Kazakov, K. Safonov, and D. Turaev (2025). Analytic proof of the emergence of new type of Lorenz-like attractors from the triple instability in systems with $\mathbb{Z}_4$-symmetry. Journal of Differential Equations, 430, 113189.

[3] E. Karatetskaia, A. Kazakov, K. Safonov, and D. Turaev (2025). Robust chaos in a totally symmetric network of four phase oscillators. Physical Review Letters, 134(16), 167201.

Deterministic and probabilistic transitions in the dynamics of Earth co-orbitals

V. V. Sidorenko

Keldysh Institute of Applied Mathematics RAS, Moscow, Russia

Earth co-orbitals are asteroids moving in the 1:1 mean motion resonance with our planet. They may occupy several qualitatively different regimes, including quasi-satellite (QS), horseshoe (HS), Trojan, and compound states [1]. Slow variations of the orbital elements can produce repeated transformations between these regimes and transitions between resonant and non-resonant motion. The starting point of the present construction is the perturbative theory developed by Sidorenko et al. [2]. Here, this approach is extended from the restricted three-body problem to a multiplanet model applicable to real Earth co-orbitals.

We focus on a subgroup termed *dynamically warm Earth co-orbitals*. It consists of objects with moderate inclinations (in practice, $i \gtrsim 5^\circ$) for which the resonant and secular time scales remain sufficiently well separated. We additionally require $\sigma < \sigma_\star \approx 0.277$, where σ, a quantity related to the von Zeipel–Lidov–Kozai integral, bounds the possible variations of eccentricity and inclination). This condition guarantees the absence of close approaches to Venus and to Mars. The low-inclination population and the Trojan branch are outside the scope of the present study.

The model retains the resonant interaction with Earth and includes secular perturbations from Venus, Mars, Jupiter, and Saturn. Averaging over the fast orbital motions produces a resonant subsystem for the resonant phase and its conjugate momentum and a slow subsystem describing the evolution of the eccentricity e and argument of perihelion ω. For fixed slow variables, the resonant subsystem is a one-degree-of-freedom Hamiltonian system. Its action is an adiabatic invariant of the problem. A second averaging along periodic trajectories of this subsystem yields evolutionary equations for e and ω. Their phase portraits contain different branches corresponding to QS, HS, and compound QS+HS motion.

Transitions are controlled by curves of uncertainty in the (e, ω) plane. The points of these curves correspond to separatrix solutions of the resonant subsystem, whose periods become infinite. Near such curves, averaging loses accuracy, the action undergoes small phase-dependent jumps, and several continuations of the slow evolution may become possible. The transitions between coexisting resonant regimes can be deterministic or quasi-probabilistic,

with the transition probabilities calculated using the formulas of Artemyev et al. [3].

The theory is applied to the Earth quasi-satellites Cardea and Kamo'oalewa and compared with direct numerical integrations including all planets. For Cardea, the first QS-to-HS transition is deterministic. At a subsequent transition, the probabilities of returning from the HS regime to the QS and compound QS+HS regimes are ≈ 0.95 and ≈ 0.05, respectively. For Kamo'oalewa, the corresponding probabilities are ≈ 0.85 and ≈ 0.15, which explains why compound motion interrupts its QS–HS sequence earlier than in the case of Cardea.

Thus, repeated QS–HS transformations, compound motions, and transitions between resonant and non-resonant motion in the dynamics of Earth co-orbitals can be interpreted within a unified semi-analytical framework.

References

[1] Pan N., Gallardo T., An attempt to build a dynamical catalog of present-day Solar System co-orbitals, *Celestial Mechanics and Dynamical Astronomy*, 2025, vol. 137:2.

[2] Sidorenko V. V., Neishtadt A. I., Artemyev A. V., Zelenyi L. M., Quasi-satellite orbits in the general context of dynamics in the 1:1 mean motion resonance: perturbative treatment, *Celestial Mechanics and Dynamical Astronomy*, 2014, vol. 120, pp. 131–162.

[3] Artemyev A. V., Neishtadt A. I., Zelenyi L. M., Ion motion in the current sheet with sheared magnetic field – Part 1: Quasi-adiabatic theory, *Nonlinear Processes in Geophysics*, 2013, vol. 20, pp. 163–178.

Stabilization of underactuated mechanical systems with unknown build-in controllers

I. M. Tarabukin, O. Yu. Sumenkov

Sirius University of Science and Technology, Sirius, Russia

This paper addresses the control problem for underactuated dynamic systems when force (torque) control is not available. This scenario is commonly encountered in industrial robotic systems, e.g., manipulators, where the interface does not expose torque commands and allows only the velocity and/or position of a link to be commanded [1].

Such behaviour stems from an built-in controller whose dynamics are unknown and difficult to identify. Nevertheless, it is assumed that the available input (desired velocity and/or position) and the system output satisfy certain input–output relations.

Under these assumptions, this paper proposes a constructive method that reduces the problem of stabilizing an equilibrium of an underactuated system governed by an unknown built-in controller to that of stabilizing an auxiliary linear time-invariant (LTI) system subject to parametric uncertainties and external disturbances. Stability proofs are provided for several input–output relationships enforced by the unknown built-in controller, specifically when: (i) the input exactly matches the system output after some finite time; (ii) the tracking error remains bounded by a prescribed constant; and (iii) the output tracks the reference trajectory with a constant delay.

The proposed results have been validated in simulations and in experiments on stabilizing a Ball-on-Disk system, where the disk is actuated by commanding the drive of an ABB IRB 2400 manipulator in velocity mode.

This work was supported by a grant of the Russian Science Foundation (project No. 24-11-20009)

References

[1] Sumenkov, O., Medvedeva, T., Gusev, S., and Fridman, L., Super-Twisting Algorithm Gain Adjustment Strategy for Manipulator Position Control, in *Interactive Collaborative Robotics*, A. Ronzhin, J. Savage, R. Meshcheryakov (Eds.), *Lect. Notes in Comp. Sci.*, 2024, vol. 14898, Cham: Springer, pp. 15–29.

Numerical modeling of three-dimensional motion of a spherical robot with electromagnetic drive

A. M. Tuzikov[1,2]

[1] *Lobachevsky State University of Nizhny Novgorod, Nizhny Novgorod, Russia*
[2] *Sirius University of Science and Technology, Sirius Federal Territory, Russia*

Spherical robots (SRs), originally proposed as a lightweight and robust alternative to wheeled platforms for planetary exploration [1], cannot tip over, have their drive and electronics protected by the shell, and can roll in any direction, which makes them attractive for underwater and planetary exploration and for inspection of tunnels, pipes, and contaminated sites.

We consider an SR with an electromagnetic drive (SRED), which is fundamentally new for robots of this kind. It consists of two concentric spherical shells: the inner one carries S electromagnets (EMs), and the outer one carries M neodymium permanent magnets (PMs), so that the design resembles a spherical motor [2]; the robot moves due to the interaction between the magnets on the two shells. Such a drive enables omnidirectional, smooth motion with much smaller delays and no slip between the drive and the shell. The goal of the work is to formulate a magnet placement principle and to verify by numerical simulation that motion along prescribed trajectories is realizable with the selected layout.

Control system and drive model. Following [3], the control vector $\boldsymbol{Q}$ that brings the SR to the reference trajectory is the sum of a feedforward control and a corrective control, the latter being a linear state feedback. Its gains are found from a Pareto-optimal bicriteria problem (deviation from the trajectory vs. control effort) solved by semidefinite programming.

The drive model is built for a pair of a thick solenoid (EM) and a cylindrical PM [4] (Fig. 1a): the Biot–Savart–Laplace law gives the PM field $\boldsymbol{B}$ at the EM, and Ampère's law in the coil's cylindrical coordinates (ρ, θ, z_0) gives the force $\boldsymbol{F}$ on the EM and the torque $\boldsymbol{Q}^{in}$.

The desired torque $\boldsymbol{Q}^{in}_{ref}$ is given by the optimal controller, and the actual torque by the drive model, $\boldsymbol{C}\boldsymbol{I} = \boldsymbol{Q}^{in}$, where $\boldsymbol{C} \in \mathbf{R}^{3\times S}$ is the torque map and $\boldsymbol{I}$ is the vector of coil currents. The energy-optimal currents are obtained with the regularized pseudoinverse

$$\boldsymbol{I} = \boldsymbol{C}^{\top}\left(\boldsymbol{C}\boldsymbol{C}^{\top} + \lambda E_3\right)^{-1}\boldsymbol{Q}^{in}_{ref}, \tag{1}$$

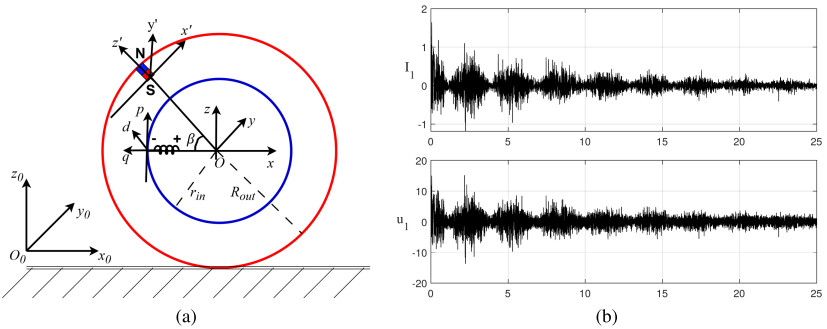


Figure 1. (a) Planar scheme of the SRED; (b) current I_1 (A) and voltage u_1 (V) of one EM vs. time (s)

where $\lambda > 0$ is small and E_3 is the identity matrix; the coil voltages follow from Kirchhoff's equations with the back-EMF induced by the relative motion of the shells.

Placement of magnets on the spherical shells. The drive must produce a torque about any axis for any orientation of the shells. The magnets are placed at the vertices of inscribed polyhedra, but the equations of motion and the control scheme of [3] are valid only if the inertia tensors of both shells are scalar. A sufficient condition for this is that the point symmetry group of the placement acts irreducibly on $\mathbf{R}^3$. Only the cubic (T, T_d, T_h, O, O_h) and icosahedral (I, I_h) point groups satisfy this condition; all others leave an invariant axis. The vertex-transitive convex polyhedra (excluding prisms and antiprisms) with such symmetry are exactly the 5 Platonic and 13 Archimedean solids.

Choice of PM placement. Among the candidates with $N \geq 20$ vertices, the one with the smallest coverage gap $\theta_{gap}^{\max}$ (maximal angular distance to the nearest vertex) is preferred, since the PM–EM torque decays rapidly with angular distance. Among the four Archimedean solids with $N = 60$ (truncated dodecahedron, truncated icosahedron, snub dodecahedron, rhombicosidodecahedron), the rhombicosidodecahedron has the smallest gap, $22.4°$, and is selected for the PMs.

Choice of EM placement. The key indicator is $\tau_{\min}$, the minimal torque about any axis for any orientation of the shells at unit current norm. A numerical check (10^4 random relative orientations from $SO(3) \times 10^5$ directions) for $S \in \{8, 12, 20, 24, 30\}$ shows that the guaranteed torque grows monotonically with the number of EMs. The truncated octahedron ($S = 24$, group O_h) provides $\tau_{\min} = 0.118$ N·m at $\|\boldsymbol{I}\| = 1$ A. Using $S = 30$ EMs (icosido-

decahedron) gives only about 29% more torque at the cost of extra mass and control channels.

Numerical simulation of three-dimensional motion. The motion of the SRED along a three-dimensional trajectory over a Gaussian bell-shaped surface with dry friction coefficient $\kappa = 0.8$ was simulated, the initial position of the robot being offset from the reference trajectory. Typical current $I_1(t)$ and voltage $u_1(t)$ of one of the 24 coils (Fig. 1b; the others are similar) decay with time and have peak values of about 1.6 A and ± 16.5 V, respectively. Their fast oscillations are due to the large number of magnets and the fairly high rate of relative rotation of the shells, about 20 rad/s. Thus, the proposed drive produces a torque sufficient for motion over uneven surfaces with voltages within the range of modern low-voltage power drivers.

This work was supported by the Ministry of Education and Science of the Russian Federation (project no. FSWR-2026-0007), and by the Research and Education Mathematical Center Mathematics for Future Technologies.

References

[1] Halme A., Schönberg T., Wang Y., Motion Control of a Spherical Mobile Robot, in *Proc. 4th IEEE Internat. Workshop on Advanced Motion Control*, 1996, pp. 259–264.

[2] He J., Li G., Zhou R., Torque Modelling and Validation for a Spherical Motor with Stepped Permanent Magnets, *J. Electr. Eng. Technol.*, 2020, vol. 15, pp. 2661–2673.

[3] Balandin D. V., Biryukov R. S., Tuzikov A. M., Optimal Control of the Movement of a Spherical Robot on Uneven Surfaces, *J. Comput. Syst. Sci. Int.*, 2026, vol. 65, pp. 134–151.

[4] Balandin D. V., Tuzikov A. M., Biryukov R. S., Polovinkin A. V., Spherical Robot with Electromagnetic Drive: Modeling and Control, *Russian J. Nonlinear Dyn.*, 2025, vol. 21, no. 4, pp. 649–671.

On the first caustic of elliptical billiards

A. D. Uskova

National Research University Higher School of Economics, Moscow, Russia

A point source of light is placed inside a billiard with a smooth, convex, closed boundary. For any integer n, the n-th caustic by reflection, denoted by Γ_n, is the envelope of light rays that have undergone n reflections in such a billiard after emanating from the source.

It has been conjectured by Gil Bor and Serge Tabachnikov [2] that for an elliptical billiard, Γ_n has exactly four ordinary cusps; this problem is a billiard variation of Jacobi's Last Geometric Statement, which concerns the number of cusps in the conjugate locus of a point on an ellipsoid [1]. Gil Bor, Mark Spivakovsky, and Serge Tabachnikov have proven that Γ_n has at least four ordinary cusps [3]; however, the upper bound for the number of cusps is unknown at this moment.

We proved that Γ_1 in elliptical billiards has exactly four ordinary cusps, using billiards in complex spaces introduced by Glutsyuk [5], [6]. This approach potentially makes it possible to obtain upper bounds on the number of cusps of Γ_n with $n > 1$.

References

[1] Itoh, J., Kiyohara, K., The cut loci and the conjugate loci on ellipsoids, *Manuscr. Math.*, 2004, no. 114, pp. 247–264.

[2] Bor, G., Tabachnikov, S., On Cusps of Caustics by Reflection: Billiard Variations on the Four Vertex Theorem and on Jacobi's Last Geometric Statement., *The American Mathematical Monthly.*, 2023, no. 130:5, pp. 454–467.

[3] Bor, G., Spivakovsky, M., Tabachnikov, S., Cusps of caustics by reflection in ellipses, *Journal of the London Mathematical Society*, 2024, no. 110:6 pages e70033.

[4] Bruce, J.W., Giblin, P.J., Gibson, C.G., On Caustics of Plane Curves, *The American Mathematical Monthly*, no. 88(9), pp. 651–667.

[5] Glutsyuk, A., On quadrilateral orbits in complex algebraic planar billiards, *Moscow Mathematical Journal*, 2014, no. 14, pp. 239–289

[6] Glutsyuk, A., On Odd-periodic Orbits in complex planar billiards, *Journal of Dynamical and Control Systems*, 2014, no. 20, pp. 293–306

[7] Cayley, A., A Memoir upon Caustics, *Philosophical Transactions of the Royal Society of London*, 1857, Vol. 147, pp. 273–312.

[8] Tabachnikov, S. *Geometry and Billiards*, American Mathematical Society, 2005.

Normal forms for an equilibrium with a triple-zero eigenvalue in $\mathbf{Z}_4$-symmetric systems: bifurcations and attractors

R. A. Uvarov

HSE University, Nizhny Novgorod, Russia

Classical Shimizu-Morioka system turns out to be a normal form for axially $\mathbf{Z}_2$–symmetric systems undergoing a bifurcation of an equilibrium point with three zero eigenvalues [1]. For certain open set of parameters this system has the famous Lorenz attractor - pseudo-hyperbolic and robustly transitive attracting set [5,6]. This gives one possible explanation for ubiquity of Lorenz attractors.

Instead of axial reflective symmetry other $\mathbf{Z}_2$ and related symmetries have been studied by several authors [1, 4]. It is natural to ask what happens for other group actions such as $\mathbf{Z}_4$. In $\mathbf{R}^3$ there are essentially only two possible cases for $\mathbf{Z}_4$ symmetries corresponding to the matrices

$$S_1 = \begin{pmatrix} 0 & -1 & 0 \\ 1 & 0 & 0 \\ 0 & 0 & -1 \end{pmatrix}, \quad S_2 = \begin{pmatrix} 0 & -1 & 0 \\ 1 & 0 & 0 \\ 0 & 0 & 1 \end{pmatrix}$$

The first case has been studied in [2] where pseudo-hyperbolic Lorenz-like attractors were proven to exist for an open set of parameters.

In this work we begin studying the second case by obtaining the normal form of this bifurcation and analyzing how the equilibria bifurcate and what possible attractors may occur.

The result was prepared within the framework of the project "International academic cooperation" HSE University (HSE-BR-2025-81).

References

[1] Shil'nikov, A. L., Shil'nikov, L. P., Turaev D. V., Normal forms and Lorenz attractors, *IJBC*, 1993, vol. 03, no. 05, pp. 1123–1139.

[2] Karatetskaia E. Yu., Kazakov A. O, Safonov K. A, Turaev D. V., Analytic proof of the emergence of new type of Lorenz-like attractors from the triple instability in systems with $\mathbf{Z}_4$-symmetry, *Journal of Differential Equations*, 2025, vol. 430, 113189.

[3] Arneodo, A., Coullet, P.H., Spiegel, E.A., Tresser, C., Asymptotic chaos, *Physica D: Nonlinear Phenomena*, 1985, 14(3), pp. 327-347.

[4] Gonchenko, S. V, Karatetskaia, E. Yu., Kazakov, A. O, Kruglov V. P., Conjoined Lorenz twins—a new pseudohyperbolic attractor in three-dimensional maps and flows. *Chaos: An Interdisciplinary Journal of Nonlinear Science*, 2022, 32(12).

[5] Shilnikov A. L, Bifurcations and chaos in the Shimizu–Morioka system in Methods of Qualitative Theory of Differential Equations (Gorky: Gorky State University) pp. 180–193

[6] Shilnikov A, L., On bifurcations of the Lorenz attractor in the Shimizu–Morioka model, *Physica D*, 62(1–4) 338–346

Control of a circular foil motion using an attached source

E. V. Vetchanin, E. M. Artemova

Ural Mathematical Center, Udmurt State University, Izhevsk, Russia

The problem of controlling the motion of a balanced circular foil in an ideal incompressible fluid by means of rotor rotation and an attached source is considered. The motion is described by the following system of ordinary differential equations [1].

$$\begin{gathered} m\dot{u}_x = \frac{\rho q R^2}{r_1^2}u_x + m\omega u_y + \frac{\rho q^2 R^2}{2\pi r_1(r_1^2 - R^2)} - \frac{\rho R^2}{r_1}\dot{q}, \\ m\dot{u}_y = -m\omega u_x - \frac{\rho q R^2}{r_1^2}u_y - \frac{\rho q R^2}{r_1}\omega, \\ \dot{Z}_c = (u_x + iu_y)e^{i\vartheta}, \quad \dot{\vartheta} = \omega, \end{gathered} \tag{1}$$

where the angular velocity ω and the source strength q are the controls. Equations (1) are written relative to the moving reference frame attached to the body (see Fig. 1)

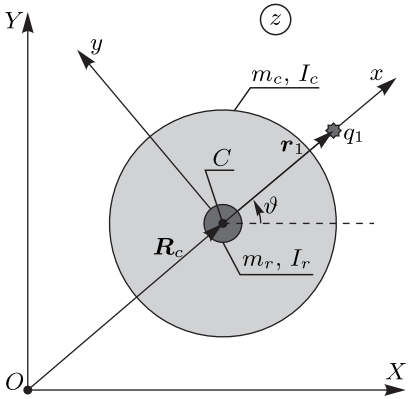


Figure 1. Diagram of the system under consideration.

In the case of a piecewise constant control

$$\begin{pmatrix} q \\ \omega \end{pmatrix} = \sum_{j=1}^{M} \begin{pmatrix} Q_j \\ \Omega_j \end{pmatrix} \big(\Theta(t-\tau_j) - \Theta(t-\tau_{j+1})\big), \quad Q_j = \text{const}, \quad \Omega_j = \text{const}, \tag{2}$$

equations (1) can be integrated explicitly. In this case, at the moments of change in the source strength, the longitudinal component of the system velocity also changes in a jump:

$$u_x(\tau_j + 0) = u_x(\tau_j - 0) - \frac{\rho R^2}{m r_1}(Q_j - Q_{j-1}). \tag{3}$$

Using the explicit solutions found, a trajectory control algorithm is formulated that enables the system to move near a prescribed trajectory (see the example in Fig. 2).

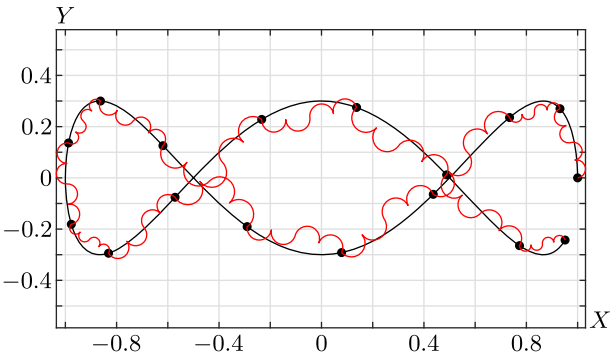


Figure 2. An example of the implementation of the trajectory control algorithm.

The work was carried out within the framework of the state assignment of the Ministry of Science and Higher Education of Russia (FEWS-2024-0007).

References

[1] Vetchanin E. V., Artemova E. M., Control of the motion of a circular foil using attached sources and internal mechanisms, *Izvestiya Vysshikh Uchebnykh Zavedeniy. Applied Nonlinear Dynamics*, 2026, vol. 34, no. 2, pp. 223-246

Structurally stable systems with codimension one attractors

E. V. Zhuzhoma

HSE University, Nizhny Novgorod, Russia

Axiom A systems (in short, A-systems) were introduced in Dynamical Systems by Steve Smale as the systems whose non-wandering set is hyperbolic and the closure of periodic points. Well known that a non-wandering set of such system splits into so-called basic sets (invariant and transitive components). Basic sets of maximal dimension are codimension one ones.

We consider A-flows (dynamical systems with continuous time) and A-diffeomorphisms (dynamical systems with discrete time) with codimension one basic sets on closed manifolds. One shows that such basic set is either an attractor or repeller. Mainly, we consider two-dimensional attractors of structurally stable systems on 3-manifolds.

The work was prepared within the framework of the project "International academic cooperation" HSE University.

Flexible hinges with a given characteristic for a gravity compensator

A. N. Zotov[1], A. R. Valeev[2], A. P. Tokarev[2], D. N. Mazidullin[2], and D. P. Danilov[2]

[1] *Sirius University of Science and Technology, Sirius Federal Territory, Russia*
[2] *Ufa State Petroleum Technological University, Ufa, Russia*

Recently, there has been growing interest in the field of passive gravity compensators within robotics [1, 2]. This is a promising area that enables a significant expansion of human capabilities when handling heavy loads, thereby reducing the risk of injury and increasing work efficiency. This paper examines a gravity compensator based on a flexure joint with a specific characteristic; its schematic diagram is shown in Fig. 1a. A spring 1 with stiffness c is housed within a casing 2, which can rotate about center O and move along guides 3, and is rigidly connected to a rod 4; a second flexure joint 5 of identical design is located at the end of this rod. Spring 1 makes contact with guides 3 via a roller 6. Fig. 1b illustrates the proposed gravity compensator. The flexure joints are located at points O and A.

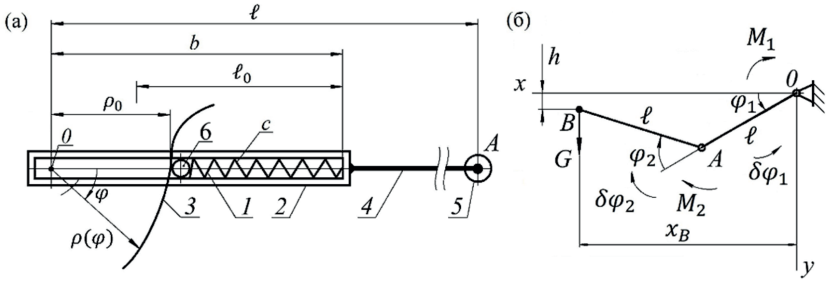
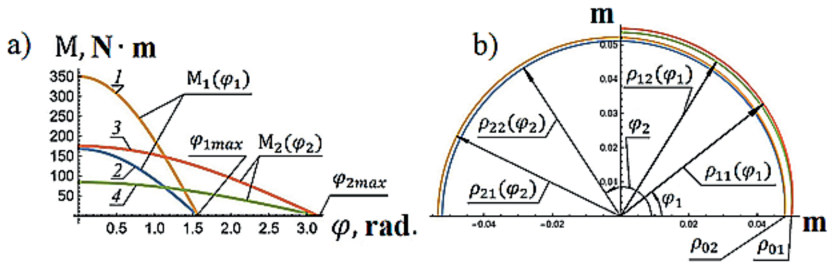


Figure 1. Schematic diagram of an elastic hinge with a given characteristic

Under static conditions, the problem of calculating the shape of the guides 3 — defined by the function $\rho(\varphi)$ (Fig. 1a) — was solved. Initially, this dependence was determined assuming the radius of roller 6 to be zero and disregarding friction. To simplify the solution, it was initially assumed that $h = 0$. To this end, the dependencies $M_1(\varphi_1)$ and $M_2(\varphi_2)$ were determined (Fig. 1a). Subsequently, first-order differential equations incorporating the functions $\rho_1(\varphi_1)$, $\rho_2(\varphi_2)$, $M_1(\varphi_1)$, and $M_2(\varphi_2)$ were solved. Once $\rho_1(\varphi_1)$

and $\rho_2(\varphi_2)$ were determined, the curves equidistant to them were calculated, taking into account the radii of roller 6 (Fig. 1b). Fig. 2a shows the dependencies $M_1(\varphi_1)$ and $M_2(\varphi_2)$ for various values of the load weight G. Fig. 2b presents the polar coordinate dependencies $\rho_{11}(\varphi_1)$ ($G = 500$ N) and $\rho_{12}(\varphi_1)$ ($G = 240$ N) — defining the guide shapes for the hinge at point O (Fig. 1b) — and $\rho_{21}(\varphi_2)$ ($G = 500$ N) and $\rho_{22}(\varphi_2)$ ($G = 240$ N) — defining the guide shapes for the hinge at point A (Fig. 1b).



$b = 0.16$ m; $l_0 = 0.12$ m; $l = 0.35$ m; $h = 0$;

a) $1, 3 - G = 500$ N; $2, 4 - G = 240$ N;

$\varphi_{1\,\max} = \pi/2$ — maximum hinge rotation angle at the point O;

$\varphi_{2\,\max} = \pi$ — maximum hinge rotation angle at the point A;

b) $\rho_{11}(\varphi_1), \rho_{21}(\varphi_2) - G = 500$ N; $c = 6 \cdot 10^6$ N/m; $\rho_{01} = 0.050$ m;

$\rho_{12}(\varphi_1), \rho_{22}(\varphi_2) - G = 240$ N; $c = 4 \cdot 10^6$ N/m; $\rho_{02} = 0.048$ m.

Figure 2. Dependencies of moments and polar coordinates

Given the characteristics of the gravity compensator shown in Fig. 1b, a load of weight G will be counterbalanced during horizontal movement. It is assumed that for small values of h, only minimal muscular effort will be required when operating with a tool of weight G. The results of previous studies on this topic can be found, for example, in [3]. Future plans involve replacing the springs with pneumatic springs, which offers additional possibilities for adjusting the gravity compensator's parameters.

This work was supported by a grant from the Russian Science Foundation (No. 25-29-00314). No additional grants were received for conducting or supervising this specific study.

References

[1] Lixing Jin, Xiaolong Zhu, Jiale Huan, Changsheng Li, and Xingguang Duan. Passive Gravity Compensation for Parallel Mechanism With Spatial Translations and Angular Rotations. *IEEE Robotics and Automation Letters*, 2024, vol. 9, no. 3, pp. 2279–2286.

[2] Ulrich N. et al. Passive mechanical gravity compensation for robot manipulators. In *Proc. of the IEEE Int. Conf. on Robotics and Automation (ICRA)*, Sacramento, USA, April 9–11, 1991, pp. 1536–1541.

[3] Zotov A., Valeev A., and Sviridov A. Exoskeleton Based on Elastic Hinges with a Given Characteristic for Passive Gravitational Compensation of Heavy Objects. In A. A. Radionov and V. R. Gasiyarov, editors, *Proceedings of the 6th International Conference on Industrial Engineering (ICIE 2020). ICIE 2021. Lecture Notes in Mechanical Engineering*. Springer, Cham, 2021.

Motion planning for a spherical robot on uneven terrain using PPO

I. S. Zvonarev, Yu. L. Karavaev

Kalashnikov Izhevsk State Technical University, Izhevsk, Russia

This study addresses motion planning for an underactuated spherical robot on uneven terrain using direct torque commands for the pendulum and rotor actuators. The aim is to determine how terrain irregularities influence the paths followed by the robot under a control policy trained using proximal policy optimization (PPO).

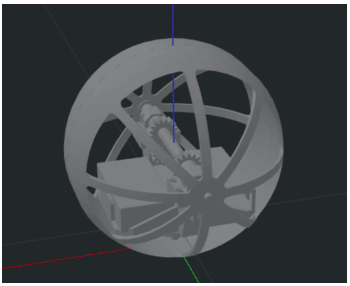


Figure 1. Spherical robot in simulation

The motion of the spherical robot (Fig. 1) is governed by inertial coupling between the shell and the internal mechanisms, as well as by contact with the supporting surface [1]. Motion over uneven terrain requires consideration of changes in the direction of the surface normal, possible slip, and pendulum oscillations, since these factors affect the resulting path and the robot's dynamics.

Control of spherical robots with internal rotors has been investigated in [2], while an overview of designs and control algorithms is presented in [3]. Feedback controllers for motion stabilization have been proposed for spherical robots of the combined and pendulum types [4, 5]. Recent approaches include deep deterministic policy gradient (DDPG) for trajectory tracking [6] and predictive control with obstacle avoidance [7]. The present study investigates the paths generated on uneven terrain by a policy trained using PPO [8] to directly command actuator torques.

The task is to move the robot from its initial state to a specified goal region subject to constraints on actuator torques and internal mechanism states.

The terrain is represented by a height map with regions that differ in slope and in the amplitude and spatial scale of surface irregularities. Simulation experiments are planned in NVIDIA Isaac, with terrain characteristics and the coefficient of friction varied across experiments. The policy's ability to generalize will be evaluated on terrain configurations and contact conditions not encountered during training.

PPO [8] was selected as the training algorithm because it performed best in a preliminary comparison with soft actor-critic (SAC) and twin delayed deep deterministic policy gradient (TD3). The comparison considered the mean episodic return over the final 100 episodes, its standard deviation, the median and range across independent runs, the number of runs with negative return at the end of training, and training time. Here, episodic return is the sum of rewards over all time steps of an episode.

The policy produces two normalized control commands in the range from -1 to 1, which are scaled according to the torque limits of the pendulum and rotor actuators. The commanded torques are held constant between successive control steps. The observations used to generate the commands include the goal coordinates in a reference frame attached to the internal mechanism, the linear and angular velocities of the shell, the pendulum deflection angle and angular velocity, the rotor angular velocity, and the previous action. Terrain geometry is represented by a local map of relative heights, constructed from the environment model and expressed in the same reference frame. Planning and control are thus combined through the sequential generation of actuator torque commands from current observations.

The reward function encourages progress toward the goal and penalizes torque magnitude, changes in control commands, pendulum oscillations, and travel time. Normalization of the reward components and the choice of their weights determine the relative emphasis on rapid progress, smooth control inputs, and limited pendulum oscillations. The goal is considered reached when the positioning accuracy and velocity requirements remain satisfied for a specified time interval. Episodes terminated because of constraint violations or upon reaching the time limit are recorded separately.

Paths on terrains with different surface irregularities will be compared using the same set of observed variables, common criteria for reaching the goal, a common set of initial and goal positions, and an equal number of interactions with the environment. Reproducibility will be assessed through independent training runs with different random seeds. Motion performance will be evaluated in terms of the success rate, the length of the three-dimensional path, time to reach the goal, positioning error, pendulum oscillation amplitude, and the fraction of time spent at the actuator torque limits. The cumulative

absolute mechanical work of the actuators will also be computed by integrating the sum of the absolute values of their mechanical powers over time. Each actuator's mechanical power is the product of its torque and the corresponding relative angular velocity. Results will be reported with measures of variability and confidence intervals.

The analysis will compare the paths followed by the robot across different terrains with shortest paths on the corresponding surface maps. It will examine under which terrain conditions the learned policy guides the robot across an uneven region or around it, and how this affects path length and success in reaching the goal. The study is expected to establish a relationship between terrain irregularities, path geometry, and the success rate.

References

[1] Kilin A. A., Karavaev Yu. L., Experimental Research of Dynamic of Spherical Robot of Combined Type, *Nelineinaya Dinamika*, 2015, vol. 11, no. 4, pp. 721–734 (in Russian).

[2] Borisov A. V., Kilin A. A., Mamaev I. S., How to Control Chaplygin's Sphere Using Rotors, *Regul. Chaotic Dyn.*, 2012, vol. 17, nos. 3–4, pp. 258–272.

[3] Karavaev Yu. L., Mamaev I. S., Kilin A. A., Pivovarova E. N., Spherical Rolling Robots: Different Designs and Control Algorithms, *Proc. CLAWAR 2020*, 2020, pp. 195–202.

[4] Borisov A. V., Kilin A. A., Karavaev Yu. L., Klekovkin A. V., Stabilization of the Motion of a Spherical Robot Using Feedbacks, *Appl. Math. Model.*, 2019, vol. 69, pp. 583–592.

[5] Klekovkin A. V., Karavaev Yu. L., Nazarov A. V., Stabilization of a Spherical Robot with an Internal Pendulum During Motion on an Oscillating Base, *Rus. J. Nonlin. Dyn.*, 2024, vol. 20, no. 5, pp. 845–858.

[6] Nor N. V., Reinforcement Learning in the Task of Spherical Robot Motion Control, *Rus. J. Nonlin. Dyn.*, 2024, vol. 20, no. 2, pp. 295–310.

[7] Keymasi-Khalaji A., Mokhtari P., Bathaei F., Predictive Control for the Navigation of Spherical Robots in Obstacle-Rich Environments, *Sci. Rep.*, 2025, vol. 15, article 13859.

[8] Schulman J. et al., Proximal Policy Optimization Algorithms, *arXiv:1707.06347*, 2017.

Visual localization of an unmanned aerial vehicle using onboard camera imagery

V. K. Zykov, P. N. Deryushev, R. T. Mrakov, and Yu. L. Karavaev

Kalashnikov Izhevsk State Technical University, Izhevsk, Russia

The objective of this work is to develop a visual localization system for an unmanned aerial vehicle (UAV) using georeferenced satellite imagery. Matching onboard camera frames to a map provides an additional source of position estimates when satellite navigation signals are unavailable or corrupted.

Frames from a downward-looking camera are matched to map patches around the estimated UAV position after rotation correction using telemetry. A common position estimation pipeline has been implemented with SIFT, SuperPoint with LightGlue [1], and RoMa [2]. RoMa is selected as the primary method because it estimates a dense correspondence field rather than relying solely on independently detected keypoints and is designed to handle changes in scale, illumination, and viewpoint [2]. These properties are relevant when matching UAV frames to satellite imagery acquired under different conditions. SIFT and SuperPoint with LightGlue serve as comparison methods; the computational cost of RoMa is considered in further adaptation to an onboard computer.

Correspondences are verified using RANSAC to estimate a projective transformation between the frame and the map. The image center is mapped to the satellite image and converted to geographic coordinates. Reliability is assessed using the number and proportion of inliers, the image registration error, and the spatial distribution of the correspondences. The shape and size of the projected image footprint and the availability of map data at the estimated position are also checked. No position is reported if these criteria are not met. These checks reject spurious matches and solutions supported by only a small image region. The method assumes near-nadir imaging and locally planar terrain.

A tracking mode uses GPS for initialization over the first ten processed frames. Subsequently, the search region is predicted from previous positions and the estimated velocity, then updated using accepted visual position estimates. This restricts the search to a local map patch. Subsequent GPS measurements are used only for accuracy evaluation. A graphical interface provides synchronized displays of the video and the estimated trajectory.

Experiments use the AirLock+ dataset [3], which contains seven DJI Air 2S flight sequences recorded over Austin, USA. The dataset includes nadir

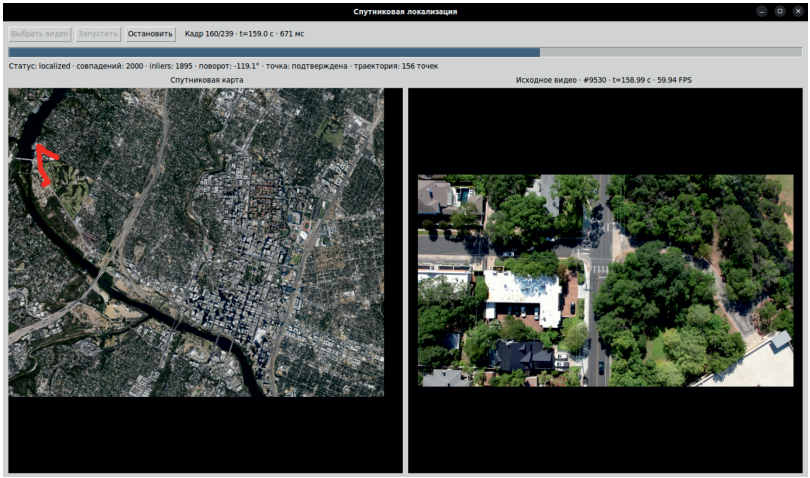


Figure 1. Visualization of UAV localization using RoMa on DJI_1005: satellite map with the estimated trajectory and an onboard camera frame

video, per-frame UAV telemetry, and georeferenced satellite maps. The experiments use 1920×1080-pixel video at 59.94 frames/s and a Mapbox Satellite map in GeoTIFF format. Two video sequences were selected: DJI_1002, approximately 6 min 30 s long, recorded at 118–156 m above ground level, and DJI_1005, approximately 3 min 58 s long, recorded at 149–150 m.

The selected sequences were processed using RoMa with GPS initialization, sampling one frame per second. The proportion of all sampled frames with an accepted position estimate and an error of at most 20 m was 83.3% for DJI_1002 (390 frames) and 97.9% for DJI_1005 (239 frames). The median errors among accepted estimates were 13.32 and 5.41 m, respectively. Rotation telemetry was used throughout both sequences; these results apply to the evaluated conditions. Figure 1 illustrates the interface for DJI_1005: the satellite map and the accepted visual trajectory in red are shown on the left, and the corresponding onboard camera frame is shown on the right.

The experiments demonstrate the feasibility of visual tracking after initial position acquisition. Further work focuses on robustness to viewpoint and terrain changes, relocalization after tracking loss, and faster processing.

References

[1] Lindenberger P., Sarlin P.-E., Pollefeys M., LightGlue: Local Feature Matching at Light Speed, *Proc. IEEE/CVF ICCV*, 2023, pp. 17627–17638.

[2] Edstedt J., Sun Q., Bökman G., Wadenbäck M., Felsberg M., RoMa: Robust Dense Feature Matching, *Proc. IEEE/CVF CVPR*, 2024, pp. 19790–19800.

[3] Deng Z., Case A., Sentis L., AirLock+: Scaling UAV-to-Satellite Image Registration for Target Geolocalization and Geospatial Augmented Reality, *Proc. IEEE/CVF WACV*, 2026, pp. 3340–3349.

Notes

ANS Conference Series

Regular and Chaotic Dynamics:

Nonlinear Dynamics, Mechanics and Robotics

November 23–27, 2026

Book of Abstracts

Подписано в печать 16.11.2026. Формат $60 \times 84\,{}^{1}/_{8}$.
Гарнитура «Times New Roman». Печать цифровая.
Усл. печ. л. 6,74. Уч.-изд. л. 6,72. Тираж 100 экз. Заказ № 26-57.

АНО «Ижевский институт компьютерных исследований»,
426053, г. Ижевск, ул. Ворошилова, д. 123.
http://ics.com.ru E-mail: mail@rcd.ru Тел./факс: +7 (3412) 26-36-34
Отпечатано в цифровой типографии
АНО «Ижевский институт компьютерных исследований».